

# 1 Newly identified climatically and environmentally significant high- 2 latitude dust sources

3 Outi Meinander<sup>1</sup>, Pavla Dagsson-Waldhauserová<sup>2,3</sup>, Pavel Amosov<sup>4</sup>, Elena Aseyeva<sup>5</sup>, Cliff Atkins<sup>6</sup>,  
4 Alexander Baklanov<sup>7</sup>, Clarissa Baldo<sup>8</sup>, Sarah Barr<sup>9</sup>, Barbara Barzycka<sup>10</sup>, Liane G. Benning<sup>11,23</sup>, Bojan  
5 Cvetkovic<sup>12</sup>, Polina Enchilik<sup>5</sup>, Denis Frolov<sup>5</sup>, Santiago Gassó<sup>13</sup>, Konrad Kandler<sup>14</sup>, Nikolay Kasimov<sup>5</sup>,  
6 Jan Kavan<sup>15,b</sup>, James King<sup>16</sup>, Tatyana Koroleva<sup>5</sup>, Viktoria Krupskaya<sup>5,6</sup>, Markku Kulmala<sup>18</sup>, Monika  
7 Kusiak<sup>19</sup>, Hanna K Lappalainen<sup>18</sup>, Michał Laska<sup>11</sup>, Jerome Lasne<sup>20</sup>, Marek Lewandowski<sup>19</sup>, Bartłomiej  
8 Luks<sup>19</sup>, James B McQuaid<sup>10</sup>, Beatrice Moroni<sup>21</sup>, Benjamin J Murray<sup>10</sup>, Ottmar Möhler<sup>22</sup>, Adam Nawrot<sup>19</sup>,  
9 Slobodan Nickovic<sup>13</sup>, Norman T. O'Neill<sup>23</sup>, Goran Pejanovic<sup>13</sup>, Olga B. Popovicheva<sup>5</sup>, Keyvan  
10 Ranjbar<sup>23,a</sup>, Manolis N. Romanias<sup>20</sup>, Olga Samonova<sup>5</sup>, Alberto Sanchez-Marroquin<sup>10</sup>, Kerstin  
11 Schepanski<sup>24</sup>, Ivan Semenov<sup>5</sup>, Anna Sharapova<sup>11</sup>, Elena Shevnina<sup>1</sup>, Zongbo Shi<sup>9</sup>, Mikhail Sofiev<sup>1</sup>,  
12 Frédéric Thevenet<sup>20</sup>, Throstur Thorsteinsson<sup>25</sup>, Mikhail A. Timofeev<sup>5</sup>, Nsikanabasi Silas Umo<sup>22</sup>, Andreas  
13 Uppstu<sup>1</sup>, Darya Urupina<sup>20</sup>, György Varga<sup>26</sup>, Tomasz Werner<sup>19</sup>, Olafur Arnalds<sup>2</sup>, and Ana Vukovic  
14 Vimic<sup>27</sup>

15

16 <sup>1</sup>Finnish Meteorological Institute, Helsinki, 00101, Finland

17 <sup>2</sup>Agricultural University of Iceland, Reykjavik, 112, Iceland

18 <sup>3</sup>Czech University of Life Sciences Prague, Prague, 16521, Czech Republic

19 <sup>4</sup>INEP Kola Science Center RAS, Apatity, Russia

20 <sup>5</sup>Lomonosov Moscow State University, Moscow, 119991, Russia

21 <sup>6</sup>Institute of Geology of Ore Deposits, Petrography, Moscow, 119017, Russia

22 <sup>7</sup>Te Herenga Waka—Victoria University of Wellington, Wellington, 6012, New Zealand

23 <sup>8</sup>World Meteorological Organization, WMO, Geneva, 1211, Switzerland

24 <sup>9</sup>University of Birmingham, Birmingham, B15 2TT, United Kingdom

25 <sup>10</sup>University of Leeds, Leeds, LS2 9JT, United Kingdom

26 <sup>11</sup>University of Silesia in Katowice, Sosnowiec, 41-200, Poland

27 <sup>12</sup>German Research Centre for Geosciences, Helmholtz Centre Potsdam, 14473, Germany

28 <sup>13</sup>Republic Hydrometeorological Service of Serbia, 11030, Belgrade, Serbia

29 <sup>14</sup>University of Maryland, College Park MD, 20742, United States of America

30 <sup>15</sup>Technical University of Darmstadt, Darmstadt, 64287, Germany

31 <sup>16</sup>Masaryk University, Brno, 61137, Czech Republic

32 <sup>17</sup>University of Montreal, Montreal, H3T 1J4, Canada

33 <sup>18</sup>Institute for Atmospheric and Earth System Research, University of Helsinki, Helsinki, 00101, Finland

34 <sup>19</sup>Institute of Geophysics, Polish Academy of Sciences, Warsaw, 01-452, Poland

35 <sup>20</sup>Institut Mines-Télécom Nord Europe, Université de Lille, Center for Energy and Environment, Lille, 59000, France

36 <sup>21</sup>University of Perugia, Perugia, 06123, Italy

37 <sup>22</sup>Institute of Meteorology and Climate Research, Karlsruhe Institute of Technology, Karlsruhe, 76227, Germany.

38 <sup>23</sup>Université de Sherbrooke, Sherbrooke, J1K, Canada

39 <sup>24</sup>Free University of Berlin, Berlin, 12165, Germany

40 <sup>25</sup>University of Iceland, Reykjavik, 102, Iceland

41 <sup>26</sup>Research Centre for Astronomy and Earth Sciences, Budapest, 1112, Hungary

42 <sup>27</sup>University of Belgrade, Faculty of Agriculture, Belgrade, 11080, Serbia

43 <sup>a</sup>now at: Flight Research Laboratory, National Research Council Canada, Ottawa, ON, Canada

44 <sup>b</sup>now at: University of Wroclaw, Wroclaw, 50-137, Poland

45

46

47

48 *Correspondence to:* Outi Meinander ([outi.meinander@fmi.fi](mailto:outi.meinander@fmi.fi))

49 **Abstract.** Dust particles from high latitudes have a potentially large local, regional, and global significance to climate and the  
50 environment as short-lived climate forcers, air pollutants, and nutrient sources. Identifying the locations of local dust sources  
51 and their emission, transport, and deposition processes is important for understanding the multiple impacts of High Latitude  
52 Dust (HLD) on the Earth's systems. Here, we identify, describe, and quantify the Source Intensity (SI) values, which show the  
53 potential of soil surfaces for dust emission scaled to values 0 to 1 concerning globally best productive sources, using the Global  
54 Sand and Dust Storms Source Base Map (G-SDS-SBM). This includes sixty-four HLD sources in our collection for the  
55 Northern (Alaska, Canada, Denmark, Greenland, Iceland, Svalbard, Sweden, and Russia) and Southern (Antarctica and  
56 Patagonia) high latitudes. Activity from most of these HLD dust sources shows seasonal character. It is estimated that high-  
57 latitude land areas with higher ( $SI \geq 0.5$ ), very high ( $SI \geq 0.7$ ), and the highest potential ( $SI \geq 0.9$ ) for dust emission cover  $>1$   
58  $670\,000\text{ km}^2$ ,  $>560\,000\text{ km}^2$ , and  $>240\,000\text{ km}^2$ , respectively. In the Arctic HLD region ( $\geq 60^\circ\text{N}$ ), land area with  $SI \geq 0.5$  is  
59 5.5% ( $1\,035\,059\text{ km}^2$ ), area with  $SI \geq 0.7$  is 2.3% ( $440\,804\text{ km}^2$ ), and with  $SI \geq 0.9$  is 1.1% ( $208\,701\text{ km}^2$ ). Minimum SI values  
60 in the north HLD region are about three orders of magnitude smaller, indicating that the dust sources of this region greatly  
61 depend on weather conditions. Our spatial dust source distribution analysis modeling results showed evidence supporting a  
62 northern High Latitude Dust (HLD) belt, defined as the area north of  $50^\circ\text{N}$ , with a 'transitional HLD-source area' extending  
63 at latitudes  $50\text{--}58^\circ\text{N}$  in Eurasia and  $50\text{--}55^\circ\text{N}$  in Canada, and a 'cold HLD-source area' including areas north of  $60^\circ\text{N}$  in Eurasia  
64 and north of  $58^\circ\text{N}$  in Canada, with currently 'no dust source' area between the HLD and LLD dust belt, except for British  
65 Columbia. Using the global atmospheric transport model SILAM, we estimated that 1.0% of the global dust emission  
66 originated from the high-latitude regions. About 57% of the dust deposition in snow- and ice-covered Arctic regions was from  
67 HLD sources. In the south HLD region, soil surface conditions are favorable for dust emission during the whole year. Climate  
68 change can decrease snow cover duration, retrieval of glaciers, and increase drought, heatwave intensity, and frequency,  
69 leading to the increasing frequency of topsoil conditions favorable for dust emission, which increases the probability of dust  
70 storms. Our study provides a step forward to improve the representation of HLD in models and to monitor, quantify, and assess  
71 the environmental and climate significance of HLD going forward.

## 72 **1 Introduction**

73 Mineral dust is an essential and relevant climate and environmental variable with multiple socioeconomic effects on, e.g.,  
74 weather and air quality, marine life, climate, and health (Creamean et al., 2013; Terradellas et al., 2015; Shepherd et al., 2016;  
75 Querol et al., 2019; Nemuc et al., 2020). Mineral dust is transported from local sources of high-latitude dust (HLD,  $\geq 50^\circ\text{N}$  and  
76  $\geq 40^\circ\text{S}$ , Bullard et al., 2016), low-latitude dust (LLD, mostly  $0\text{-}35^\circ\text{N}$ ), and the so-called ‘global dust belt’ (GDB, Prospero et  
77 al., 2002), defined to extend into the Northern Hemisphere from the west coast of North Africa, over the Middle East (West  
78 Asia), Central and East Asia, and south-west North America (Ginoux et al., 2012), with only minor sources in Southern  
79 Hemisphere (Prospero et al., 2002; Ginoux et al., 2012; Bullard et al., 2016; Terradellas et al., 2017). Dust is often associated  
80 with hot, subtropical deserts, but the importance of dust sources in the cold, high latitudes has recently increased (Arnalds et  
81 al., 2016; Bullard et al., 2016; Groot Zwaafting et al., 2016, 2017; Kavan et al., 2018, 2020a,b; Boy et al., 2019; Gassó and  
82 Torres, 2019; IPCC, 2019; Tobo et al., 2019; Bachelder et al., 2020; Cosentino et al., 2020; Ranjbar et al., 2021; Sanchez-  
83 Marroquin et al., 2020). Dust produced in high latitudes and cold climates (Iceland, Greenland, Svalbard, Alaska, Canada,  
84 Antarctica, New Zealand, and Patagonia) can have regional and global significance (Bullard et al., 2016). Local HLD dust  
85 emissions are increasingly being recognized as driving the local climate, biological productivity, and air quality (Groot  
86 Zwaafting et al., 2016, 2017; Moroni et al., 2018; Crocchianti et al., 2021; Varga et al., 2021). HLD can induce significant  
87 direct (blocking sunlight) and indirect (clouds and cryosphere) radiative forcing (Kylling et al., 2018) on solar radiation fluxes  
88 and snow optical characteristics, strongly impacting Arctic amplification, including glacier melt (Boy et al., 2019).

89  
90 HLD aerosols consist of a variety of different dust particle types with various particle sizes and shapes distributions, as well  
91 as physical, chemical, and optical properties that differ from the crustal dust of the Sahara or American deserts (Shepherd et  
92 al., 2016; Arnalds et al., 2016; Bachelder et al., 2020; Baldo et al., 2020; Crucius, 2021). Therefore, impacts on climate,  
93 environment, and human health can differ from those of LLD. For example, Icelandic dust is of volcanic desert origin, often  
94 dark, and has higher proportions of heavy metals than crustal dust (Arnalds et al., 2016). The IPCC special report (IPCC, 2019)  
95 recognizes dark dust aerosols as a short-lived climate forcer (SLCF) and light-absorbing aerosols connected to cryospheric  
96 changes. Light-absorbing HLD particles can induce direct effects on solar radiation fluxes as SLCF and snow optical  
97 characteristics impacting cryosphere melt via radiative feedback (Peltoniemi et al. 2015; Boy et al., 2019; Dagsson-  
98 Waldhauserová and Meinander, 2019, 2020; IPCC, 2019; Kylling et al., 2018). HLD significantly affects the formation and  
99 properties of clouds (Abbatt et al., 2019; Sanchez-Marroquin et al., 2020; Murray et al., 2021).

100

101 Dust is connected to climate change: Historical dust (paleo dust) is not only a contributor to climate change but a record of  
102 previous dust and climate conditions (Lamy et al., 2014; Lewandowski et al., 2020). Dust can significantly contribute to air  
103 pollution mortalities (Terradellas et al., 2015; Nemuc et al., 2020). Deposition at high latitudes can provide nutrients to the  
104 marine system; mineral and organic matter on glaciers, including natural and anthropogenic dust, can form cryoconite granules.

105 Cryoconite, dust, and ice algae can reduce surface albedo and accelerate the melting of glaciers (Lutz et al., 2016; McCutcheon  
106 et al., 2021). Monitoring dust in remote, high-latitude areas has crucial value for climate change assessment and understanding  
107 the impacts of global warming on natural systems and socioeconomic sectors. Bullard et al. (2016) summarized natural HLD  
108 sources as covering over 500 000 km<sup>2</sup> and producing particulate matter of ca. 100 Mt dust per year.

109  
110 Dust emissions respond to changes in wind speed, soil moisture, and other parameters affected by climate change; changes in  
111 land cover and surface properties by human activities can affect dust emissions (Kylling et al., 2018). The fundamental  
112 processes controlling aeolian dust emissions in high latitudes are essentially the same as in temperate regions. However, there  
113 are other processes specific to or enhanced in cold regions. Low temperatures, humidity, strong winds, permafrost, and niveo-  
114 aeolian processes, which can affect the efficiency of dust emission and distribution of sediments, were listed in Bullard et al.  
115 (2016).

116  
117 The modeling of emissions, transport, and deposition complemented with available observations, can provide essential  
118 information related to dust's impact on the climate and environment in the high latitudes (IPCC, 2019). The locations and  
119 characteristics of local dust sources are two of the major observations documented for inputting information into numerical  
120 models to predict or simulate the HLD process from its emission to downwind deposition. In some cases, model results can  
121 indicate possible but not yet identified dust sources in the HL regions. A general lack of observational and long-range transport  
122 modeling studies results in poor HLD monitoring and predicting. Models have predictive capacity and, without the  
123 observations, can constitute a source of information and indicate where more direct observations are needed. The first long-  
124 range transport modeling studies show that main transport pathways from HLD sources clearly affect the High Arctic (>80°N)  
125 and European mainland (Baddock et al., 2017; Beckett et al., 2017; Đorđević et al., 2019; Groot Zwaafting et al., 2016, 2017;  
126 Moroni et al., 2018). The World Meteorological Organization Sand and Dust Storm Warning Advisory and Assessment System  
127 (WMO SDS-WAS) monitors and predicts dust storms from the world's major deserts (<https://www.wmo.int/sdswas>), where  
128 HLD sources have recently been included in the SDS-WAS dust forecasts. Europe's largest desert is at a high latitude in  
129 Iceland (Arnalds et al., 2016), with dust transport observed over the North Atlantic to European countries (Ovadnevaite et al.,  
130 2009; Prospero et al., 2012; Beckett et al., 2017; Đorđević et al., 2019).

131  
132 HLD is a short-lived climate forcer, air pollutant, and nutrient source, showing the need to identify the geographical extent  
133 and dust activity of the HLD sources (Arnalds et al., 2014, 2016; Dagsson-Waldhauserová et al., 2014, 2015; Terradellas et  
134 al., 2015; USGCRP, 2018; IPCC, 2019). Bullard et al. (2016) designed the first HLD map based on visibility and dust  
135 observations, combined with field and satellite observations of high-latitude dust storms, resulting in 129 locations described  
136 in 39 papers. Here, we compile and describe sixty-four HLD sources in the northern and southern high latitudes. This work's  
137 main aim is to:

138 (i) identify new and previously unpublished HLD sources ,

- 139 (ii) estimate the high-latitude land area with potential dust activity and calculate the source intensity (SI) for the  
140 identified sources
- 141 (iii) provide model results on HLD emission, long-range transport and deposition at various scales of time and  
142 space
- 143 (iv) specify key climatic and environmental impacts of HLD and related research questions, which could improve  
144 our understanding of HLD sources, with the help of literature surveys on clouds and climate feedback,  
145 atmospheric chemistry, marine environment, cryosphere, and cryosphere-atmosphere feedbacks.  
146

147 We focus on high latitudes with natural dust sources and include some anthropogenic dust sources, such as road dust, when  
148 unpaved roads serve as a significant dust source. Direct emissions of volcanic eruptions and road dust formed via abrasion and  
149 wear of pavement or traction control materials are excluded. Identifying dust sources is the first step to understand the HLD  
150 life-cycle (dust emission, transport, and deposition). After that, impacts and feedback mechanisms can be identified and  
151 quantified as physical, chemical, and optical properties of dust from these source areas. Their properties during emission,  
152 transport, and deposition are needed to be characterized to allow a holistic understanding.

## 153 **2 Materials and methods**

### 154 **2.1 Identification and characteristics of dust sources**

155 Three topical workshops in Russia, Finland, and Iceland (Meinander et al., 2019a,b) on HLD were organized in 2019 to  
156 identify, describe, and assess new high-latitude dust sources ( $\geq 50^\circ\text{N}$  and  $\geq 40^\circ\text{S}$ , according to Bullard et al. 2016, and including  
157 the Arctic as a subregion at  $\geq 60^\circ\text{N}$ ). The HLD source map and observations on dust properties provided here are based on:

- 158 (i) new field and satellite observations not described in published academic papers  
159 (ii) newly identified HLD source locations reported in recent literature but not included in previous collections  
160 (iii) updated observations on previously documented sources.

161 Each location was assessed to classify each source: Category 1 refers to an active dust source with high ecological significance,  
162 category 2 to a semi-active source with moderate ecological significance, and category 3 to new sources with unknown activity  
163 and importance. Moreover, SI values for each HLD location in the Northern and Southern (Antarctica and Patagonia) high  
164 latitudes were quantified, and the potential land surface area for dust emissions in the north, Arctic, and south HLD regions  
165 was calculated (Section 2.2).

### 166 **2.2 High-latitude dust sources from UNCCD G-SDS-SBM**

167 The Global Sand and Dust Storms Source Base Map (G-SDS-SBM), developed by the United Nations Convention to Combat  
168 Desertification (UNCCD) in collaboration with the United Nations Environment Programme (UNEP) and World  
169 Meteorological Organization (<https://maps.unccd.int/sds/>; Vukovic, 2019, 2021) represents gridded values of SDS source

170 intensity (SI, values 0 to 1) on a resolution of 30 arcsec. The Source Base Map was developed by including the information on  
 171 soil texture, bare land fraction, and NASA satellite Moderate-resolution Imaging Spectroradiometer Enhanced Vegetation  
 172 Index, MODIS EVI, as well as the data on land cover, topsoil moisture, and temperature. Values of SI represent topsoil's  
 173 potential to emit soil particles under windy conditions, assigning the highest values of source intensity to the most productive  
 174 surfaces. SI values are derived under the assumption they are exposed to the same velocity of surface wind. Input data, which  
 175 change depending on the weather (and possibly human activities) for bare land fraction, moisture, and temperature data, are  
 176 defined for four months (January, April, July, October—each month representing one season) by using extreme values. This  
 177 was observed from 2014 to 2018, providing favorable conditions for surfaces to act as sources. Thus, sources that may appear  
 178 during heatwaves and drier conditions (or drought), when the surface in high latitudes is unfrozen, snow-free, and more  
 179 susceptible to wind erosion, are included in this map. Such weather extremes under climate change are becoming more frequent  
 180 and are projected to increase (IPCC, 2013), justifying the source mapping approach using the information on extreme topsoil  
 181 conditions. Using the maps produced for the four seasons, maximum and minimum values are determined for each grid point  
 182 to explore the potential of high-latitude land surfaces to act as dust sources, their seasonality, and to compare values of source  
 183 intensity with marked locations of HLD sources.

### 184 **2.3 Methods used to identify and study the dust sources**

185 Various methods identified the HLD sources (Table 1), including direct observations and measurements; satellite data;  
 186 emission, long-range transport and deposition modeling; media, social media, and literature sources (e.g., web pages,  
 187 conference abstracts). More details and literature references can be found in each source section. Dust emission, long-range  
 188 transport, and deposition modeling calculations were made to study if the HLD sources have local, regional, or global  
 189 significance. Two well-established dust atmospheric models—SILAM and DREAM—were used to simulate the atmospheric  
 190 dust process over high latitudes. Both models have been thoroughly evaluated for other deserts where the accuracy of their  
 191 results has been verified.

192

193 **Table 1. Methods used to identify and study the dust sources**

<b>Method</b>	<b>Sources</b>
Direct observation: photographs and visual observations	Marambio, Antarctic Peninsula, Schirmacher Oasis, East Antarctica, McMurdo Sound/Ross Sea
Satellite images: Meteosat-11 images	Denmark, Sweden, Iceland
Instrumentation: SEM	Svalbard

Instrumentation: LOAC	James Ross Island
Instrumentation: SL-501 surface and snow albedo	Marambio, Antarctic Peninsula
Instrumentation: Magnetic susceptibility upon heating, magnetic hysteresis parameters	Svalbard
Instrumentation: ICP-MS, AES-ICP, XRD, XRF	Russia (sources no. 2–5 of Fig.1)
Instrumentation: high performed liquid chromatography, potentiometry	Russia (sources no. 7–8 of Fig.1)
Passive deposition samplers	James Ross Island
Snow samples	Svalbard (Hornsund, Pyramiden), Antarctica
Social media: Twitter account (@SanGasso) and hashtag (#highlatitudedust)	South America (Patagonia), Alaska, Greenland, Iceland
Literature sources	Denmark, Sweden
SILAM model	Arctic
DREAM model	Arctic, Antarctic

194

195

196 Estimates of the emission and deposition of global and Arctic dust were computed separately to assess Arctic dust’s global  
197 impact using the SILAM model (Sofiev et al., 2015)—a global to meso-scale atmospheric dispersion and chemistry model—  
198 applied for air quality and atmospheric composition modelling. The dust emission estimate is driven by the European Centre  
199 for Medium Range Weather Forecast ECMWF IFS meteorological model at a resolution of 0.1 x 0.1 degrees. The computations  
200 were performed using ECMWF ERA5 meteorological reanalysis data for 2017 at a resolution of 0.5 x 0.5 degrees. The dust  
201 emission model was validated against AERONET (AErosol RObotic NETwork, www.aeronet.com) aerosol optical density  
202 (AOD) data and provided unbiased results for the main dust emission areas. For Arctic areas, where dust is not contributing to  
203 the AOD as much, the simulated AOD from all aerosols is unbiased concerning the measurements. While the simulation’s  
204 relatively coarse resolution cannot capture the smaller point-like dust sources, it is still expected to give a good approximation  
205 of the overall patterns and magnitudes of dust emission and deposition. The SILAM results are presented in sections 3.3 (Fig.  
206 4) and 3.4 (Fig. 12 and Fig. 15).

207

208 DREAM is a fully dynamic numerical prediction model for atmospheric dust dispersion originating from soil. The dust  
209 component of this system (Pejanovic et al., 2011; Nickovic et al., 2016) is online and driven by the atmospheric model NMME  
210 (Janjic et al., 2001). Dust concentration in the model is described with eight particle bins, with radii ranging from 0.18 to 9  
211  $\mu\text{m}$ . DREAM-ICELAND is the model version to predict dust transport emitted from Iceland's largest European dust sources  
212 (Cvetkovic et al., 2021, submitted). The size distribution of particles in the model is specified according to in situ measurements  
213 in the Icelandic hot spots. The model horizontal resolution of  $\sim 3.5$  km is sufficiently fine to resolve the Icelandic dust sources'  
214 rather heterogeneous and small-scale character. As the first operational numerical HLD model in the international community,  
215 DREAM-ICELAND is used daily, having predicted Icelandic dust since April 2018. DREAM results are included in sections  
216 3.4 (Fig. 8 and 11) and 3.6 (Fig. 16), and as a supplementary animation.

217

## 218 **3 Results and discussion**

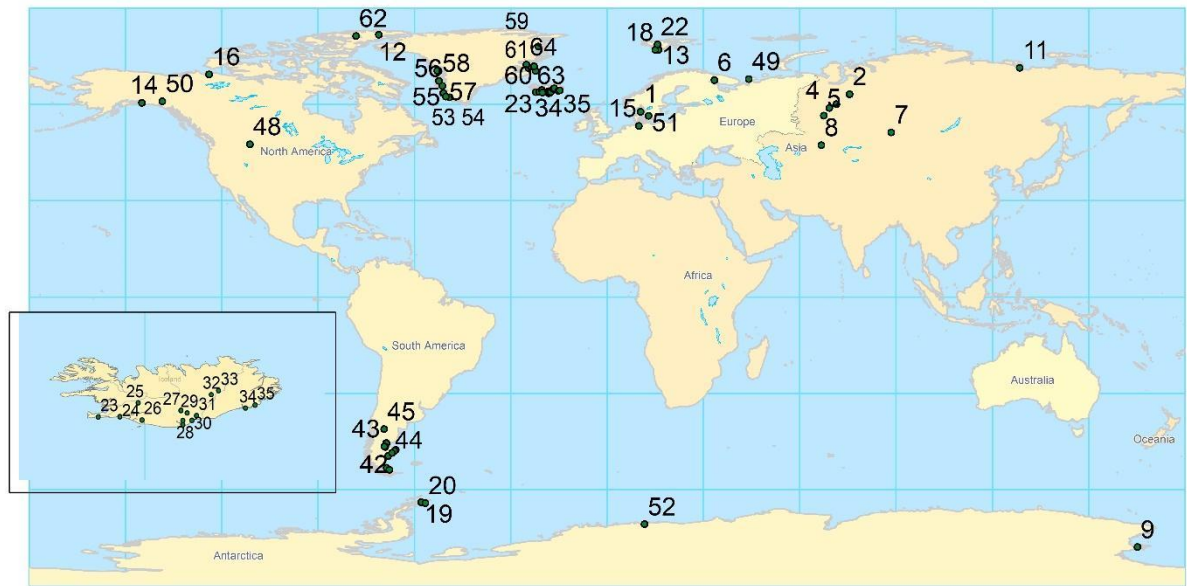
219

### 220 **3.1 Locations of the HLD sources**

221

222 Sixty-four HLD sources at northern and southern high latitudes (Fig. 1) were identified. In the north HLD region are 49  
223 locations (47 locations  $\geq 50^\circ\text{N}$  and two  $>47^\circ\text{N}$ ) in Alaska, Canada, Denmark, Greenland, Iceland, Svalbard, Sweden, and  
224 Russia, of 35 are in the Arctic HLD subregion ( $\geq 60^\circ\text{N}$ ). In the south HLD region ( $\geq 40^\circ\text{S}$ ), 15 sources were identified in  
225 Antarctica and Patagonia, South America. The sources included the Arctic and Antarctic, boreal, remote, rural, mountain,  
226 marine and coastal, river sediments, mining, unpaved roads, soils (Podzols, Retisols, Gleysols, Phaeozems, and Stagnosols;  
227 USS Working Group WRB, 2015), and glacial dust. The observational periods for these locations varied from days or weeks  
228 to multiple years and included data from ground-based measurements, remote sensing data, and modeling results. Results on  
229 the calculated source intensity and areas of high-latitude surface land with higher ( $\text{SI} \geq 0.5$ ), very high ( $\text{SI} \geq 0.7$ ), and the highest  
230 potential ( $\text{SI} \geq 0.9$ ) for dust emission are shown in Section 3.2. Observations and characteristics of the identified dust sources  
231 in our collection (Fig. 1) are presented in Section 3.4 and the Supplement Tables S1-S7 (including the contemporary  
232 classification for each source into categories 1–3, based on the currently available observations, in S1; satellite observations  
233 on new HLD sources in Iceland in S2; observations on new HLD sources in Greenland and Canada in S3; SI values for each  
234 source in S4 and S5, including latitude and longitude; and results from Russian HLD sources in S6-S7).



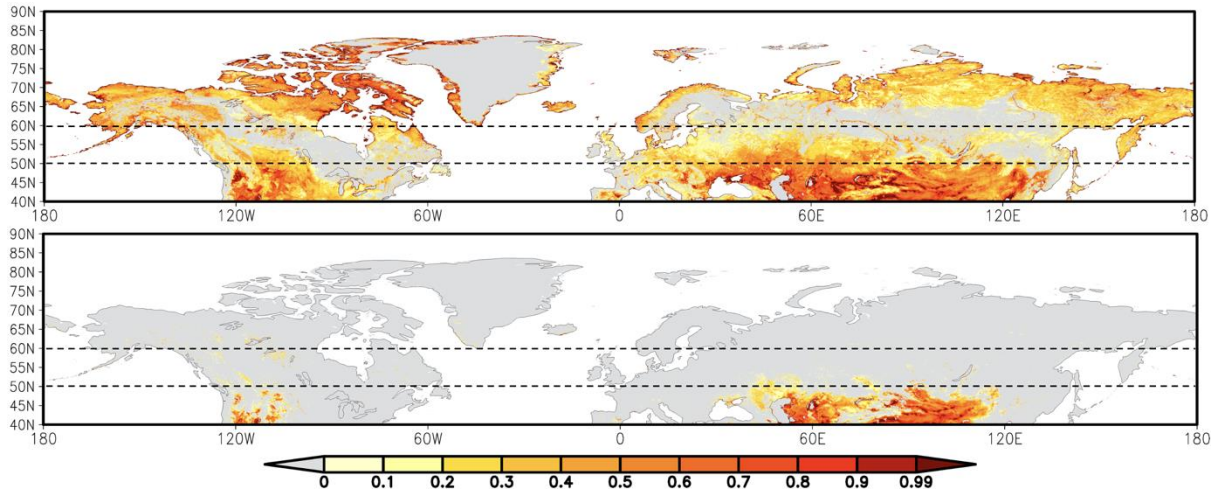


235  
236  
237  
238

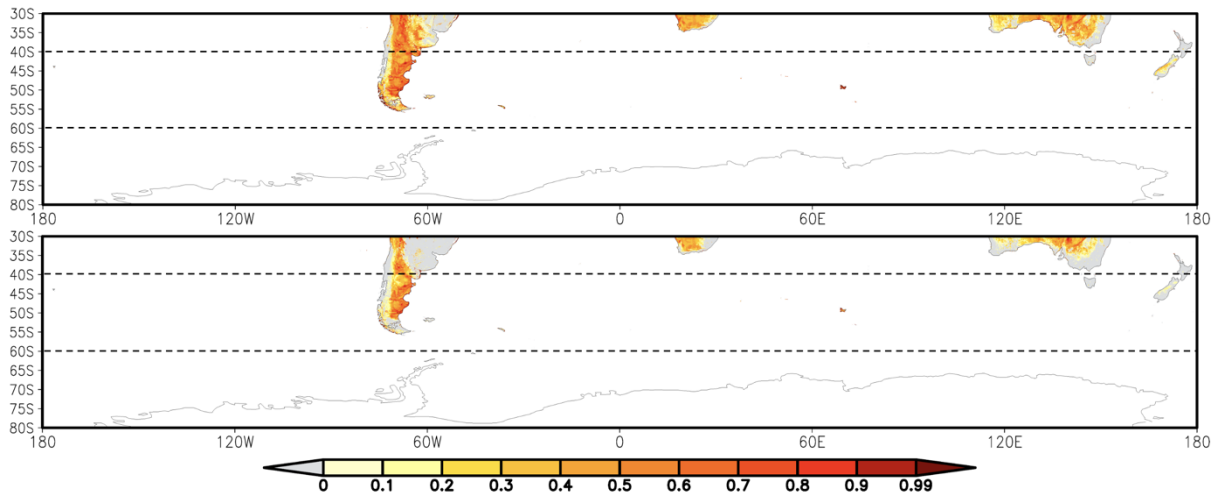
**Figure 1. Map of the locations of the northern (north of 50°N) and southern (south of 40°S) high-latitude dust (HLD) sources identified and included in this study. The numbers are the identified 64 dust sources, as shown in Figure 1.**

239 **3.2 Source intensity from UNCCD G-SDS-SBM**

240 Figure 2 presents the G-SDS-SBM source intensity values (maximum and minimum) for the north HLD region. The north  
 241 HLD region includes the area north of latitude 50°N and the Arctic region (as a subregion of the HLD region) north of 60°N.  
 242 HLD dust sources show extreme seasonal characteristics, with some exceptions. The sources appear and disappear (or change  
 243 SI values) seasonally or appear (or increase source intensity values) only during favorable extreme weather conditions. Figure  
 244 3 shows G-SDS-SBM source intensity values for the south HLD region (south of 40°S) without values for Antarctica since G-  
 245 SDS-SBM does not include areas south of 60°S. Supplementary Tables S4 and S5 give the values of SI for specific locations  
 246 marked in Figure 1. Further analysis consists of assessing the areal coverage of sources, with different thresholds for SI values  
 247 in absolute values (km<sup>2</sup>) and the percentage they occupy concerning the total land surface area in the defined HLD regions.



249  
250  
251  
252 **Figure 2. UNCCD Global Sand and Dust Storms Source Base Map (G-SDS-SBM) for annual maximum (upper panel) and**  
253 **minimum (lower panel) source intensity for the north HLD region and Arctic sub-region (north of 50°N and 60°N, respectively,**  
254 **marked with dashed lines).**  
255  
256



257  
258  
259 **Figure 3. UNCCD Global Sand and Dust Storms Source Base Map (G-SDS-SBM) for annual maximum (upper panel) and**  
260 **minimum (lower panel) source intensity for the south HLD region (south of 40°S) without Antarctica (south of 60°S), marked with**  
261 **dashed lines.**  
262  
263

264 The total surface area of dust sources with a higher potential for dust emission ( $SI \geq 0.5$ ) over the north HLD region (north of  
265 50°N) is 3.9% of the total land surface (1 364 799 km<sup>2</sup>). The area with a very high potential for dust emission ( $SI \geq 0.7$ ) is 1.5%  
266 (509 965 km<sup>2</sup>). The area with the highest dust emission potential ( $SI \geq 0.9$ ) is 0.7% of the total land area (233 336 km<sup>2</sup>) (Table

267 2). In the Arctic region (north of 60°N)—the subregion of the north HLD area—dust sources with a higher potential for dust  
 268 emission ( $SI \geq 0.5$ ) are 5.5% of the total land surface (1 035 059 km<sup>2</sup>). The area with a very high potential for dust emission  
 269 ( $SI \geq 0.7$ ) is 2.3% (440 804 km<sup>2</sup>). The area with the highest dust emission potential ( $SI \geq 0.9$ ) is 1.1% (208 701 km<sup>2</sup>). The surface  
 270 of dust-productive areas with minimum seasonal SI values in the north HLD region is about three orders of magnitude smaller  
 271 than the maximum, meaning the north HLD dust sources highly depend on weather conditions. Maximum surfaces contain  
 272 dust-productive regions that are defined under the most favorable weather conditions for soil exposure to wind erosion  
 273 (including extreme weather). All sources defined here are not necessarily active every year nor in the same period, meaning  
 274 these surfaces can seasonally or occasionally (under severe weather) appear as dust sources.

275

276 For the south HLD region (40°S–60°S, area without Antarctica), the land surface is only 2% of the total surface area (Table  
 277 3). The surface area of dust sources with  $SI \geq 0.5$  is 22.6% of the total land surface (309 520 km<sup>2</sup>). The area with  $SI \geq 0.7$  is 4.5%  
 278 (61 527 km<sup>2</sup>). The area with the highest dust emission potential ( $SI \geq 0.9$ ) is 0.6% (8 630 km<sup>2</sup>). The surface areas for minimum  
 279 SI values above these thresholds are two to three times smaller than the surfaces for maximum SI values compared to the  
 280 difference in the north HLD region. This means that soil surface conditions in the south HLD region are favorable for dust  
 281 emission over the whole year. Especially in locations of HLD markers, SI maximum and minimum values do not change over  
 282 most locations or decrease by 0.1 or 0.2, except for one location (no. 38), which has SI values changing from 0.9 to 0 at the  
 283 location of an HLD marker.

284

285

286 **Table 2. Relevant surfaces for the north HLD and Arctic regions: surface of total area of the region, surface of land area within**  
 287 **the region (in km<sup>2</sup> and % of total surface), total surface (in km<sup>2</sup> and % of land surface) of areas with SI values above thresholds**  
 288 **(0.5 for surfaces with at least “higher” dust emission potential, 0.7 for surfaces with at least “high” dust emission potential, and 0.9**  
 289 **for surfaces with “highest” dust emission potential) in maximum (max) and minimum (min) seasonal values; values are derived**  
 290 **from UNCCD G-SDS-SBM.**

291

<b>NORTH HLD REGION (NORTH OF 50°N)</b>				
	<b>total area (km<sup>2</sup>)</b>	<b>land area (km<sup>2</sup>)</b>		<b>land area (%)</b>
	64392015	34695710		54
	<b>max</b>		<b>min</b>	
	<b>surface area (km<sup>2</sup>)</b>	<b>surface area (%)</b>	<b>surface area (km<sup>2</sup>)</b>	<b>surface area (%)</b>
SI ≥ 0.5	1364799	3.9	1916	0.006
SI ≥ 0.6	803372	2.3	1053	0.003
SI ≥ 0.7	509965	1.5	718	0.002
SI ≥ 0.8	342913	1.0	562	0.002
SI ≥ 0.9	233336	0.7	451	0.001

---

**ARCTIC REGION (NORTH OF 60°N)**

---

	<b>total area (km<sup>2</sup>)</b>	<b>land area (km<sup>2</sup>)</b>	<b>land area (%)</b>	
	36876709	18853826	51	
	<b>max</b>		<b>min</b>	
	<b>surface area (km<sup>2</sup>)</b>	<b>surface area (%)</b>	<b>surface area (km<sup>2</sup>)</b>	<b>surface area (%)</b>
SI ≥ 0.5	1035059	5.5	515	0.003
SI ≥ 0.6	665082	3.5	350	0.002
SI ≥ 0.7	440804	2.3	297	0.002
SI ≥ 0.8	303521	1.6	264	0.001
SI ≥ 0.9	208701	1.1	217	0.001

292  
293  
294  
295  
296 **Table 3. Relevant surfaces for the south HLD region: surface of total area of the region, surface of land area within the region (in**  
297 **km<sup>2</sup> and % of total surface), total surface (in km<sup>2</sup> and % of land surface) of areas with SI values above thresholds (0.5 for surfaces**  
298 **with at least “higher” dust emission potential, 0.7 for surfaces with at least “high” dust emission potential, and 0.9 for surfaces**  
299 **with “highest” dust emission potential) in maximum (max) and minimum (min) seasonal values; values are derived from UNCCD**  
300 **G-SDS-SBM.**  
301

---

**SOUTH HLD REGION (SOUTH OF 40°S)**

---

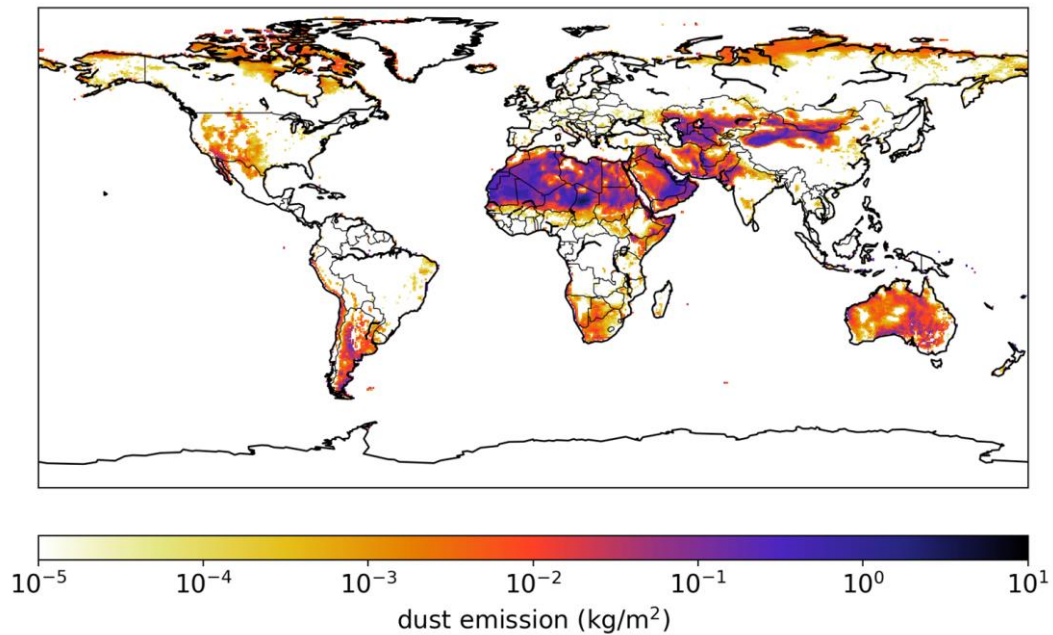
	<b>total area (km<sup>2</sup>)</b>	<b>land area (km<sup>2</sup>)</b>	<b>land area (%)</b>	
	61435208	1367987	2	
	<b>max</b>		<b>min</b>	
	<b>surface area (km<sup>2</sup>)</b>	<b>surface area (%)</b>	<b>surface area (km<sup>2</sup>)</b>	<b>surface area (%)</b>
SI ≥ 0.5	309520	22.6	186266	13.616
SI ≥ 0.6	151480	11.1	81522	5.959
SI ≥ 0.7	61527	4.5	29256	2.139
SI ≥ 0.8	25416	1.9	10842	0.793
SI ≥ 0.9	8630	0.6	2747	0.201

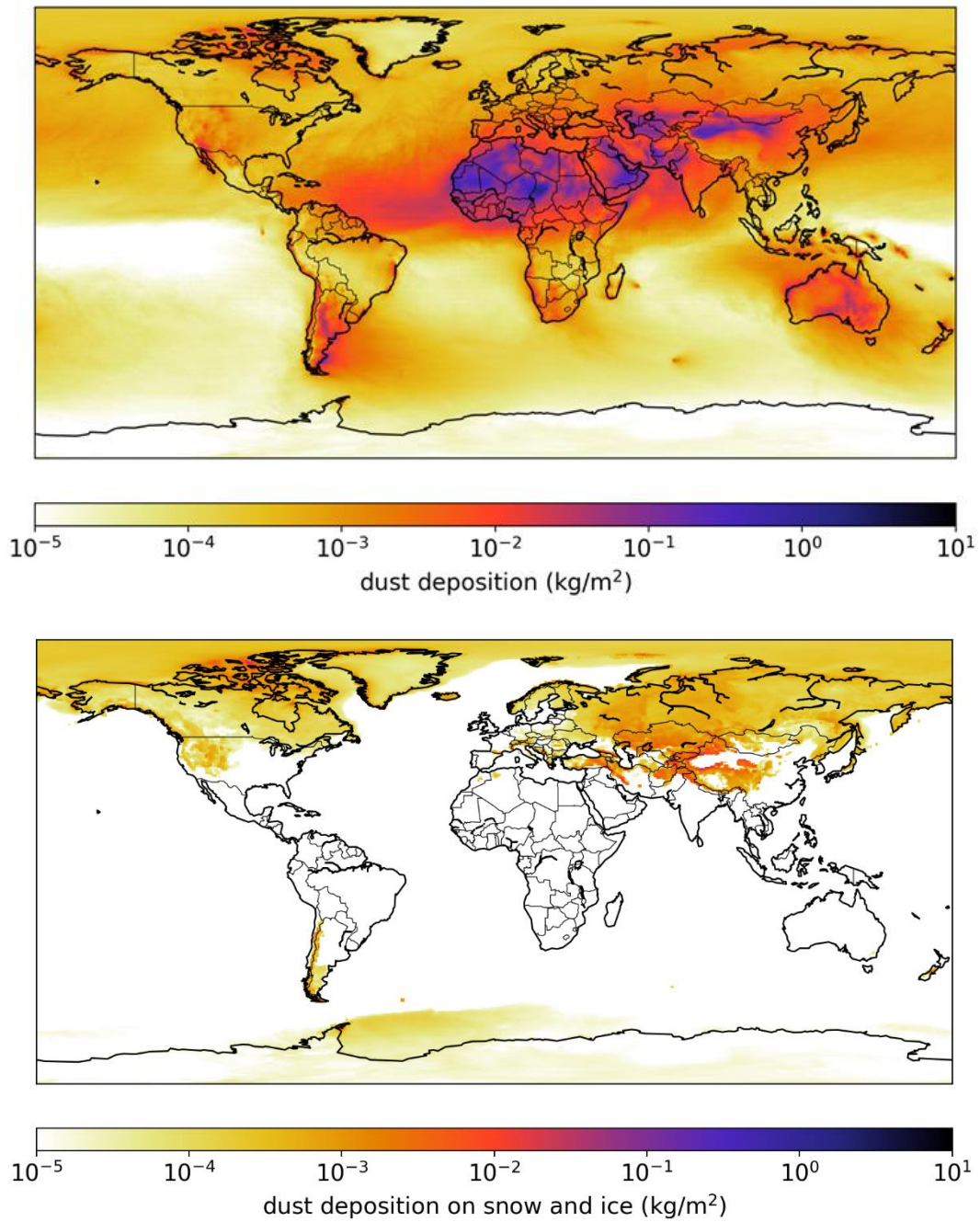
302  
303  
304 **3.3 Emission and deposition of global and Arctic dust**

305 The SILAM model estimated the total emission of annual dust and its deposition (data for 2017) onto snow-covered land,  
306 frozen sea, and total sea surfaces (frozen and non-frozen) (Fig. 4). The computations were also performed for Arctic dust and  
307 total global dust, with results for overall dust (diameter less than 30 μm) and fine dust (diameter less than 2.5 μm) separately  
308 (Fig. 15 of Section 3.5). Based on the model, the total emission of Arctic dust equals approximately 1.0% of the globe’s total

309 dust emission. The deposition of Arctic dust onto snow- and ice-covered surfaces equals about 19% of the total dust deposition  
310 onto these areas and around 57% of the deposition onto the areas explicitly located in the Arctic region. For fine dust, the  
311 corresponding figures are 7% and 22%. Compared to the deposition of black carbon (anthropogenic sources and wildfires  
312 combined; Fig. 15 of Section 3.5) onto snow and ice, the deposition of fine Arctic dust is about 70% higher globally and around  
313 580% higher in the Arctic regions. While these figures provide a general quantification of the deposited amounts, detailed  
314 calculations of the thermal and optical properties of dust and black carbon deposited on snow would be required to compare  
315 the deposited substances' net impacts on the climate.

316





317

318 **Figure 4. SILAM emission and deposition modeling results of dust emission (above), dust deposition (middle) and dust deposition**  
 319 **on snow and ice (below), in  $[\text{kg/m}^2]$ .**

320

### 321 **3.4 The identified dust sources**

322 Observations of the identified sixty-four dust sources in our collection (Fig. 1) are presented and discussed in alphabetical  
323 order as follows: 1. Alaska (sources no. 14 and 50 in Fig. 1); 2. Antarctica (no. 9, 19, 20, 52); 3. Canada (no. 2, 16, 48, 62); 4.  
324 Denmark and Sweden (no. 1, 15, 51); 5. Greenland (no. 53–61, 64); 6. Iceland (no. 23–45); 7. Russia (no. 2–11); 8. South  
325 America and Patagonia (no. 17, 21, 46, 47, 49, 52, 63); and 9. Svalbard (no. 13, 18, 22). Dust events originating simultaneously  
326 from Greenland, Iceland, and northern America are demonstrated in the Supplementary animation. The numbers are the  
327 identified 64 dust sources shown in Figure 1. Additional information, including latitude, longitude, and SI values, can be found  
328 in Supplement (Tables S1-S4).

#### 329 **3.4.1 Alaska, Copper River Valley, USA**

330 Alaskan dust sources were identified over a century ago (Tarr and Martin, 1913). However, limited satellite detection due to  
331 abundant cloud cover and isolated location resulted in sparse information on this region (Crusius et al., 2011). The main  
332 identified sources are piedmont glaciers (Malaspina, Bering), resuspension of ash from past eruptions (Hadley et al., 2004),  
333 and major rivers carrying glacial sediment (Copper, Yukon, Tanana, and Alsek) (Gassó, 2020a,b; 2021a,b). Resuspension of  
334 glacial dust transported by these rivers can be abundant, often triggering air quality alerts by the Alaska Department of  
335 Environment (USGCRP, 2018). The largest and most active of such dust sources is the Copper River (Fig. 5), estimated to  
336 transport 69 million tons of suspended sediment annually (Brabets, 1997). Transported sediment is deposited on the Copper  
337 River Delta, an alluvial floodplain covering an area of 2800 km<sup>2</sup>. When conditions allow, sediment is resuspended, resulting  
338 in dust plumes that can extend hundreds of kilometers over the Gulf of Alaska. Dust events, often lasting several days or weeks  
339 (Schroth et al., 2017), are most common in late summer and autumn when the river discharge and snow cover are at their  
340 minimum and high wind speeds are commonplace (Crusius, 2021). However, these occurrences have been observed year-  
341 round (Gassó, 2021a; January 2021). Dust reaches the open waters beyond the continental shelf and the influence of coastal  
342 sediments (Crusius et al., 2017). Thus, it has been proposed that dust from coastal sources such as the Copper River Delta can  
343 be an important source of bioavailable iron in the Gulf of Alaska (Crusius et al., 2011; Crusius, 2021; Schroth et al., 2017).  
344 Further work is also needed to investigate the relative importance of dust emissions from Alaska and East Asia (Bishop et al.,  
345 2002) in other areas. Also, dust from this region may initiate ice production in supercooled clouds, which is crucial for climate  
346 feedback (Murray et al., 2021). Regarding the magnitude and seasonal variability of emissions of sources in southern Alaska,  
347 a few dedicated studies have focused on dust from the Copper River Delta (Crusius, et al., 2017; Schroth et al., 2017; Crusius,  
348 2021). However, to our knowledge, no dust activity and source characterization has been carried out along the coast of the  
349 Gulf of Alaska. Moreover, resuspended road dust is a major air quality issue throughout Alaska.

350



351

352



353

354

355 **Figure 5. Satellite image (left) of the Copper River region and photo (right) taken at the Copper River Delta on the same day (14th**  
356 **October 2019). The common occurrence of clouds prevents directly viewing the dust in suspension, illustrating the difficulty of**  
357 **observing dust activity from space. (Satellite image from NASA Worldview; photo by Sarah Barr).**

358

### 359 **3.4.2 Antarctica**

#### 360 **3.4.2.1 James Ross Island, Ulu Peninsula**

361 The northern part of James Ross Island—Ulu Peninsula—represents one of Antarctica’s largest ice-free areas (312 km<sup>2</sup>). Its  
362 bare surface, consisting mainly of weathered sedimentary rocks, is an active HLD source (Kavan et al., 2018). Suspended  
363 sediments originate from outside the local fluvial systems based on the elemental ratios of Sr/Ca and Rb/Sr (Kavan et al.,  
364 2017). The wind speed threshold of 10 ms<sup>-1</sup> is needed for activating local dust sources, with most of the particles captured (by  
365 mass) in size bins between 2.5–10 μm. Mean (median) mass concentrations of the PM<sub>10</sub> were 6.4 ± 1.4 (3.9 ± 1) μg m<sup>-3</sup>, while  
366 the PM<sub>2.5</sub> was 3.1 ± 1 (2.3 ± 0.9) μg m<sup>-3</sup> for the whole measurement period from January to March 2018. Mean PM<sub>10</sub> values  
367 are comparable to background stations in Northern Europe. The highest daily aerosol concentration was 57 μg m<sup>-3</sup> for PM<sub>10</sub>,  
368 with hourly PM<sub>10</sub> with > 100 μg m<sup>-3</sup>. Higher aerosol concentration occurs in late austral summer when the soil water content  
369 in the upper soil layer is significantly lower than in early summer. Long-range transport of dust originating in Patagonia was  
370 observed during aerosol measurements (Kavan et al., 2018). A higher proportion of long-range transported dust was found in  
371 snow pits on higher elevated glaciers compared to a higher proportion of locally transported dust in lower elevated glaciers  
372 (Kavan et al., 2020b). Kňázková et al. (2020) identified a redistribution of mineral material within the HLD source area in  
373 Abernethy Flats, impacting the local microtopography.



### 374 **3.4.2.2 Marambio, Antarctic Peninsula**

375 The Marambio Base (64°14'S, 56°37'W, 198 m a.s.l.) on Marambio Island, Graham Land, Antarctic Peninsula, is a member  
376 of the Global Atmosphere Watch (GAW) programme of the WMO, with personnel available year-round. This region has ice-  
377 free areas and cold desert soils (Cryosols) that can be seasonally susceptible to wind erosion and weathering. The removal of  
378 fine materials occurs mainly by wind action. The Finnish-Argentinian co-operative research in Marambio includes  
379 measurements of ozone, solar irradiance, aerosols, and ultraviolet (UV) albedo (Aun et al., 2020). The UV Biometer Model  
380 501 from Solar Light Co. (SL501) UV albedo data of 2013–2017 in Marambio were used to analyze the effects of local HLD  
381 on measured snow UV albedo and solar UV irradiance and differences in simulated UV irradiances (Meinander et al., 2018;  
382 data not presented here). For validating the UV albedo data, surface photos were taken regularly. The surface photos and UV  
383 albedo measurements show that local dust can be detected on the snow and ice. Also, the optical dome of the SL-501 sensor  
384 was found to be sandblasted by the windblown dust when returning to Finland for maintenance. These findings suggest that in  
385 Marambio, local dust can decrease surface snow/ice albedo, possibly enhance the cryosphere melt, and contribute to warming  
386 in the Antarctic Peninsula due to the ice-albedo feedback mechanism.

### 387 **3.4.2.3 McMurdo Sound, Antarctica**

388 The McMurdo Sound area of the Ross Sea region is widely recognized as the dustiest place in Antarctica, where locally sourced  
389 aeolian accumulation is up to two to three orders of magnitude above global background and dust fallout rates for the continent  
390 (Chewings et al., 2014; Winton et al., 2014). The area includes the McMurdo Dry Valleys (MDV), the largest ice-free area (4  
391 800 km<sup>2</sup>) in Antarctica. The MDV has high but extremely variable fluxes of locally derived aeolian sand (e.g., Speirs et al.,  
392 2008; Lancaster et al., 2010; Gillies et al., 2013; Diaz et al., 2020) and common aeolian landforms. Such has led to the  
393 assumption that the MDV is a significant regional dust source (e.g., Bullard, 2016). Some modeling studies suggest the MDV  
394 could supply large volumes of dust to a wide area of the Southern Ocean (e.g., Bhattachan et al., 2015). However, field-based  
395 observations show that very little sediment is transported out of the MDV (Ayling and McGowan, 2006; Atkins and Dunbar,  
396 2009; Chewings et al., 2014; Murray et al., 2013) because the valleys have already been extensively winnowed into a well-  
397 developed deflation surface and large coastal piedmont glaciers form a topographic barrier, preventing aeolian sediment from  
398 escaping. The dominant source of aeolian sediment in the McMurdo Sound area is the debris-covered surface of the McMurdo  
399 Ice Shelf (1500 km<sup>2</sup>), with minor contributions from local ice-free headlands. This ice shelf is unusual because it has high  
400 surface ablation and a continuously replenishing supply of fine-grained sediment advected from the seafloor. The sediment is  
401 blown off the ice shelf by frequent intense southerly wind events, forming a visible sediment plume onto coastal sea ice. Within  
402 a few km of the ice shelf, accumulation rates on sea ice are up to 55g m<sup>-2</sup>yr<sup>-1</sup>, reducing rapidly downwind to an average of  
403 1.14 g m<sup>-2</sup> yr<sup>-1</sup>, equating to 0.6 kt yr<sup>-1</sup> of aeolian sediment entering McMurdo Sound annually (Atkins and Dunbar, 2009;  
404 Chewings et al., 2014). Some sediment is transported at least 120 km from the source and could travel much farther,  
405 contributing iron-rich dust to the Ross Sea (Winton et al., 2014). Coastal areas and lowland parts of the MDV are on the

406 threshold of climatically driven change with observed increases in ablation and seasonal meltwater flow incising into  
407 permafrost (Fountain et al., 2014), suggesting the dust potential of McMurdo Sound and MDV could rapidly change. The  
408 McMurdo Dry Valleys (4800 km<sup>2</sup>) is estimated to best fit Category 3 (source with unknown activity, Table S1). The McMurdo  
409 Ice Shelf ‘debris bands’ are estimated to best fit Category 2 (moderately active source).

#### 410 **3.4.2.4 Schirmacher Oasis, East Antarctica**

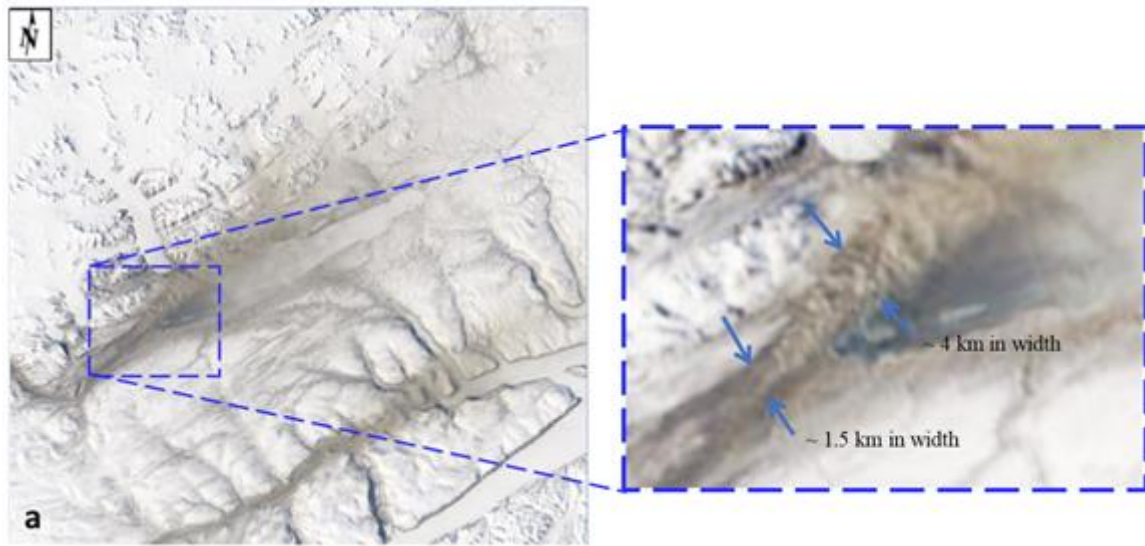
411 The Schirmacher Oasis (70° 45′ 30″ S, 11° 38′ 40″ E) is approximately 80 km from the coast of Lazarev Sea, Queen Maud  
412 Land, East Antarctica. The oasis is an ice-free area of over 35 km<sup>2</sup> with typically hilly relief. The oasis and surrounding  
413 area have been explored since the early 1960s. However, no systematic studies of dust on local ice and snow have been done.  
414 Most of this region’s dust is assumed to be formed with the soils blown in the air because of strong winds. Human activity  
415 produces some of the dust in this region: The oasis shelters four bases, which use diesel oil and petrol to supply heat and  
416 transport operations. Two airports are nearby, which operate during the summer—lasting from late November to late February.  
417 In December 2019, we collected the snow samples on eleven sites near the local ice roads, bases, and airports. These data will  
418 contribute to our future study.

#### 419 **3.4.3 Canada**

##### 420 **3.4.3.1 Lake Hazen, Ellesmere Island**

421 Evidence of dust activity in Canada has been reported, e.g., in the prairie, crater lake, and river valley environments (e.g.,  
422 Wheaton et al., 1990; Neuman, 1990; Wheaton, 1992; Hugenholz and Wolfe, 2010; Fox et al., 2012). Satellite observations  
423 of high-latitude dust events over water are relatively common (see, for example, Bullard et al., 2016). Whether directly  
424 concerning explicit plume remote sensing or indirectly regarding plume deposition, the detection of such events has remained  
425 largely unreported. Ranjbar et al. (2021) recently reported detecting a drainage-flow induced dust plume over (frozen) Lake  
426 Hazen, Nunavut, Canada, using a variety of remote sensing techniques (Lake Hazen is the Arctic’s largest lake, by volume, at  
427 81.8°N latitude in the northernmost portion of Ellesmere Island). Figure 6 shows a true-color georeferenced RGB MODIS-  
428 Terra image acquired on 19 May 2014 at 19:50 UT (15:50 EDT) over Lake Hazen. The authors employed MISR stereoscopy,  
429 CALIOP, and CloudSat vertical profiling, as well as MODIS thermal IR techniques, to identify and characterize the plume as  
430 it crossed over a complex springtime terrain of snow, ice, and embedded dust. While limited by the lack of dedicated dust  
431 remote sensing algorithms over snow and ice terrain, the plume characterization boded well for developing systematic,  
432 satellite-based, high-latitude dust detection approaches using current and future generations of aerosol and cloud remote  
433 sensing platforms.

434



435

436 **Figure 6. MODIS-Terra satellite image on 19 May 2014 at 19:50 UTC (a) True-color image: MODIS channels 1 (620–670nm), 3**  
 437 **(459–479 nm), and 4 (545–565 nm) were loaded into the RGB channels of the display. The sub-image is a zoom of the most discernible**  
 438 **part of the plume (outlined by the blue broken-line square).**

### 439 **3.4.3.2 Kluane Lake, Yukon**

440

441 Within the St. Elias Mountain range at the north end of the Pacific Coast Range on the continental side of the Yukon Territory  
 442 lies the Kluane Lake region (KLR), which contains Lhù'ààn Mân' (Kluane Lake) (no. 50 in Fig. 1). The lake is fed primarily  
 443 from the meltwater of the Kaskawulsh glacier down the A'äy Chù (formally the Slims River) and snowmelt from the  
 444 surrounding regions in the springtime. This seasonal discharge has, in recent history, been known to be highly variable as the  
 445 glacier terminates at the fork of two distinct watersheds—one draining into the Bering Strait through the Yukon River and the  
 446 other into the Gulf of Alaska—supplying the two watersheds' inconstant ratios. In 2016, most of the glacier's discharge was  
 447 diverted to the Gulf of Alaska in an intense discharge event, dramatically decreasing the Lhù'ààn Mân's water levels and  
 448 increasing the dust emission potential from the A'äy Chù (Shugar et al., 2017). This drastic change makes the KLR an excellent  
 449 natural laboratory for investigating the impact of pro-glacial hydrology on dust emission potential under past and future  
 450 climates. Research was conducted in the early 1970s in this same valley as a comprehensive set of dust flux measurements as  
 451 part of several publications (Nickling, 1978; Nickling and Brazel, 1985). Nickling (1978) concluded that there is a dynamic  
 452 relationship between soil moisture (driven by precipitation and nighttime radiation insolation) and wind, resulting in periodicity  
 453 of dust emissions from the valley in all but the mornings throughout the snow-free seasons. Within a more recent study by  
 454 Bachelder et al. (2020), soil and aerosol samples were collected within the Ä'äy Chù delta, where air quality thresholds were  
 455 exceeded, indicating a negative impact on local air quality throughout May. Notably, daily particle size distributions of PM10

456 were very fine (mode of 3.25  $\mu\text{m}$ ) compared to those measured at more well-characterized, low-latitude dust sources.  
457 Moreover, mineralogy and elemental composition of ambient PM<sub>10</sub> were found to be enriched in trace elements (e.g., As and  
458 Pb) compared to dust deposition, bulk soil samples, and fine soil fractions ( $d < 53 \mu\text{m}$ ). Finally, through a comparison of the  
459 elemental composition of PM<sub>10</sub>, dust deposition, and fine and bulk soil fractions, as well as meteorological factors measured,  
460 Bachelder et al. (2020) propose that the primary mechanisms for dust emissions from the Ä'äy Chù are the rupture of clay  
461 coatings on particles and the release of resident fine particulate matter.

#### 462 **3.4.4 Denmark and Sweden**

463 In Denmark, large areas with severe wind erosion have been documented (Kuhlman, 1960). Published literature on the activity  
464 of dust sources in Denmark is rare; some documentation is only in Danish. On 23 April 2019, a dust plume from Denmark's  
465 west coast, with dust plumes from Sweden 12 km long Mellbystrand around the mouth of the Lagan River (no. 51 in Fig. 1);  
466 Poland could be observed in Meteosat-11 Dust RGB and Natural Colour images, 23 April 12:30 UTC. These dust plumes were  
467 observed to travel to the North Sea (Meteosat, 2019). The source in Denmark appears to be from Holmsland Dunes (no. 15 in  
468 Fig. 1). Other potential dust sources in Denmark include, e.g., the Råbjerg mile (no. 1 in Fig. 1), the largest moving dune in  
469 Northern Europe with an area of around 2 km<sup>2</sup> (Doody et al., 2014), located between Skagen and Frederikshavn. Råbjerg Mile  
470 moves at approximately 15 meters per year due to wind and has moved around 1.5 km further east in the last 110 years. The  
471 drifting sand is not considered to be transported very far. In general, dust storms in Denmark are considered small, and locally  
472 based dust storms can be expected when farmers prepare the arable soils in spring, creating dust in case of a very dry April  
473 month. In Tilviden, flying sand took over (after King Frederik II cut the oak trees for building ships in 1600). Also, a regional  
474 soil and sand event in Denmark, reportedly common in April, was recently documented between Mejrup and Holtebro on 6  
475 April 2021 (Television Midtvest, 2021; not identified in Fig. 1; coordinates are estimated as 56°23'N, 8°41'E). This location  
476 between Mejrup and Holtebro remains to be marked as a potential dust source for future observations. The event was observed  
477 over roadways in several parts of the region, reducing visibility due to a long period without rain and with strong winds for >  
478 24 hours, causing the soil to blow off the harrowed fields.

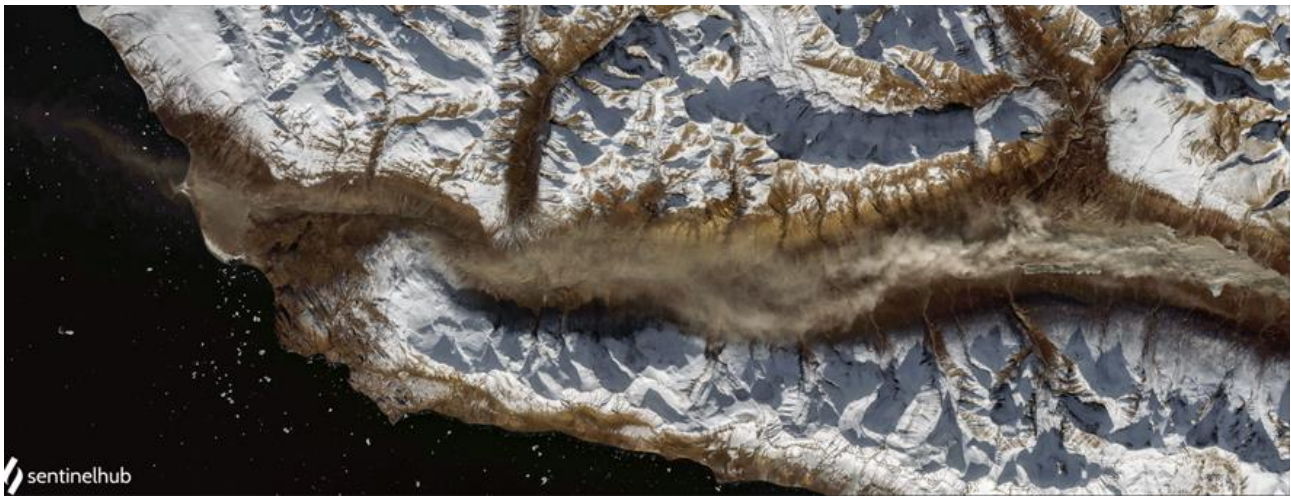
#### 479 **3.4.5 Greenland**

480 Greenland's ice-free areas have long been identified as locally important dust sources (Hobbs, 1942), with dust storms  
481 described as reaching >100 m high (Dijkmans and Törnqvist, 1991). These storms can cause the darkening of the Greenland  
482 Ice Sheet by deposition, which may affect albedo and rates of ice melt (Wientjes et al., 2011; McCutcheon et al., 2021).  
483 Potential dust source areas in Greenland are mapped in the recently issued global dust atlas by A. Vukovic (UNCCD, 2021).  
484 Dust input to soils and lakes may also have substantial ecological impacts (Anderson et al., 2017). Bullard and Mockford  
485 (2018) investigated the seasonal and decadal variability of dust emissions in southwest Greenland and presented the first long-  
486 term assessment of dust emissions. Dust emissions occur all year but peak in spring and early autumn. The evidence linking  
487 increased dust emissions to preceding jökulhlaup (a type of glacial outburst flood) events is inconclusive, requiring further

488 exploration. The decadal record confirmed that dust-storm magnitude may have increased from 1985 to the 1990s (Bullard  
489 and Mockford, 2018). Amino et al. (2020) also showed that dust deposition on the southeastern dome in Greenland has  
490 increased in recent decades. They link this increase to dust emissions in coastal Greenland, where snow cover is decreasing.  
491 However, further work is needed to characterize the magnitude of dust events at the source and how their emissions are  
492 changing. Bullard and Mockford (2018) also presented preferential dust-event pathways from Kangerlussuaq, indicating that  
493 most events travel toward the Davis Strait and the Labrador Sea, where the dust might impact boundary layer of mixed-phase  
494 clouds (Murray et al., 2021).

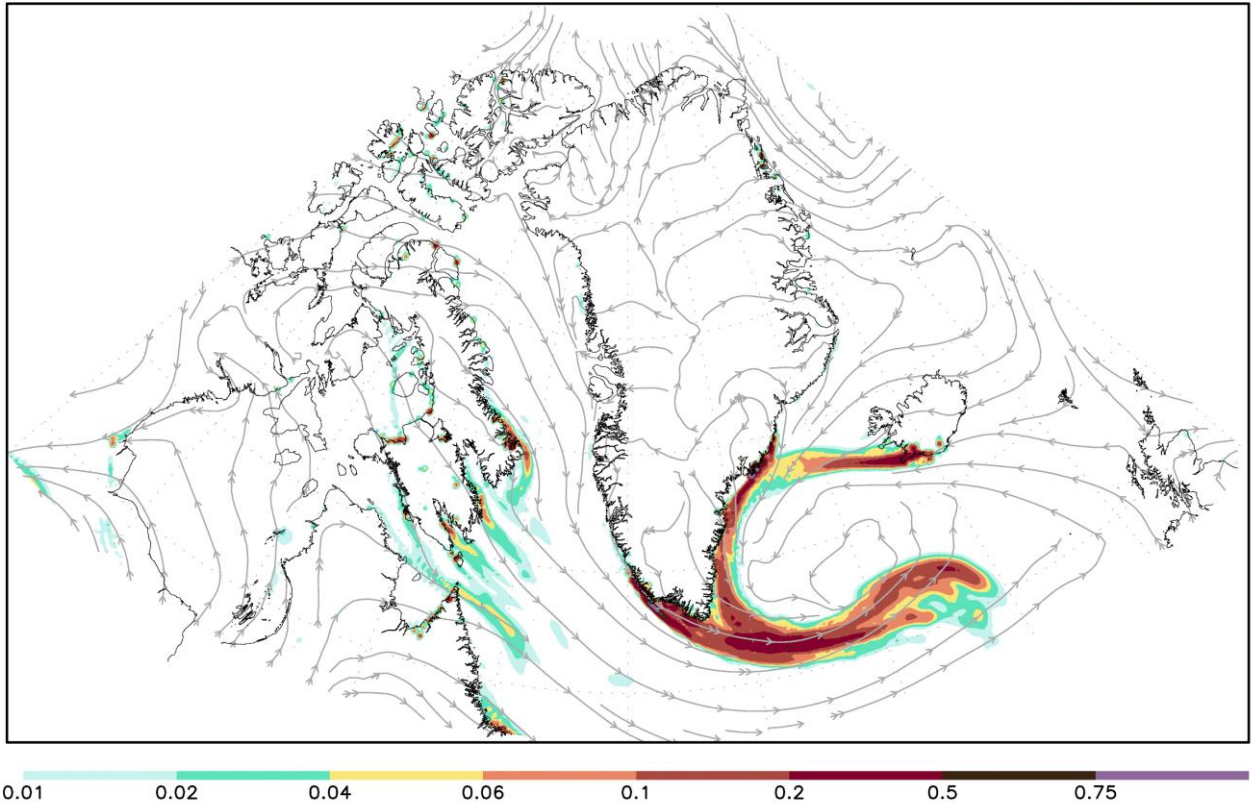
495 Modern satellite remote sensing methods can detect dust storm events in Greenland's different valleys and coastal areas. The  
496 new HLD sources identified in this study based on satellite observations are in Supplementary Table S3. Figure 7 illustrates  
497 one such dust storm episode on the Nuussuaq Peninsula, Greenland, on 1 October 2020 (Markuse, 2020). One example of  
498 DREAM regional-scale modeling of atmospheric transport of dust from Greenland potential dust sources is demonstrated in  
499 Figure 8 (animation available in Supplementary), where the DREAM circumpolar prediction experiment example shows the  
500 predicted surface dust concentration for 4 November 2013 and Icelandic volcanic desert dust to reach Greenland, as discussed,  
501 e.g., in Meinander et al. (2016).

502



503

504 **Figure 7. High-latitude dust storm on the Nuussuaq Peninsula, Greenland – 1 October 2020 (Markuse, 2020; cc-by-2.0.2020)**



505

506

Figure 8. DREAM model predicted dust load for 4 November 2013 (animation available in Supplementary).

507

508

### 3.4.6 Iceland

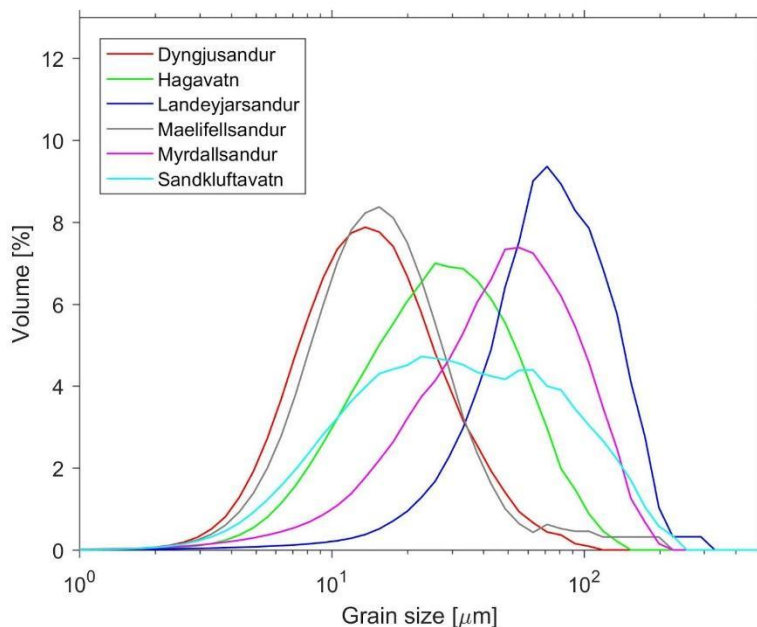
509

Iceland has been recognized for a while as a potentially important dust source. In our collection, 13 new sources in Iceland were included (Table S2), compared to previous sources, in which eight Icelandic dust hot spots were identified (Arnalds et al., 2016). Sandkluftavatn, Kleifarvatn, Skafta jökulhlaup deposits and other areas have also been found to produce large amounts of dust (Dagsson-Waldhauserová et al., 2019). In recent years, increased dust activity has been reported in Flosaskard and Vonaskard (Gunnarsson et al., 2020). These dust hotspots cover almost  $500 \text{ km}^2$ , while deserts are over  $45\,000 \text{ km}^2$  (Arnalds et al., 2016). Most of the dust hotspots are near glaciers: glacial floodplains, old lakes, jökulhlaup (a type of glacial outburst flood) deposit areas, or sandy beaches. Glacio-fluvial plains receive a massive amount of unconsolidated silty material during the melting of nearby glacial regions.

516



517 New dust sources with the number of events are identified here and presented based on satellite image observations from 2002  
518 to 2011 (Supplementary Table S2), suggesting that Iceland's entire southern coast could be considered one source. However,  
519 previous results on Icelandic dust suggest that nearby locations may have different particle characteristics (Fig. 9). Therefore,  
520 each source must be studied independently. For example, the grain size distribution curves of the samples from Dyngjúsandur,  
521 Hagavatn, Landeyjarsandur, Maelifellsandur, Myrdallsandur, and Sandklúftavatn showed generally unimodal distributions  
522 with a rather diverse character (average diameters ranging from 19.8 to 97.7  $\mu\text{m}$ , Fig. 9). Richards-Thomas et al. (2021)  
523 identified a range in particle diameter between 0.4  $\mu\text{m}$  and 89  $\mu\text{m}$ , with the medians ( $d_{50}$ ) of the distributions from 12 to 25  
524  $\mu\text{m}$ ). Some hotspot particles are bimodal with peaks at 2  $\mu\text{m}$  and 30  $\mu\text{m}$  and a more significant proportion of the sample within  
525 the silt-size range.



526

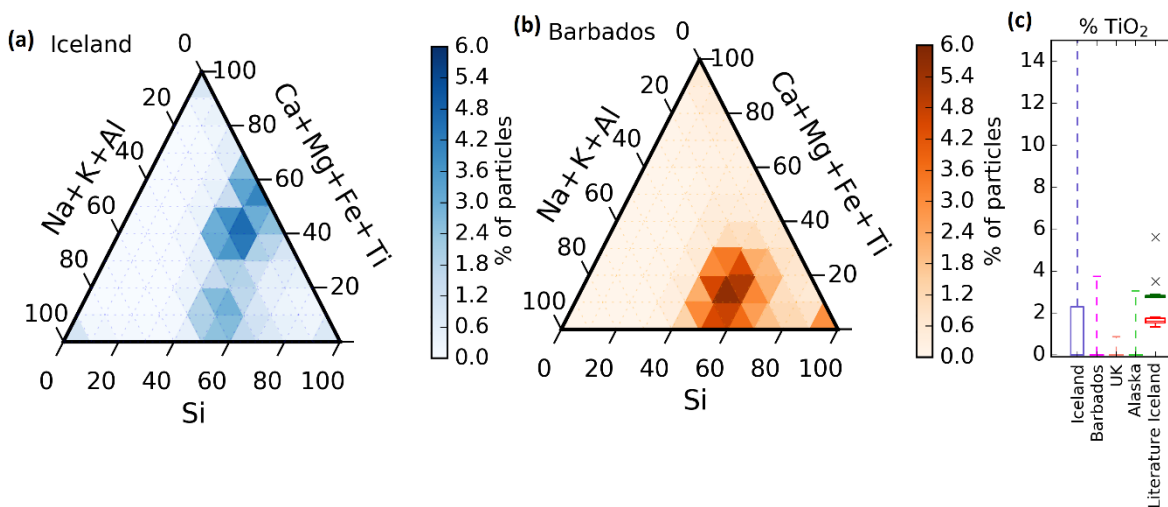
527 **Figure 9.** Grain size distributions of samples from Icelandic source areas (redrawn from Varga et al., 2021)

528 Icelandic dust particles have different shapes, lower densities, higher porosity, increased roughness, and darker colors than  
529 other desert dust (Butwin et al., 2020; Richards-Thomas et al., 2021). Those greater than 20  $\mu\text{m}$  retain the volcanic  
530 morphological properties of fresh volcanic ash. Dust and fresh volcanic ash particles less than 20  $\mu\text{m}$  are crystalline and blocky.  
531 Icelandic dust particles contain amorphous glass, large internal voids, and copious dustcoats comprised of nano-scale flakes.  
532 The amorphous basaltic material is mostly aluminosilicate glass ranging from 8 wt% (Hagavatn hotspot) to 60–90 wt%, with  
533 relatively high total Fe with higher Fe solubility and magnetite fraction than low-latitude dust (10–13 wt%, Baldo et al., 2020).  
534 PM10 concentrations measured during severe Icelandic dust storms well exceeded 7000  $\mu\text{g}\text{m}^{-3}$  (Dagsson-Waldhauserová et

535 al., 2014, 2015; Mockford et al., 2018). Submicron particles contribute with high proportions (> 50%) to PM10 mass  
536 concentrations and number concentrations (Dagsson-Waldhauserová et al., 2014, 2016, 2019). Aeolian transport of 11 t of  
537 dust over one meter transect was measured during the severe dust/ash storm in 2010, when grains > 2 mm were uplifted  
538 (Arnalds et al., 2013).

539 As well as differences in Icelandic dust sources, the chemical composition of the aircraft-collected Icelandic dust particles has  
540 a different chemical signature than, e.g., airborne Saharan dust particles transported to Barbados (Sanchez-Marroquin et al.,  
541 2020). This difference can be observed in Figs. 10a and 10b, where the chemical composition of most Icelandic dust particles  
542 falls in a different area of the chemical composition ternary diagram than the Saharan dust particles from Barbados. One of the  
543 most prominent differences between these types of dust is Ti's presence in ~ 30% of the Icelandic dust particles, while this  
544 element is almost absent in the Saharan dust particles and dust collected elsewhere, shown in Fig. 10c. Furthermore, the  
545 chemical composition of the aircraft-collected Icelandic dust is consistent with surface scooped samples of dust or volcanic  
546 ash from Iceland. Moreover, a droplet freezing-based assay confirmed that the sampled Icelandic dust has a high ice-nucleation  
547 ability and can influence the radiative and lifetime properties of clouds containing water and ice.

548



549

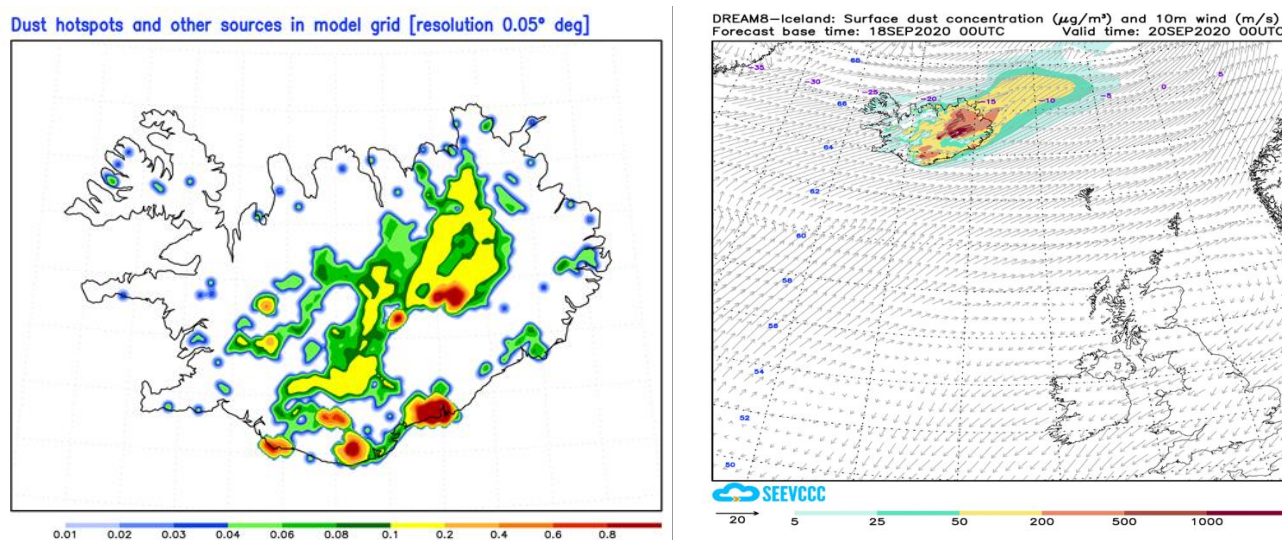
550 **Figure 10.** Ternary graphs of the chemical composition of Icelandic dust particles (a) and Saharan dust particles collected in  
551 Barbados (b). Each graph contains a heat map with the percentage of dust particles in each sample compositional bin. The chemical  
552 composition of each aerosol has been recalculated from the weight percentages given by the SEM software, excluding elements that  
553 are not Si, Al, Fe, Mg, Ca, Na, K, Ti, Mn, and P. (c) The box represents particles in the Q3 percentile of the percentage of the  
554 composition of Ti in all the dust particles in each sample (Icelandic dust, Saharan dust collected in Barbados, dust collected in the  
555 UK, and dust collected in Alaska). The whiskers represent the composition of all particles between the median plus and minus two



556 standard deviations. The data has been compared with the Ti weight percentage of different Icelandic dust and ash samples from  
557 the literature. (Figure extracted from the Supplementary Material of Sanchez-Marroquin, 2020).

558 No direct observations or measurements of the new sources were available. Instead, two model computations are presented for  
559 Iceland because of the lack of observations and complexity of the AOD interpretation in polar and subpolar regions. Without  
560 high uncertainty of direct measurements, the importance of the HLD modeling rises; models validated over better-observed  
561 regions may become an important or primary source of information. Results using the DREAM model, with a horizontal  
562 resolution of ~3.5 km, were used here to resolve the heterogeneous and small-scale character of the Icelandic dust sources  
563 (Fig. 11). As the first operational numerical HLD model, DREAM-ICELAND predicted the Icelandic dust for the example  
564 case of 18 September 2020 (Fig. 11).

565  
566



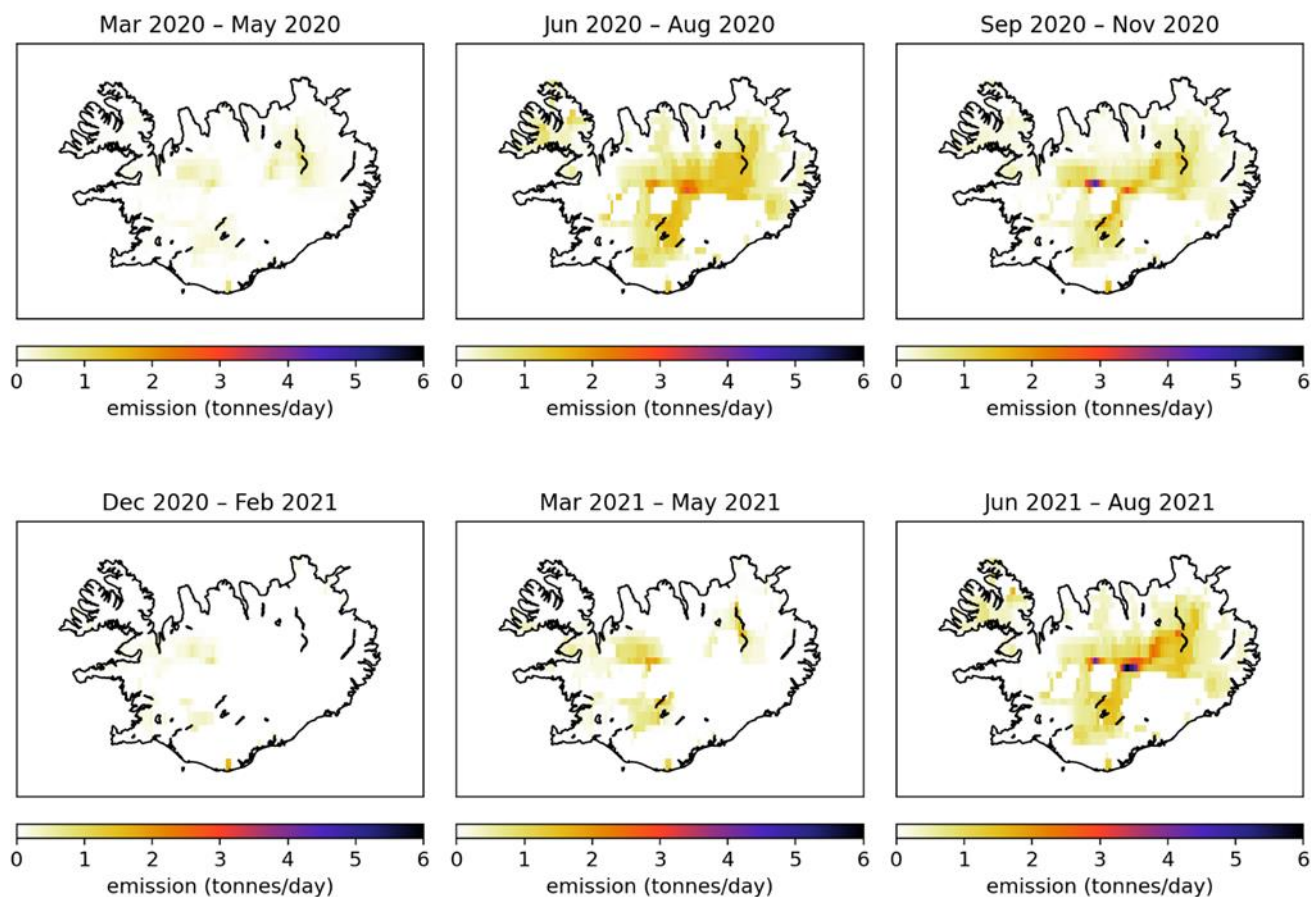
567

568 **Figure 11. Left panel: dust sources in DREAM-ICELAND model grid with areas vulnerable to erosion and containing hot spots**  
569 **(Arnalds et al., 2016). Right panel: An example of the operational Icelandic dust surface concentration forecast for 18 September**  
570 **2020 (available at the Republic Hydrometeorological Service of Serbia site, <http://www.seevccc.rs/?p=8>).**

571

572 In Figure 12, dust emissions in Iceland are presented in three-months periods for March 2020–August 2021. The modeled  
573 results clearly show the seasonal nature of the dust sources. The summer season (June–August) appears to be the strongest  
574 dust season. However, there are also dust emissions in wintertime with snow-covered land surfaces, according to observations  
575 of dust events during snowfall (e.g., Dagsson-Waldhauserová et al., 2015). The 2021 summer season in these modeled emission

576 results appears in the same locations as summer 2020 but with more severe emissions in the highlands in 2021, agreeing with  
577 the field observations in Vatnajökull national park during the HiLDA measurement campaign in the 2021 season  
578 (<https://gomera.geo.tu-darmstadt.de/wordpress/>), where the most severe dust events were measured.



579  
580 **Figure 12. SILAM modeled dust emissions (tonnes/day) in Iceland for three months periods in March 2020 – August**  
581 **2021.**

582  
583 **3.4.7 Russia**

584 The Russian Arctic and subarctic are the most relevant regions connected to the HLD sources. In these territories, atmospheric  
585 dust is produced due to burning gas (Novy Urengoy is named the gas capital of Russia) and forest fires (especially in Siberia;  
586 see MODIS or Sentinel images for Novy Urengoy on 3-8 August 2021), dusting of abandoned and non-reclaimed heaps).  
587 Wind erosion is followed by vegetation destruction from gas and oil extraction, especially in Western Siberia. Some Russian

588 sources included in our collection (e.g., no. 7 and 8 of Fig. 1) could be identified as dust sources on the periphery of HLD and  
 589 low-latitude source regions. Source no. 7 of Fig. 1 is the Altai Mountains. Some parts of these territories are covered by  
 590 permafrost, where winter lasts for 5–6 months. From October, in lower mountains (less than 1000 m a.s.l.), and from  
 591 September, in higher mountains (more than 1500 m a.s.l.), a stable snow cover persists. The mean daily air temperature during  
 592 winter within the lower, middle, and higher mountains is  $-21^{\circ}\text{C}$ ,  $-29^{\circ}\text{C}$ , and below  $-30^{\circ}\text{C}$ , respectively. Source no. 8 is in  
 593 Central Kazakhstan. From late December to early March, a stable snow cover from 5 cm to 30 cm occurs within plains and up  
 594 to 50 cm within hollows. Periods of snow cover and thaw correspond to transitions of the mean daily temperature of air through  
 595  $0^{\circ}\text{C}$ , which, on average, are the 7 November and 23 March plus/minus 10–12 days. From early January to late February, the  
 596 air's mean daily temperature can be as low as  $-20^{\circ}\text{C}$ . Soil Atlas of the Northern Circumpolar Region  
 597 (<https://esdac.jrc.ec.europa.eu/content/soilatlas-northern-circumpolar-region>) covers all land surfaces in Eurasia and North  
 598 America above the latitude of  $50^{\circ}\text{N}$ . Thus, these territories are considered high-latitude.

### 599 3.4.7.1 Western Siberia, Altai Mountains, and Central Kazakhstan

600 In the most widespread undisturbed soils (Gleysols, Phaeozems, Podzols, Retisols, and Stagnosols) in Western Siberia  
 601 (Semenkov et al., 2015a, 2015b)—the vastest plain in the world—mineralogical and elemental composition (Supplementary  
 602 Table S6) were studied using X-ray diffractometry, X-ray fluorescence spectrometry, ICP-MS, ICP-AES, and content of total  
 603 organic carbon (TOC), as reported in detail in (Semenkov et al., 2019; Semenkova and Koroleva, 2019; Semenkova and  
 604 Yakushev, 2019). At locations no.7 and no. 8 of Fig. 1 (Table 4), the concentration of N-containing substances, pH values,  
 605 dust content and dust deposition rate were measured in snow in winter from 2009 to 2019 (Koroleva et al., 2016, 2017;  
 606 Semenkova et al., 2021; Sharapova et al., 2020).

607 **Table 4. Major ions (mg/L), pH value, dust content ( $\text{mg}/\text{m}^2$  in snow), and deposition rate ( $\text{mg}/\text{m}^2/\text{d}$ ) during winter at HLD sources**  
 608 **no. 7 and no. 8 in Fig. 1.**

HLD no	M	SD	Me	Min	Max	N
No. 7						
Dust content $\text{mg}/\text{m}^2$	316	439	112	0	1542	30
$\text{NH}_4^+$ mg/L	0.75	0.98	0.30	0	3.60	43
$\text{NO}_2^-$ mg/L	0.015	0.019	0.008	0	0.08	107
$\text{NO}_3^-$ mg/L	2.3	3.4	1.4	0	20.4	118
pH	6.6	0.8	6.7	4.1	8.4	129

---

No. 8						
Dust deposition rate mg/m <sup>2</sup> /d	1.67	1.67	1.08	0.05	6.6	38
NH <sub>4</sub> <sup>+</sup> mg/L	0.20	0.009	0.10	0	1.34	682
NO <sub>2</sub> <sup>-</sup> mg/L	0.027	0.007	0	0	0.61	127
NO <sub>3</sub> <sup>-</sup> mg/L	0.47	0.02	0.19	0	3.93	697
pH	6.1	0.02	6.1	4.6	8.0	585

---

609 M – mean, max – maximum, Me – median, min – minimum, N – number of observations, SD – standard deviation

610

### 611 3.4.7.2 Murmansk region: Apatity, Kirovsk, Kovdor

612 Large amounts of displaced rock have been breaking the balance of geological emissions of gas and dust from mining, dumps,  
613 and tailing pits (e.g., Csavina, et al. 2012). Over 150 Mt of industrial wastes are disposed of in the Murmansk region annually,  
614 achieving about 8 Gt (Supplementary Table S7). The dusting of processing tailing is one of the main sources of air pollution  
615 resulting from suspended matters near the mining enterprises. About 30% of all suspended matter is released from the mining  
616 enterprises into the atmosphere due to wind-induced dusting of beaches and slopes of tailings dumps. Elevated concentrations  
617 of suspended matter are registered every summer in Apatity's atmosphere. Dust storms from technogenic dust sources of the  
618 mining industry on the Kola Peninsula are presented, e.g., in Baklanov and Rigina (1998), Baklanov et al., (2012), and Amosov  
619 and Baklanov (2015).

### 620 3.4.7.3 Tiksi

621 Aerosol characterization was performed at the Hydrometeorological Observatory (HMO) Tiksi (71.36N; 128.53E) on the coast  
622 of the Laptev Sea in Northern Siberia from 2014 to 2016 (Popovicheva et al., 2019). FTIR analyses of functionalities and ionic  
623 and elemental components provided insight into the dust source-influenced and season-dependent composition of East Siberian  
624 Arctic aerosols. Analysis of wind and aerosol pollutants roses, with long-range transport analysis, helped identify the dust  
625 sources at Tiksi, demonstrating impacts from lower latitudes or local emissions from the adjacent urban Tiksi area. In warm  
626 periods, Na<sup>+</sup>, Cl<sup>-</sup>, K<sup>+</sup>, and Mg<sup>2+</sup> are found to be the major ions in the sea-salt aerosols, which are ubiquitous in the marine  
627 boundary layer, significantly impacting the dust concentrations in the coastal region. However, Cl<sup>-</sup> and K<sup>+</sup> could also originate  
628 from biomass burning during the warm period. Ammonium is mainly produced by the soil and emission from biota and the  
629 ocean, commonly found in the form of (NH<sub>4</sub>)<sub>2</sub>SO<sub>4</sub> and NH<sub>4</sub>Cl. Like sulfates, ammonium is influenced by regional sources of

630 secondary aerosol formation and transport. Bands of carbonates  $\text{CO}_3^{2-}$  (at  $871\text{ cm}^{-1}$ ) and ammonium  $\text{NH}_4^+$  ( $3247\text{ cm}^{-1}$ ) indicate  
631 the dominance of dust carbonates in the natural inorganic aerosol. Also, S, Fe, Na, Al, Si, Ca, Cl, K, Ti, Mn, Co, Cu, Zn, Ga,  
632 Sr, Ba, Hg, and Pb were detected in the background dust, with sulfur displaying the highest concentration, followed by Fe, Na,  
633 and Al.

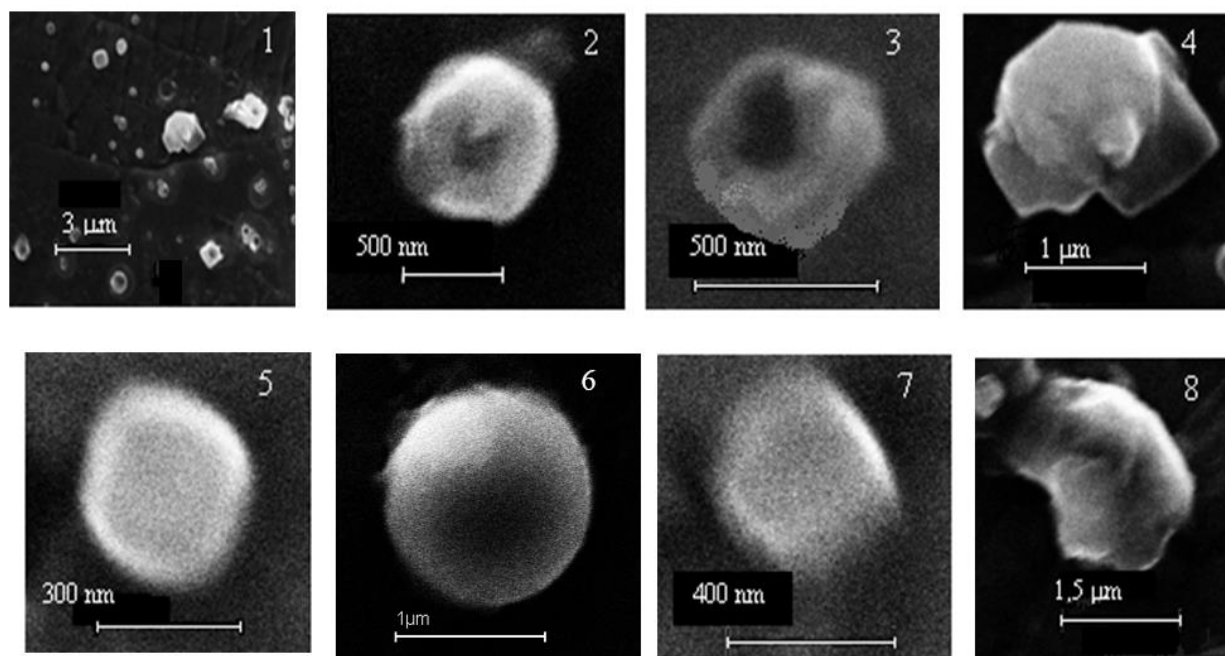
634 According to individual particle analyses by SEM-EDX, during the summer and autumn, when the wind comes from the  
635 southwest and air masses arrive from the ocean, aerosol particles demonstrate a large variability in shapes, sizes, and  
636 composition (Fig. 13.1). Elemental composition is characterized by a dominant weight percentage of C, K, Na, Cl, O, and Fe.  
637 The distribution of elements over particles is heterogeneous, with greater amounts of Cl, K, and Na than C and O in around  
638 50% of particles, indicating that background aerosols contain soil, salts, minerals, and carbonaceous compounds. Group Na-  
639 rich with dominant Na and Cl is the most abundant at 32.5%, originating from sea spray near the ocean (Fig. 13.2). The other  
640 particles contain small amounts of K, Ca, and Mg from seawater impurities, as well as S, gained through acid displacement.

641 The second most abundant group of individual particles is Group K-rich at 28.8%, dominated by K and Cl, which are not of  
642 marine origin because the concentration of NSS  $\text{K}^+$  ions significantly exceeds K's possible concentration in SSA. Instead,  
643 Group K-rich particles are of natural mineral sylvite (KCl), transformed from genuine ones because the average weight ratio  
644 of K/Cl was found to be equal to 3.3—significantly higher than 1.1—in sylvite (Fig. 13.3). KCl is water-soluble and may react  
645 in a polluted atmosphere. The variation of wt% of K vs. Cl shows the lack of Cl compared to genuine sylvite and the formation  
646 of complex chemical compounds  $\text{K}_x\text{Cl}_y$  with various K and Cl atoms. A representative micrograph of particles in Group K-  
647 rich demonstrates the reacted sylvite in Fig. 13.3, with slight damage by an electronic beam that can prove the presence of  
648 nitrates that were easily evaporated during EDX analyses. A part of Group Na-rich and K-rich, 20% and 5%, respectively,  
649 contains Na, Cl, and K and is assumed to be particles comprised of natural sylvite from alternative layers of halite and sylvite  
650 ( $n\text{NaCl} + m\text{KCl}$ ) (Fig. 13.4). They have distinctive mineral shapes and are stable regarding evaporation by an electron beam.  
651 About 14.8% of individual particles composed of Group Organic made almost exclusively from C and O. These particles are  
652 roughly spherical or liquid-like shaped (Fig. 13.5): Around half contain only C and O, being probably secondary organic  
653 aerosol from the biogenic source; the other half come from the seawater of the Arctic Ocean, as demonstrated by trace amounts  
654 of Na, Cl, and Mg. The oxidation of volatile organic compounds, humic-like substances (HULIS) in the marine environment,  
655 perhaps contributes to observed organic matter.

656 Finally, a few biogenic particles such as pollen, spore, algae, bacteria, and plant or insect remnants are found in natural aerosols,  
657 indicated by the specific shape and presence of K, S, Si, and Cl with C. The remaining groups—Fe-rich (14.4%), Ca-rich  
658 (6.4%), and Al, Si-rich (3%)—are representative of atmospheric dust derived from the Earth's crustal surface. Dust particles  
659 have solid irregular shapes of round and euhedral morphology. Analyses of the soil sample taken near the CAF showed stony  
660 material with minimal fertile ground cover. EDX analyses demonstrated 27.7 and 9.8 wt% of Si and Al, 46 and 10.6 wt% of  
661 O and Fe, respectively, and 3.5 w% of K in various Fe,K—aluminosilicates containing small additives (less than 1.7 wt%) of

662 Na and Mg. Since the tiny dust of stony soil may be easily dispersed into the atmosphere by wind, we assume that Group Al,  
663 which is Si-rich, and around half of Group Fe-rich, is composed of Fe,K—aluminosilicates (Fig. 13.6). Group Fe-rich  
664 containing Fe, Ni, Ca, and Si is composed of soil particles of iron-nickel ore (Fig. 13.7). Finally, Ca carbonates and sulfates  
665 with Ca, C, S, and O are found in Group Ca-rich (Fig. 13.8), according to the observation of  $\text{Ca}^{2+}$ ,  $\text{CO}_3^{2-}$ , and  $\text{SO}_4^{2-}$  ions  
666 described above. With aluminosilicates, they are most likely windblown dust.

667  
668



669

670 **Figure 13. 1. Panorama and representative micrographs of natural background aerosols at HMO Tiksi; 2. reacted sea salt NaCl in**  
671 **Group Na-rich; 3. reacted sylvite KCl and 4. sylvinites (nNaCl + mKCl) in Group K-rich; 5. an organic particle in Group Organic;**  
672 **6. Fe, Ca- aluminosilicate in Group Al, Si-rich; 7. Fe/Ni particle in Group Fe-rich and 8. CaCO<sub>3</sub> in Group Ca-rich of natural aerosols**  
673 **on 27.09.2014. New unpublished results of Popovicheva et al. (2019) investigation.**

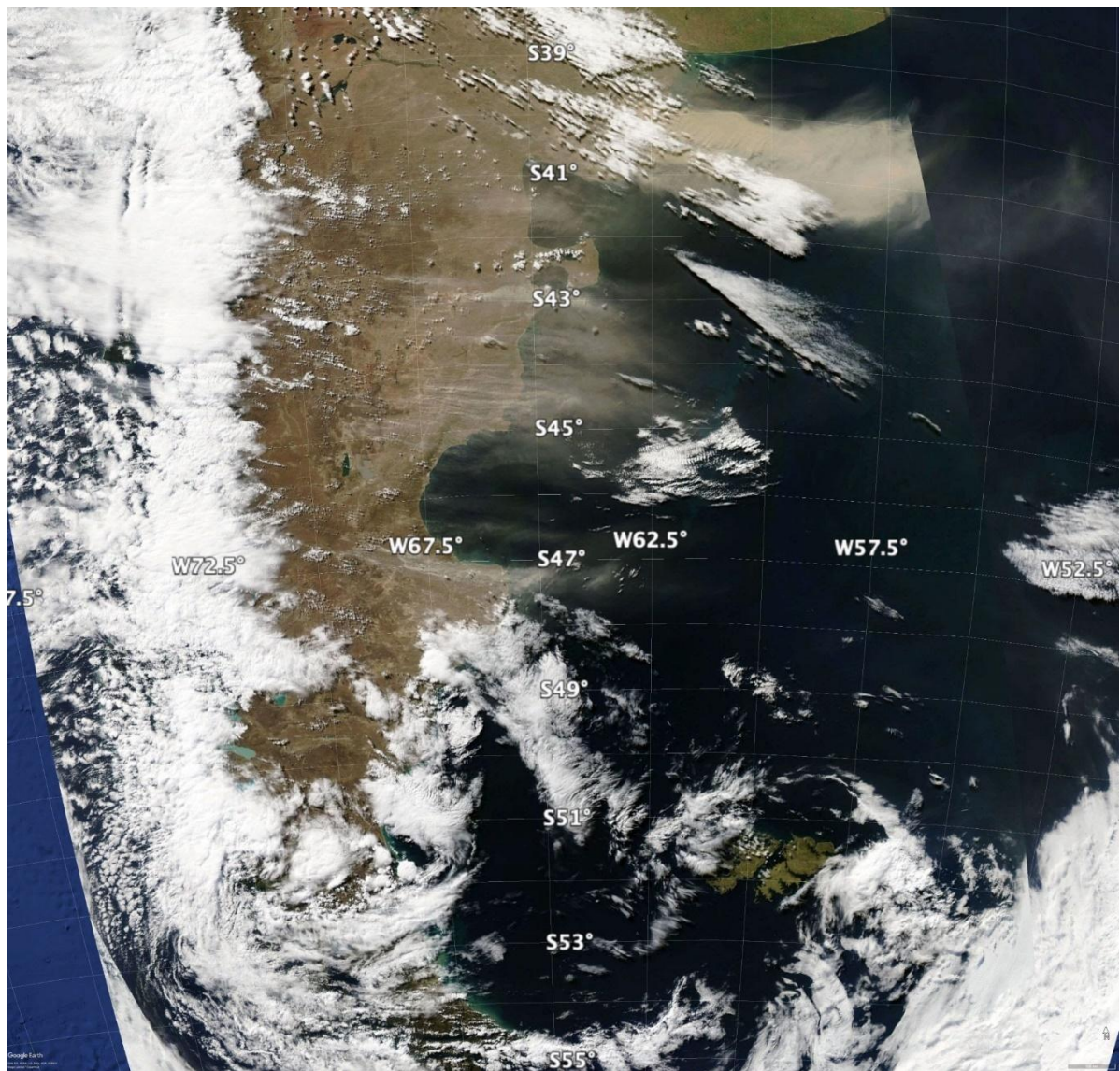
674

### 675 3.4.8 South America and Patagonia

676 Extending from 39°S to 54°S, with an area of 600 000 km<sup>2</sup>, dust activity (Fig. 14) from this large desert remains largely  
677 unknown. Some basic facts must be formally assessed, such as the location of sources and geomorphological features  
678 associated with dust, as well as the seasonality and frequency of the dust's activity. To date, limited surveys of dust activity

679 (Crespi-Abril et al., 2017; Gaiero et al., 2003; Gassó and Torres, 2019) and case studies of individual sources exist (Gassó et  
680 al., 2010; Gassó and Stein, 2007; Johnson et al., 2011). Recently, a list of dust activities and sources in Tierra del Fuego  
681 (Cosentino et al., 2020) has been published. Generally, dust sources in Patagonia are at topographic lows, and the river valleys  
682 (e.g., the Deseado and Santa Cruz rivers) (Coronato et al., 2017; Hernández et al., 2008) are associated with the late Holocene  
683 para-glacial environments. The most active modern source of dust is the drying of Colhué Huapi Lake (CHL) in Central  
684 Patagonia (45.5°S and 68°W) (Montes et al., 2017)—a shallow lake with variable water levels exposed to intense  
685 evapotranspiration. An anthropogenic component appears to be linked to intense farming, oil prospection, and supplying water  
686 to urban centers (Gaitán et al., 2009; Hernández et al., 2008; Mazzonia and Vazquez, 2009; Valle et al., 1998). CHL has been  
687 steadily shrinking (Llanos et al., 2016) and was dried up by the summer of 2020. Consequently, dust activity originating in  
688 CHL has increased with frequent blowouts large enough to be easily detected from space (Gassó and Torres, 2019).





689

690 **Figure 14. A dust event spanning the north and central sections of the Patagonian Desert (+1000 km) on March 28, 2009. Events this**  
691 **large occur about once every one to three years. This event is typical in that it was triggered by the passage of a powerful low-**  
692 **pressure center commonly found in these high latitudes. Also, this event is singular in that a large portion of it is cloudless, enabling**  
693 **a direct view from space (most dust activity in Patagonia occurs under cloudy conditions). The thick dust cloud in the upper right**  
694 **corner is from an area used for cattle farming, which was undergoing a drought, whereas the active sources further south can be**  
695 **considered more naturally occurring with less anthropogenic interference. Source: NASA’s Worldview interface image processed**  
696 **with Google Earth.**

697



698 Overall, satellite detection in the Patagonia region remains challenging. There are several difficulties in surveying dust activity  
699 in the area: obstructed views from space because of cloudiness, nighttime dust activity, and sparse population. Also, except  
700 for a few sources, the lack of recurrence in dust emission is a general feature of the desert: Sources that were active during one  
701 season do not reactivate until two or three seasons later. A comprehensive and dedicated survey combining surface and space-  
702 based detection networks is needed for a better understanding.

### 703 **3.4.9 Svalbard**

704 Evidence of the presence and activity of dust sources in Svalbard is only recent and quite rare. Yet, for example, dust storms  
705 in Longyearbyen are reported as a regular feature in autumn. Dörnbrack et al. (2010) documented and characterized a strong  
706 dust storm in the Adventdalen valley—the center of Spitsbergen Island—in May 2004, using airborne lidar observations and  
707 mesoscale numerical modeling. In the same area, near Longyearbyen, dust emissions from an active coal mine were  
708 documented by Khan et al. (2017). Kandler et al. (2020) also reported Svalbard measurements in Longyearbyen in September  
709 2017, with high iron and chlorite-like contributions in dust.

710 The accelerated ablation of Svalbard’s glaciers (Schuler et al., 2020) and the increasing melt rate of permafrost are causing  
711 accelerated growth in periglacial and proglacial areas. The significance of the morphogenetic processes of deflation,  
712 denudation, and sediment transport on slopes and in river channels in glaciers’ marginal zones is increasing (Zwolinski et al.,  
713 2013). Thus, these areas have become potential sources of dust and, as such, have been investigated for the physical and  
714 chemical properties of their sediments, regardless of the documented occurrences of the dust events these areas have  
715 experienced.

716 Fluvial, glaciofluvial, and weathering deposits at five different sites on the coastal plains near the Ny-Ålesund Research Station  
717 (78.92481°N, 11.92474°E), NW Spitsbergen were investigated (Moroni et al., 2018). The mineralogical assemblage is  
718 characterized by dolomite, calcite, quartz, albite, and sheet silicates (vermiculite, muscovite, clinocllore) in variable amounts,  
719 along with monazite, zircon, apatite, baryte, iron sulfate, Fe, Ti, Cu, and Zn ores as accessory minerals. With a weight fraction  
720 of 4 to 53% of particles smaller than 100 µm, these deposits should be considered a valid dust source. However, the contribution  
721 is influenced by the modest extension of bare soils (less than 4 km<sup>2</sup>) and the brief duration of the area’s driest summer. The  
722 composition of the aerosols collected at the Gruvebadet lab near Ny-Ålesund during the summer-fall period reveals the  
723 presence of such a local dust component (Moroni et al., 2016; Moroni et al., 2018). Further evidence of local dust sources in  
724 the Ny-Ålesund area and Brøgger Peninsula also results from the annual snowpack’s chemical composition (Gallet et al., 2018,  
725 Jacobi et al., 2019). The contribution of local dust sources on this site is of secondary importance compared to that of long-  
726 range transport (Moroni et al., 2015; Moroni et al., 2016; Moroni et al., 2018, Conca et al., 2019).

727 A similar study was conducted on the loose sediment deposits in the neighborhood of the Polish Polar Station Hornsund  
728 (77.00180°N, 15.54057°E), SW Spitsbergen, where a belt of nearshore plains consisting of marine terraces and nival moraine  
729 bars, with bare surfaces available for mineral dust uplift from late spring, widely outcrop (Zwolinski et al., 2013). The  
730 mineralogical assemblage consists of quartz, alkali feldspar, plagioclase, dark mica, and chlorite, with zircon, apatite,  
731 monazite, iron sulfide, and Fe ore as accessory minerals. The same assemblage was found in the aerosols and snow cover  
732 collected at the base station and the surrounding glaciers in the same period. This fact, along with the significant proportion of  
733 particles smaller than 50  $\mu\text{m}$  in the loose sediment deposits, supports the prevalence of the local dust source in the melting  
734 season. Further evaluation of the impact of local dust sources was obtained from analyzing shallow and deep cores from  
735 different glaciers in the Hornsund area (Lewandowski et al., 2020; Spolaor et al., 2020). The results suggest that for Spitsbergen  
736 glaciers with the summit close (Ny-Ålesund) or below (Hornsund) the equilibrium line, the summer dust deposition from the  
737 local sources is predominant, affecting the glacier ice's chemical composition. However, the dating of monazite grains and  
738 presence of magnetite and iron sulfide (magnetic susceptibility and SEM data, Lewandowski et al., 2020) also suggest the  
739 existence of regional wind transport from Nordaustlandet and Edgeøya, respectively. Further, a long-range component from  
740 Northern Europe, Siberia, and, to a limited extent, Greenland, Iceland, and Alaska, was also evidenced (Moroni et al., 2018;  
741 Crocchianti et al., 2021).

742 Recent estimations of dust load in Central and Southern Svalbard from different sources range from 4 g up to 4 – 5 kg m<sup>-2</sup>  
743 (Rymer, 2018; Rymer et al. 2022), with the highest values in the Ebba Valley due to frequent dust storms in this area (Strzelecki  
744 and Long, 2020). Kavan et al. (2020a) found a negative correlation between deposition rate and altitude at Pyramiden  
745 (78.71060°N, 16.46059°E), the west coast of Petuniabukta, and Ariekammen (77.00035°N, 15.53674°E), and Hornsund area.  
746 The pattern was clear up to the altitude of approximately 300 m a.s.l., suggesting the influence of local sources in the lower  
747 levels of the atmosphere and long-range transport at higher altitudes. The lower values of the deposition rates found at  
748 Ariekammen were ascribed due to the more frankly maritime climate of the Hornsund region.

### 749 **3.5 Climatic and environmental impacts of HLD**

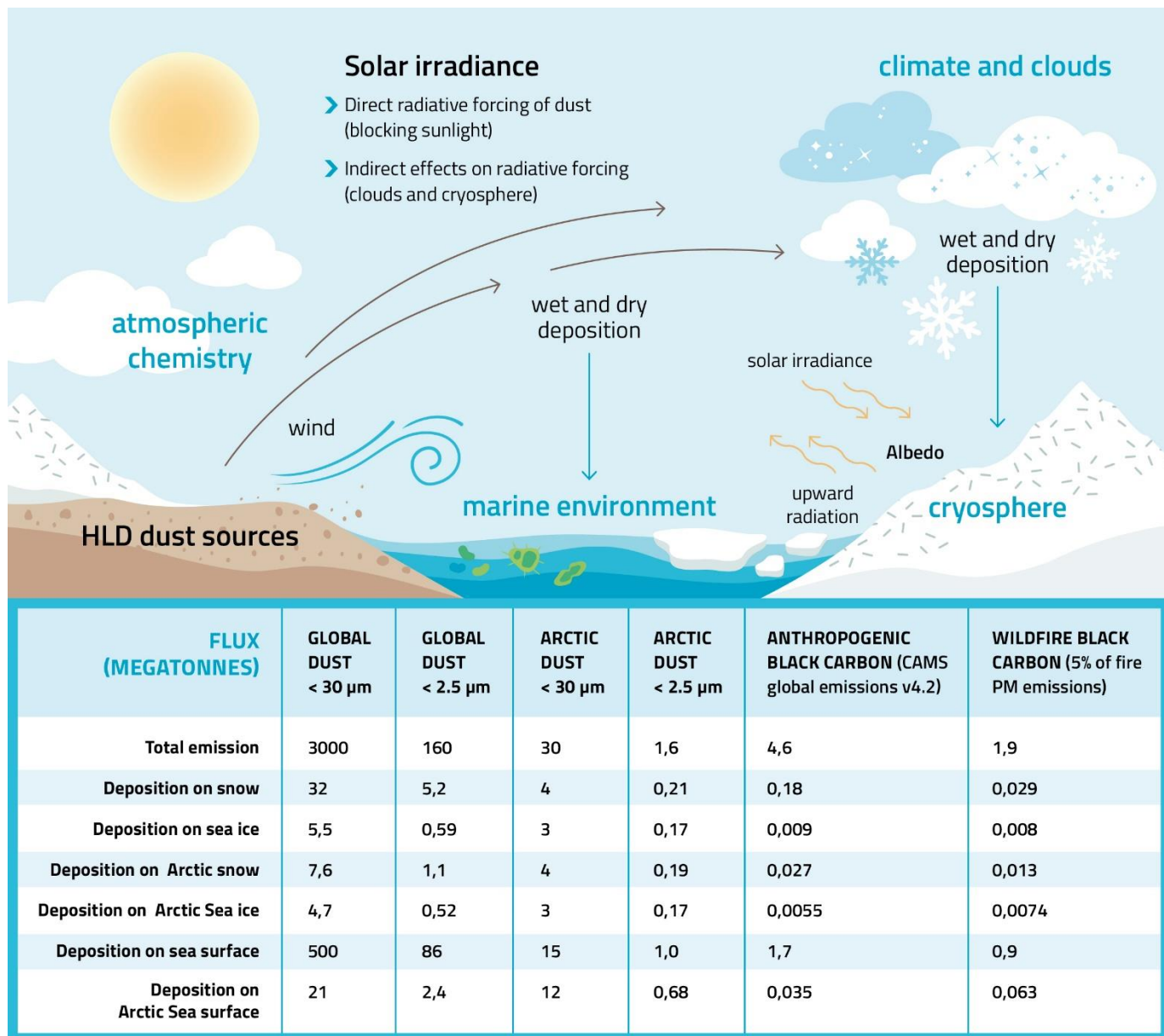
750 Climatic and environmental impacts of HLD on clouds and climate feedback, atmospheric chemistry, marine environment and  
751 cryosphere-atmosphere feedback (Fig. 15) were investigated with the help of topical literature surveys (Sections 3.5.1 - 3.5.4).  
752 Direct radiative forcing of HLD dust (blocking sunlight) and comparison of dust and black carbon as SLCF in the cryosphere  
753 are included in the cryosphere-atmosphere feedback section.

754

755 The amounts of dust emission and deposition (megatonnes) of annual global and Arctic dust (data for 2017), as compared to  
756 anthropogenic and wildfire black carbon (Fig. 15), were studied using the SILAM model (Sofiev et al., 2015). The results of  
757 black carbon emissions presented in Figure 15 were based on the Copernicus Atmosphere Monitoring Service (CAMS) global

758 emission inventory version 4.2 and black carbon originating from wildfires from the SILAM IS4FIRES fire emission model,  
 759 equaling 5 % of the total primary fire PM emissions of the model. The IS4FIRES model is based on fires observed by the  
 760 MODIS instrument onboard the Terra and Aqua satellites.

761  
 762  
 763



764

765 **Figure 15. Climatic and environmental impacts of high latitude dust include direct radiative forcing (blocking sunlight), indirect**  
766 **radiative forcing (clouds and cryosphere) as well as effects on atmospheric chemistry and marine environment. The amounts of dust**  
767 **emission and deposition (megatonnes) of global and Arctic dust, as compared to black carbon, were estimated using the SILAM**  
768 **model (Sofiev et al., 2015). The black carbon emissions are based on the CAMS global anthropogenic emission dataset v4.2 and the**  
769 **wildfire black carbon emissions are based on the IS4FIRES fire emission model, equaling 5 % of the total primary fire PM emissions**  
770 **of the model.**

### 771 **3.5.1 Impacts of HLD on atmospheric chemistry**

772 Icelandic dust, a specific HLD of volcanic origin, is constantly resuspended from the deserts. Regarding atmospheric  
773 chemistry, the most substantial impact comes from the particles in the 0.002 to 10  $\mu\text{m}$  range, as they can be carried over more  
774 considerable distances (Finlayson-Pitts, 1999). The Icelandic dust in the troposphere is not as addressed as the impact of desert  
775 dust. This HLD is very likely a long-range transporting carrier for many species adsorbed on its surface, which can act as a  
776 sink of trace gases and a subsequent platform for transferring taken-up species. Along with transport, adsorbed species may  
777 undergo different heterogeneous reactions that can lead to secondary compound formation. Such processes can influence the  
778 reactivity and balance of atmospheric species. Optical, hygroscopic, and, more generally, physicochemical properties of the  
779 HLD can change due to surface processes, implying atmospheric trace gases due to heterogeneous interactions (Usher et al.,  
780 2003). The consequences can be starkly different depending on the nature of atmospheric trace gases interacting with HLD.  
781 This section aims to illustrate the diversity of interactions between HLD and atmospheric trace gases to emphasize the various  
782 impacts of these aerosols on atmospheric physics and chemistry. In the case of ozone, if the direct heterogeneous interaction  
783 with dust does not play a major role in the atmospheric concentration decrease of the primary compound, surface processes  
784 are triggered, affecting the atmospheric budget of ozone. In the case of  $\text{NO}_2$ , heterogeneous processes on dust can significantly  
785 lead to HONO species forming, with direct impacts on gas-phase atmospheric reactivity. In the case of  $\text{SO}_2$ , beyond a complex  
786 reaction pathway, the heterogeneous process dually affects the budget of the taken-up species and the chemical and physical  
787 properties of the dust surface.

788 If the heterogeneous reaction of  $\text{NO}_2$  on various types of atmospheric particles, e.g., salts, soot, mineral dust, and proxies, was  
789 addressed in the literature (George et al., 2015), the interaction of  $\text{NO}_2$  with volcanic particles, typical HLD desert dust, under  
790 atmospheric conditions, has only been studied by Romanias et al. (2020). They explore the possible formation of a short  
791 lifetime key atmospheric species, considered a trigger of numerous atmospheric processes: HONO, a precursor of OH radicals  
792 in the atmosphere. To that end,  $\text{NO}_2$  uptake on Icelandic HLD is explored under various and contrasting atmospheric  
793 conditions. Despite the relatively close volcanic regions where the selected samples originate, uptake coefficients of  $\text{NO}_2$   
794 contrasted significantly with the dust location due to magmatic and morphological differences among samples. This point  
795 confirms that concerning heterogeneous atmospheric chemistry, sample behavior can dramatically deviate from one class of  
796 dust to another, with physical and chemical characterizations of the samples remaining key intrinsic descriptors. Nonetheless,

797 volcanic dust appears as effective NO<sub>2</sub> scavengers from the atmosphere. The interaction of NO<sub>2</sub> with HLD is evidenced as a  
798 source of NO and, more interestingly, HONO, with kinetics and formation yields highly dependent on relative humidity.  
799 Higher HONO formation yields on volcanic samples are observed for RH values exceeding 30% RH. Heterogeneous  
800 construction of HONO from NO<sub>2</sub> interaction with Icelandic dust is estimated as atmospherically significant under volcanic  
801 eruptions or, more frequently in Iceland, during typical volcanic dust storms. Such leads to HONO formation rates up to 10  
802 pptV/hr, which can significantly influence the regional atmosphere's oxidative capacity. The experimental determination of  
803 NO<sub>2</sub> uptake coefficient  $\gamma$  allows including such processes in atmospheric modeling, improving their representativeness.

804 A transient uptake of SO<sub>2</sub>—an initially important uptake of SO<sub>2</sub> that is progressively reduced—leads to low steady-state uptake  
805 coefficients of SO<sub>2</sub> after several hours of exposure in the range of 10<sup>-9</sup> to 10<sup>-8</sup>. The surface coverages were in the range of  
806 10<sup>14</sup> molecule cm<sup>-2</sup> or 10<sup>16</sup> molecule cm<sup>-2</sup> using the total surface area or the geometric surface area of aerosols, respectively  
807 (Urupina et al., 2019). Zhu et al. (2020) estimated that around 43% more volcanic sulfur is removed from the stratosphere  
808 within months due to SO<sub>2</sub> heterogeneous chemistry on volcanic particles than without. Concomitantly with SO<sub>2</sub> uptake, sulfites  
809 and sulfates are monitored on the surface of volcanic dust, with sulfates being the final oxidation product, attesting to SO<sub>2</sub>  
810 surface reaction. Through surface hydroxyl groups, the dust surface's chemical composition plays a crucial role in converting  
811 SO<sub>2</sub> to sulfites, as evidenced experimentally using lab scale but atmospheric relevant experimental setups (Urupina et al, 2019).  
812 This provides original insights into the kinetics and mechanism of SO<sub>2</sub> uptake and the transformation on volcanic material  
813 under simulated atmospheric conditions, bringing an accurate perspective on SO<sub>2</sub> heterogeneous sinks in the atmosphere on  
814 the HLD surface. The model simulations of Zhu et al. (2020) suggested that the transformation of SO<sub>2</sub> on such particles plays  
815 a key role in the stratosphere's sulfate content. Interestingly, this transformation and accumulation of sulfates on the surface  
816 of particles could turn the unreactive ozone material into reactive, especially in the stratosphere, where volcanic particles have  
817 longevity.

818 The case of SO<sub>2</sub> uptake points to the aging of the HLD surface with subsequent impacts on its chemical (e.g., hygroscopicity)  
819 and physical (e.g., optical) properties. Changes in hygroscopic properties can correlate with HLD's erratic behavior to act as  
820 cloud-or ice-nucleating particles, depending on their interactions with atmospheric gases. Similarly, sulfate and sulfuric acid's  
821 high surface coverage for volcanic dust, as reported by Urupina et al. (2019), questions the variability of the HLD refractive  
822 index and the impact on remote sensing of fresh vs. aged dust.

### 823 **3.5.2-Impacts of HLD on clouds and climate feedback**

824 Clouds across the mid- and high latitudes are of first-order importance. Climate and HLDs may play a first-order but highly  
825 uncertain role in defining their properties through the initiation of ice formation. Clouds frequently persist in a supercooled  
826 state. However, even a few droplets converting to ice crystals through heterogeneous freezing can lead to microphysical  
827 processes that dramatically reduce a cloud's liquid water content, reducing its albedo and exposing the surface underneath

828 (Murray et al., 2021; Tan and Storelvmo, 2019). Only a small subset of atmospheric aerosol can nucleate ice; concentrations  
829 of around only 1 INP per liter of air active at the cloud temperature can dramatically alter cloud albedo. In contrast, the  
830 concentration of aerosol particles capable of serving as cloud condensation nuclei (CCN) are orders of magnitude larger.  
831 Hence, dust particles in the high latitudes will rarely exist in high enough concentrations to dramatically impact cloud droplet  
832 numbers by providing additional CCN. However, high-latitude dust has been shown to serve as an effective INP in sufficient  
833 concentrations to potentially impact mixed-phase clouds (Sanchez-Marroquin, 2020). Ice formation's role in climate  
834 projections depends on the clouds' location. In the following paragraphs, we discuss two distinct classes of clouds that may be  
835 influenced by HLD particles serving as INPs.

836 For boundary layer clouds over oceans between approximately 45–70°, the amount of ice versus supercooled water, as well as  
837 albedo, is critical for global climate (Vergara-Temprado et al., 2018; Bodas-Salcedo et al., 2014). These clouds are where  
838 substantial solar insolation exists, and the contrast between a high albedo cloud and a dark ocean surface is significant. Hence,  
839 these clouds are implicated in the cloud-phase feedback, where water replaces ice, increasing their albedo as the world warms  
840 with increased carbon dioxide (Storelvmo et al., 2015). This feedback's uncertainty is very high, with the temperature rise  
841 associated with a doubling of carbon dioxide, rising from around 4 K to well above 5 K, simply by increasing the amount of  
842 supercooled water in clouds in the current climate (Frey and Kay, 2018). Hence, understanding the sources of ice-nucleating  
843 particles in the high latitudes, including HLDs, is critical to understanding these climate-relevant issues (Murray et al., 2021).

844 The second group of clouds is those occurring at high latitudes. For example, in the central Arctic, mixed-phase clouds play a  
845 critical role in the local Arctic climate and the phenomenon of Arctic amplification. In a corollary to the cloud-phase feedback,  
846 water replacing ice leads to more downward longwave radiation, resulting in positive feedback (i.e., amplification) (Tan et al.,  
847 2019). Hence, the phase of clouds and, therefore, the INP population in clouds in the present Arctic atmosphere are key for  
848 defining this feedback's strength. Moreover, any changes in the INP population with a changing climate may also provide  
849 feedback on cloud properties (Murray et al., 2021).

850 Given the apparent importance of INPs in defining cloud properties and climate feedback, surprisingly little is known about  
851 the ice-nucleating properties of HLDs. Mineral dust is one of the most important types of atmospheric INPs in clouds below  
852 approximately -15°C around the globe because of its relatively high ice-nucleating activity and abundance in the atmosphere  
853 (Murray et al., 2012). A handful of papers have also identified HLDs as significant contributors to the Arctic's INP population  
854 (Irish et al., 2019; Sanchez-Marroquin, 2020; Tobo et al., 2019; Šantl-Temkiv et al., 2019). HLDs may differ in their ice-  
855 nucleating ability from LLDs for several reasons: Firstly, the HLDs from glacial valleys, for example, are often richer in  
856 primary minerals (olivines, pyroxenes, feldspars, and amphiboles) and less rich in clays compared to LLDs. This is crucial  
857 because K-rich feldspars are known for their exceptional ice-nucleating ability, whereas clays are much less active (Harrison  
858 et al., 2019; Atkinson et al., 2013). Secondly, the most prominent LLD sources, like those in Africa, are abiotic (Price et al.,  
859 2018), whereas it has been found that HLDs can be associated with highly effective biogenic ice-nucleating material (Tobo et

860 al., 2019; Šantl-Temkiv et al., 2019). The inclusion of biological ice-nucleating material, which can be ice-active at  
861 temperatures much higher than -15 °C, may mean that these dust sources have a disproportionately greater impact on cloud  
862 glaciation and climate than their low-latitude counterparts. Much more research is needed to define and understand the ice-  
863 nucleating ability of these HLD sources.

### 864 **3.5.3 Impacts of HLD on the marine environment**

865 Mineral dust particles are a source of essential nutrients such as phosphorus (P) and iron (Fe) to the ocean ecosystems (e.g.,  
866 Jickells et al., 2005; Mahowald et al., 2005; Stockdale et al., 2016). Dust deposition onto the ocean's surface can stimulate  
867 primary productivity and enhance carbon uptake, indirectly affecting the climate (e.g., Jickells and Moore, 2015; Mahowald,  
868 2011). The extent of these impacts primarily depends on the dust deposition fluxes, its chemical properties, and the nutrients  
869 of (co)limitations patterns in the ocean waters (e.g., Boyd et al., 2007; Boyd et al., 2010; Kanakidou et al., 2018; Mahowald et  
870 al., 2010; Mills et al., 2004; Moore et al., 2013; Shi et al., 2012; Stockdale et al., 2016). Arctic Ocean is often nitrogen-limited  
871 (von Friesen and Riemann, 2020).

872 The aerosol fractional Fe solubility (%) is defined as the ratio of dissolved Fe (in the filtrate, which has passed through 0.2 or  
873 0.45 µm pore size filters) to the total Fe in the bulk aerosol (e.g., Meskhidze et al., 2019; Shi et al., 2012). This is typically  
874 used to indicate the fraction of Fe, which is likely to be bio-accessible for marine ecosystems (Meskhidze et al., 2019).

875 Sub-Arctic oceans are Fe-limited or seasonally Fe-limited. Fe limits primary productivity in the Sub-Arctic Pacific Ocean  
876 (Martin and Fitzwater, 1988). The atmospheric Fe deposition in the Gulf of Alaska is dominated by dust transported from  
877 glacial sediments from the Gulf of Alaska coastline (Crusius et al., 2011), with relatively high fractional Fe solubility—around  
878 1.4% (Schroth et al., 2017). Although the upwelling of deep water is the major source of dissolved Fe, the atmospheric flux of  
879 dissolved Fe to the Gulf of Alaska's surface water is comparable to the Fe flux from eddies of coastal origin (Crusius et al.,  
880 2011). The magnitude of glacial dust's deposition to the Gulf of Alaska varies significantly depending on the regional weather  
881 conditions. However, the extent of its impacts is still unclear (Schroth et al., 2017). Currently, the spatial resolution of global  
882 dust models is too low to accurately reproduce Alaskan dust flux, generated by anomalous offshore winds and channeled  
883 through mountains (Crusius, 2021). Recently, Crusius (2021) determined dissolved Fe inventories based on time series of  
884 dissolved Fe and particulate Fe concentrations from the Ocean Station Papa in the central Gulf of Alaska, including  
885 measurements from September 1997 to February 1999. The analysis showed 33%–70% increases in dissolved Fe inventories  
886 between September and February of successive years. These increases were possibly linked to dust fluxes from the Alaskan  
887 coastline—known to occur mostly in autumn (Crusius et al., 2011; Schroth et al., 2017). These new results support the  
888 importance of atmospheric Fe's contribution, although more work is needed to confirm the sources of dissolved Fe in the Gulf  
889 of Alaska.

890 The Sub-Arctic North Atlantic Ocean is seasonally Fe-limited (Nielsdottir et al., 2009; Ryan-Keogh et al., 2013). Natural dust  
891 from Iceland largely contributes to the atmospheric dust deposition in the North Atlantic Ocean (Bullard, 2016). Icelandic dust  
892 originates from volcanic sediments and has a relatively high total Fe content—about 10% (e.g., Arnalds et al., 2014, Baldo et  
893 al., 2020). The estimated total Fe deposition from Icelandic dust to the ocean’s surface is 0.56–1.38 Mt yr<sup>-1</sup> (Arnalds et al.,  
894 2014). The initial Fe solubility observed in dust samples from Icelandic dust hotspots is from 0.08% to 0.6%—comparable to  
895 that of mineral dust from low-latitude regions such as Northern Africa, while the fractional Fe solubility at low pH (i.e., 2) is  
896 significantly higher than typical low-latitude dust (up to 30%) (Baldo et al., 2020). Achterberg et al. (2018) argued that deep-  
897 water mixing is the dominant source of Fe in the Sub-Arctic North Atlantic Ocean’s surface water, which is up to ten times  
898 higher than the Fe supply by atmospheric Fe deposition. However, during the 2010 eruption of the Icelandic volcano  
899 Eyjafjallajökull, Achterberg et al. (2013) observed elevated dissolved Fe concentration and nitrate depletion in the Iceland  
900 Basin, followed by an early spring bloom. They measured an initial fractional Fe solubility of 0.04%–0.14% for Icelandic  
901 ash, which is below or towards the lower end of the range of values estimated for Icelandic dust (0.08%–0.6%) (Baldo et al.,  
902 2020). High deposition flux (Arnalds et al., 2016) and higher Fe solubility of Icelandic dust (Baldo et al., 2020) suggest that  
903 they may impact Fe biogeochemistry and primary productivity in the surface ocean. However, more research is needed to  
904 confirm this.

905 The Southern Ocean is known to be Fe-limited (Moore et al., 2013). Major atmospheric dust sources include, for example,  
906 Australia, southern South America, and Southern Africa (e.g., Ito and Kok, 2017). Contribution from local sources in  
907 Antarctica is also observed (e.g., Chewings et al., 2014; Winton et al., 2014; Winton et al., 2016). Winton et al. (2016) reported  
908 a background fractional Fe solubility from Antarctic dust sources of 0.7%—similar to the upper limit of Fe solubilities observed  
909 in Icelandic dust (Baldo et al., 2020). However, mineral dust originating from glacial sediments from the Gulf of Alaska  
910 coastline showed higher Fe solubilities (1.4%) (Schroth et al., 2017)—likely due to the different mineralogy and Fe speciation  
911 in the samples. The various methods used to determine the fractional Fe solubility in these studies may also contribute to this  
912 difference (Perron et al., 2020).

913 Although the upwelling of deep water is a major source of dissolved Fe, the atmospheric deposition of dissolved Fe can locally  
914 contribute to the phytoplankton bloom (Winton et al., 2014). However, evidence exists that increased dust flux enhanced  
915 primary production in the Southern Ocean in the last glacial age (Martínez-García et al., 2014). The Ross Sea is a continental  
916 shelf region around Antarctica and a highly biologically productive area in the Southern Ocean, which has important  
917 implications for global carbon sequestration (e.g., Arrigo et al., 2008; Arrigo and Van Dijken, 2007). In the Ross Sea, an  
918 additional Fe supply is required to sustain the intense phytoplankton bloom during the austral summer (Tagliabue and Arrigo,  
919 2005). Measurements conducted on snow pits and surface snow samples showed that local Antarctic dust contributes to Fe  
920 deposition. However, this contribution is only a minor component of the total Fe supply to the Ross Sea, with most being  
921 supplied by the upwelling of deep water (Winton et al., 2014; Winton et al., 2016a,b).



922 In the Polar regions, atmospheric dust is mostly delivered to the sea ice, where melting and freezing cycles (ice processing)  
923 can enhance the formation of relatively more soluble phases of Fe oxide-hydroxide minerals such as ferrihydrite. This  
924 formation can increase the flux of atmospheric dissolved Fe to the ocean (Raiswell et al., 2016).

### 925 **3.5.4 HLD impacts on cryosphere and cryosphere-atmosphere feedback**

926 The cryosphere is the frozen water part of the Earth system, including sea, lake, and river ice; snow cover, glaciers, ice caps,  
927 and ice sheets; permafrost and frozen ground. These components play a crucial role in the Earth's climate (IPCC, 2019).  
928 Temperatures in fragile areas, such as the pristine polar regions, have been increasing at twice the global average; the highest  
929 increase in the temperature on the coldest days—up to three times the rate of global warming—is projected for the Arctic  
930 (IPCC, 2021). Warming in vulnerable cold climate land areas causes glacier retreat, permafrost thaw, and a decrease in snow  
931 cover extent (IPCC, 2019). Consequently, potential HLD sources, such as glacial sediments, can increase (e.g., Nagatsuka et  
932 al., 2021). When dust is long-range transported and wet- or dry-deposited or windblown from local dust sources, the ice and  
933 snow albedo decrease and influences glacier melt (e.g., Boy et al., 2019) via the positive ice-albedo feedback mechanism  
934 (AMAP, 2015; Flanner et al., 2007; Gardner and Sharp, 2010; IPCC, 2019). Cryospheric melt processes are controlled by  
935 many environmental factors (IPCC, 2019), such as solar irradiance, ambient temperature, and precipitation (e.g., Meinander  
936 et al., 2013, 2014; Mori et al., 2019). Kylling et al. (2018) used dust load estimates from Groot Zwaartink et al. (2016) (using  
937 low-latitude dust complex refractive index for high-latitude dust) to quantify the mineral dust instantaneous radiative forcing  
938 (IRF) in the Arctic for 2012. They found that the annual-mean top of the atmosphere IRF ( $0.225 \text{ W/m}^2$ ) had the largest  
939 contributions from dust transported from Asia south of  $60^\circ\text{N}$  and Africa; high-latitude ( $>60^\circ\text{N}$ ) dust sources contributed about  
940 39% to the top of the atmosphere IRF. However, HLD had a larger impact (1 to 2 orders of magnitude) on IRF per emitted  
941 kilogram of dust than low-latitude sources. They also reported that mineral dust deposited on snow accounted for nearly all  
942 the bottom of the atmosphere IRF ( $0.135 \text{ W/m}^2$ ), with over half caused by dust from high-latitude sources north of  $60^\circ\text{N}$ .

943 For snow and ice (glacier) surface radiation balance, the net energy flux  $E_N$  is due to differences between downward ( $\downarrow$ ) and  
944 upward ( $\uparrow$ ) non-thermal shortwave (SW) and thermal longwave (LW) radiative fluxes. Such is most critically influenced by  
945 the surface characteristics of the bi-hemispherical reflectance (BHR), i.e., albedo (Manninen et al., 2021). Therefore, melt is  
946 also controlled by dark impurities in snow and ice (IPCC, 2019). Black carbon (BC) is, climactically, the most significant and  
947 best-studied dark light-absorbing aerosol particle in snow (e.g., Bond et al., 2013; Dang et al., 2017; Evangelidou et al., 2018;  
948 Flanner et al., 2007; Forsström et al., 2013; Mori et al., 2019; Meinander et al., 2020a,b). Radiation-transfer (RT) calculations  
949 indicate that seemingly small amounts of black carbon (BC) in snow, in the order of 10–100 parts per billion by mass (ppb),  
950 decrease its albedo by 1–5% (Hadley and Kirchtetter, 2012). BC has been shown to enhance snowmelt (AMAP, 2015; Bond  
951 et al., 2013; IPCC, 2019). Other light-absorbing particles include organic carbon (OC, including brown carbon BrC) and dust.  
952 Also, blooms of pigmented glacier ice algae can lower ice albedo and accelerate surface melting (McCutcheon et al., 2021),

953 showing a direct link between mineral phosphorus in surface ice and glacier ice algae biomass. They say nutrients from mineral  
954 dust likely drive glacier ice algal growth, identifying mineral dust as a secondary control on ice sheet melting. Some Icelandic  
955 dust sources have particles almost as black as black carbon by the reflectivity properties when measured as bulk material or  
956 on snow and ice surfaces (Peltoniemi et al., 2015). Unlike black carbon, Icelandic dust has been shown to melt snow quicker  
957 in small amounts and insulate and prevent melt in larger amounts (e.g., Dragosics et al., 2015; Möller et al., 2016; Boy et al.,  
958 2019). Changes related to permafrost thaw and snow and ice melt, including disappearing glaciers, rising sea levels, and  
959 drinking water shortages, are among the most serious global threats (IPCC, 2019). Water availability is vital in regions where  
960 crops depend most on snowmelt water resources (Qin et al., 2020). Snow is also essential in the catchment areas (i.e., areas  
961 supplying watercourses) and for many snow-dependent organisms, including plants, animals, and microbes (Zhu et al., 2019).  
962 Melt can also run hydroelectric power plants that supply electricity (e.g., Lappalainen et al., 2022). This all highlights the  
963 importance of investigations and continuous assessment of the temporal and spatial significance and contribution of different  
964 light-absorbing impurities in enhancing or initiating cryospheric melt in the changing climate.

### 965 **3.6 Understanding the HLD sources**

966 The HLD results are further discussed from the perspective of HLD source intensity values; comparison with available HLD  
967 information on the various regions; geological perspective on sources, focusing on a gap identified in HLD observations for  
968 the Central part of the East European Plain and dust particle properties; and local HLD sources and long-range transport of  
969 dust with the focus on results from the observations in Svalbard and Antarctica.

#### 970 **3.6.1 Source intensity values**

971 Most of the HLD study sites agree with UNCCD G-SDS-SBM source intensity (SI) values of the highest dust productive areas,  
972 identifying an environment from a given location within a distance  $\leq 0.1^\circ$ . Surfaces with higher maximum SI include a  
973 significant portion of the land surface in HLD regions. In the south HLD region, an annual change of SI exists. However,  
974 approximately half the dust productive surface stays exposed to wind erosion during the year. In the north HLD region, SI  
975 intensity varies significantly with the weather. High values of SI may not always coincide with high surface winds, meaning  
976 high values may exist but not necessarily result in a dust storm. In case emissions occur, dust may remain undetected because  
977 of the absence of ground observations over most of the HLD region and frequent cloud cover over airborne dust, obscuring  
978 remotely sensed imagery.

979 Based on the SI values, the East Greenland sources in this study (no. 58–64 in Fig. 1) are seasonal, meaning their SI minimum  
980 value is zero. Conversely, the West Greenland sources are not necessarily seasonal since their SI minimum values are  
981 somewhat reduced (but not to zero). However, the term “seasonal” regarding the SI values means the soil surface conditions

982 are suitable for dust emissions, although that doesn't mean emissions will happen. Similarly, the seasonality of all sources in  
983 this collection can be further studied.

984 When the newly identified sources are close together, such might indicate they are part of the larger dust source area, like  
985 South Iceland, West Greenland, or East Greenland. The discovered sources could be considered to represent the hot spot  
986 locations, i.e., the most emissive or active locations, of those dust-productive areas. Simultaneously, however, the land surface  
987 and soil composition can be very complex and spatially variable, and the identification of single sources justified until the  
988 source characteristics and particle properties have been characterized in more detail. For example, Icelandic sources have  
989 shown that each source, even proximate ones, may have different particle size distributions and optical properties. The results  
990 (Fig. 2) suggest two northern high-latitude dust belts. The first HLD belt would extend at 50–58°N in Eurasia and 50–55°N in  
991 Canada, and the second dust belt at >60°N in Eurasia and >58°N in Canada, with a “no dust” belt between the HLD and LLD  
992 dust belts (except for British Columbia).

993 Uncertainties about the detected locations of the HLD sources and G-SDS-SBM source intensity values arise from the  
994 methodology for determining HLD source locations. These locations are ad-hoc location sources from satellite images of dust  
995 plumes; other kinds of airborne dust observations may introduce some errors in location estimation compared to on-site land  
996 surface monitoring and the precision of available data locations. The resolution of G-SDS-SBM may be too coarse for small-  
997 scale source areas (in this case, the representative grid point value shows reduced source intensity value since it represents the  
998 whole grid box). However, the in-point (at location) values are also given maximum values in the area around the given  
999 location (one point distance: 30 arcsec, 0.1°, 0.5°, and 1° distance). Values of source intensity above 0.9 have topsoil potential  
1000 for SDS production in the top 10% of grid boxes with some emission potential in G-SDS-SBM (or in the top 10% of most  
1001 dust-productive surfaces globally in case of favorable weather conditions), above 0.8 in the top 20%, above 0.7 in the top 30%,  
1002 and so forth. Factors reducing source function value or topsoil dust productivity are sparse vegetation, coarser soil texture,  
1003 higher moisture, and temperatures near the freezing point. Uncertainties in methodology for deriving G-SDS-SBM arise from  
1004 the quality and resolution of available global datasets and the determination of thresholds for EVI in defining bare land fraction  
1005 (primarily for brown grassland, which may appear as potential dust sources but with lower productivity). Surfaces with low SI  
1006 values in favorable conditions for dust emission, in case of high winds, may produce some blowing dust events; sources with  
1007 higher values of SI may generate dust storms. Real dust production from sources depends on high winds occurring while SI is  
1008 high.

1009 Forty-nine locations were in the north HLD region (47 according to HLD definition by Bullard et al. (2016), except for two:  
1010 no. 8 and no. 48, with latitudes 47.7°N and 47.6°N, respectively), while 15 were in the south HLD region, including four south  
1011 of 60°S, where the values of SI are not provided. In the north HLD region, higher dust productive potential (SI 0.5) has 17 of  
1012 49 marked locations at the HLD source marks exact location. Also, 38 sites are where a distance from a mark point (D) is  
1013 equal to or less than 0.1° (Supplementary Table S4). Very high dust productivity, with SI 0.7, has 33 locations within D 0.1°,

1014 and 42 and 46 within 0.5° and 1°, respectively. The highest dust productive potential, with SI 0.9°, has 27 locations within D  
1015 0.1°, and 39 and 44 within 0.5° and 1°, respectively. One point has the highest SI value, with less than 0.5° and five less than  
1016 0.9° away, when considering the largest environment of the HLD source mark. Three HLD source region marks are in the sea,  
1017 so their source values are marked as -99 (undefined). In the south HLD region, 11 locations are considered (situated between  
1018 40°S and 60°S). Seven sources have very high dust productivity with SI 0.7 where the HLD source marker is; three more have  
1019 SI 0.7° in the area of the source marker with D 0.1°. The highest dust productive potential, with SI 0.9°, has seven sources in  
1020 the area with the source marker with D 0.1°, and three more in the area with D 0.5°. The source maximum and minimum  
1021 intensities in these south HLD regions differ much less than in the north HLD region.

1022 As a summary, our modeling results on the spatial distribution of the dust sources (Fig. 2) showed evidence supporting a  
1023 northern High Latitude Dust (HLD) belt, defined as the area north of 50°N, where we distinguish the following HLD-source  
1024 areas: (a) “transitional HLD-source area,” which extends at latitudes 50–58°N in Eurasia and 50–55°N in Canada, and (b)  
1025 “cold HLD-source area,” which includes areas north of 60°N in Eurasia and north of 58°N in Canada, with currently “no dust  
1026 source” area between the HLD and LLD dust belts (except for British Columbia).

### 1027 **3.6.2 Comparison of various regions**

1028 For the HLD sources identified and included in our collection, the available information varied from detailed characterizations  
1029 to the first satellite observations, waiting to be complemented with measurement data. Model output of dust transport can  
1030 provide valuable additional information. The sources are in the northern and southern high latitudes and include a variety of  
1031 environments. Particle properties, such as particle size distributions, have been determined for only some of the identified  
1032 HLD sources. For example, our study’s many Iceland south coast sources have not had any characterization done. Previous  
1033 results on the known sources in Iceland’s south coast region show that the particle size distributions vary substantially from  
1034 location to location. No assumptions can be made based on characterization in one place.

1035 For Iceland seasonality, the correlation of SILAM modeled and measured PM10 and PM2.5 total aerosol concentration in  
1036 Iceland is low, especially in 2018, which can mainly be explained by the measurement locations being far from the source  
1037 locations and showing the effects of road dust rather than long-range transported dust. Also, the Reykjavik and Akureyri dust  
1038 inventories are unrepresentative due to the challenge of fitting the modeled long-range transported dust emissions 695 to the  
1039 measurement data within the 0.1 degrees model resolution. Near Reykjavik, dust emissions, e.g., from Landeyjasandur, may  
1040 contribute to the measured dust concentrations. However, the 0.1 degrees resolution of the model is too scarce to simulate  
1041 them.

1042 The end of summer and autumn (October) are the seasons for dust activity in Greenland. For example, on 19 October 2021,  
1043 there was significant dust activity in western Greenland; several glacial valleys emitted dust along the 700-km coast. During

1044 that dust event was a good Sentinel overpass showing a long narrow valley with a great deal of haze(dust) suspended (appearing  
1045 as fuzziness in the image) (Gassó, 2021b). As far as we know, no previous observations for this source exist. Greenland's HLD  
1046 sources (no. 53–58 of Fig. 1) from its west coast are considered new and identified here using satellite observations. Currently,  
1047 further knowledge on the recurrency and area of the emission source is lacking. It is probable that these Greenland HLD  
1048 sources from the west coast have been unidentified due to frequent cloudy conditions. The representation of dust sources in  
1049 modeling approaches requires information on the location, soil characteristics, and temporal changes. A detailed specification  
1050 of the geographic distribution of potential dust sources and their physical (e.g., particle size distribution, optics) and  
1051 mineralogical/chemical (mineral fractions, chemical composition, etc.) properties is critical to accurately parameterize dust  
1052 emission's potential in numerical dust models. Various methods exist to detect new sources; remote sensing is one of the most  
1053 powerful tools, as demonstrated in Iceland's southern coast and Greenland's west and east coasts.

1054 The central part of the East European Plain, with the wide occurrence of silty soils derived from loess-like sediments and  
1055 reduced natural vegetation, is a potential aeolian dust source (Bullard et al., 2011; Sweeney and Manson, 2013). However, this  
1056 region currently lacks observations on dust lifting and transport. Therefore, this region was not included in our collection of  
1057 HLD sources. The gap for observations in the central part of the East European Plain for potential HLD source updates is filled  
1058 here with new data in the Supplement Figures S1–S4 on the partitioning of elements among the five particle-size fractions  
1059 separated from the natural soils of a rural area 100 km southwest of Moscow (Fig. S1). The study area (55°12–13'N, 36°21–  
1060 22'E) belongs to the southeastern part of the Smolensk-Moscow Upland (314 m a.s.l.), representing a marginal area of the  
1061 Middle Pleistocene (MIS 6) glaciation with moraine topography modified by post-glacial erosional and fluvial processes. The  
1062 major soil reference group is Retisol (IUSS Working Group WRB, 2015), developed on the loess-like loam. About 50% of the  
1063 soils in the interfluvial area were subjected to arable farming. A new and unpublished independent dataset on 33 elements in  
1064 topsoil horizons was obtained with a higher accuracy ICP-MS/AES analysis (compared to the DC-ARC-AES data set of  
1065 Samonova and Aseyeva, 2020).

1066 Additional dust sources with massive dust storms causing severe traffic disruption have been documented outside the dust belt  
1067 in higher latitudes. These sources were mainly arable fields, such as those in Germany and Poland, as well as Montana and  
1068 Washington state (in the US) (Hojan et al., 2019).

### 1069 **3.6.3 A geological perspective on HLD sources and particle properties**

1070 Dust sources involve very different formations and geological environments, each leaving its own imprint on the sediments.  
1071 Thus, the geomorphological, sedimentological, petrological, and geochemical study of the loose sedimentary formations in the  
1072 source areas provides information on the origin and provenance of dust when it is transported out or far away. These types of  
1073 studies—quite typical for Saharan dust—are not so well-established in the case of HLD sources. These territories are not all

1074 easily accessible. Even when they are, the time may not coincide with the dust production and/or dust emission period, which  
1075 may be one reason for this missing source area characterization.

1076 Geomorphological studies cover a wide range of subjects and topics, from characterizing specific dust sources (e.g., Arnalds  
1077 et al., 2016; Bullard and Mockford, 2018; Bertran et al., 2021) to analyzing processes (e.g., Bullard and Austin, 2011; Hedding  
1078 et al., 2015; Wolfe, 2020) to landform evolution (Heindel et al., 2017). Sedimentological studies on dust sources focus on the  
1079 particles' morphological characteristics and textural details of the loose sediment formations. The size, shape, and surface  
1080 characteristics of the particles result from morphogenetic processes. As such, these particles say a great deal about the source  
1081 areas. Furthermore, the particles' size and shape influence their lifting and transport capacity and, finally, the distance they  
1082 can reach from their site of origin. Such applies to the studies of the properties of volcanoclastic dust sources in Iceland (e.g.,  
1083 Butwin et al., 2020; Richard-Thomas et al., 2021). From the petrological and geochemical perspective, the panorama is even  
1084 wider and more varied. Save a few (e.g., Baratoux et al., 2011; Moroni et al., 2018), most studies are not aimed at studying  
1085 dust sources but comprise different targets involving the parental soils (e.g., Antcibor et al., 2014; Brédoire et al., 2015).  
1086 Although providing information on the (possible) source areas for dust, these latter studies are not explicitly aimed at studying  
1087 dust sources, so they are not functional for that purpose. Specific survey and sampling activities by a team of experts would  
1088 be required to address all aspects of dust sources and properties adequately. Thus, obtaining a database as rich and articulated  
1089 as possible on the particles' physico-chemical properties within dust would be feasible, providing the ability to predict dust  
1090 behavior within the aerosols and understand medium and long-range transport phenomena is present. A further aspect  
1091 regarding dust sources and properties is the evolution of the particles' physico-chemical properties due to the lifting and  
1092 transport mechanisms. The aerosols must be sampled in different places at different distances from the source. However, this  
1093 approach is complicated by the air masses mixing during transport, requiring a deep investigation of air mass back trajectories.  
1094 Conversely, treating the soils in the lab by re-suspending and sampling them using impactors at well-defined cut-off size ranges  
1095 can be very advantageous. Such work has been carried out on Australian soils and southern African soils (Gili et al, 2021) to  
1096 study the dust sources in Antarctica, which is now underway in Iceland (Moroni, 2021, personal communication).

#### 1097 **3.6.4 Local HLD sources versus long-range transported dust: discussing Svalbard and Antarctica**

1098 The same areas of dust lifting can also be deposition sites when particles leaving their respective source regions are deposited  
1099 there after prolonged transport pathways. The extent of the contribution of local and long-range sources may vary during the  
1100 year depending on the type of atmospheric circulation and state of the exposed surfaces, particularly the presence of bare  
1101 deglaciated soils. Such is the case of Svalbard, where the local dust sources prevail over the long-range ones, especially in  
1102 summer; the contrary occurs the rest of the year (Moroni et al., 2016; Spolaor et al., 2021). Conversely, and always in  
1103 Spitsbergen, the type of contributions—local and long-range—may also depend on the altitude due to the stratified structure  
1104 of the lower atmosphere frequently found at high latitudes (e.g., Moroni et al., 2015; Kavan et al., 2020a).

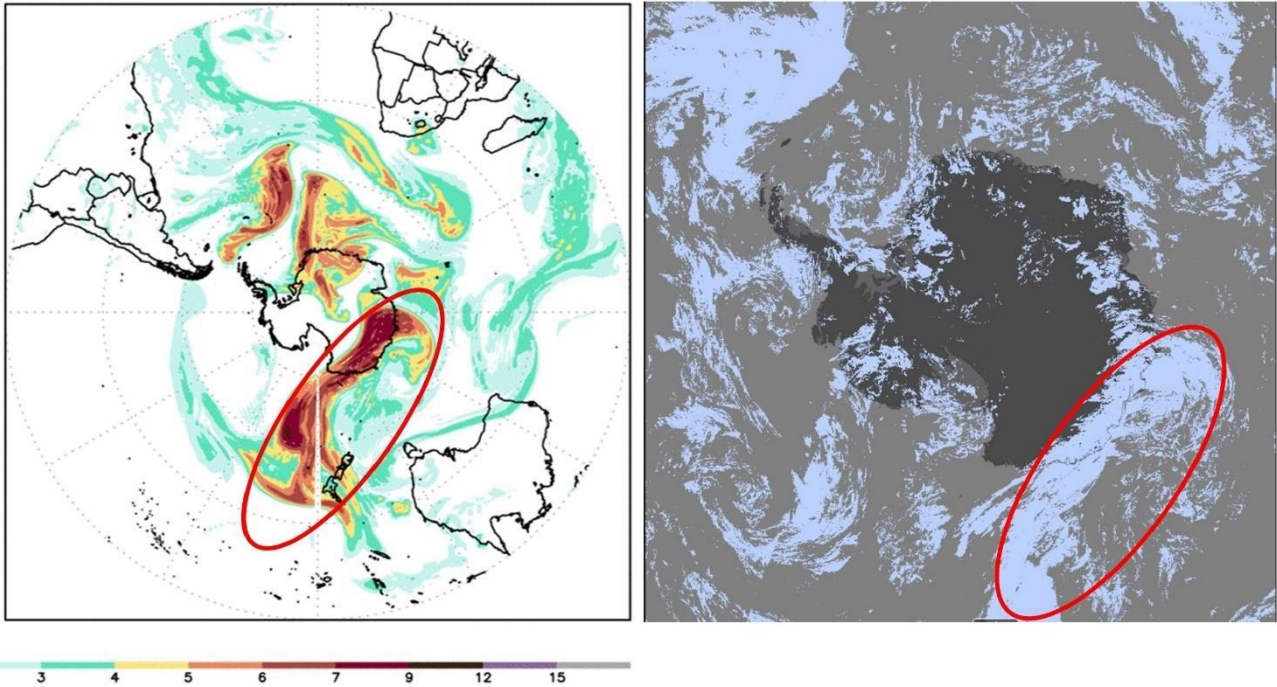
1105 Investigating the physico-chemical properties, and possibly estimating their contributions at different times of the year, is key  
1106 to identifying the source regions of dust. For example, in Spitsbergen's case, the potential Source Contribution Function  
1107 (PSCF) analysis of aerosol samples taken in Ny-Alesund clearly identified four different HLD sources in Eurasia, Greenland,  
1108 Arctic-Alaska, and Iceland (Crocchianti et al., 2021). Conversely, chemical-mineralogical investigation and single-particle  
1109 analysis recognized and estimated Icelandic dust's contribution to Ny-Alesund (Moroni et al., 2018).

1110 Kandler et al. (2020) collected dry dust deposition near sources in Northwestern Africa, Central Asia, on Svalbard, and at three  
1111 locations of the African outflow region, and studied particle sizes and composition. Their results showed low temporal variation  
1112 in estimated optical properties for each site but considerable differences among the African, Central Asian, and Arctic regions.  
1113 An insignificant difference was found between the K-feldspar relative abundances, indicating comparable ice-nucleation  
1114 abilities. The mixing state between calcium and iron compounds differed for near-source and transport regimes, potentially  
1115 and partially due to size-sorting effects. Thus, in certain situations (high acid availability, limited time), atmospheric processing  
1116 of the dust is expected to lead to less iron solubility for near-source dust (for Central Asian ones) than for transported ones  
1117 (particularly those of Sahelian origin).

1118 In the southern part, under certain meteorological conditions, dust from lower latitudes can be transported far toward polar  
1119 regions. Such was the case when a massive dust storm formed over Australia on 22 January 2020. Two days later, dust moved  
1120 southward, covering a large part of Antarctica's eastern coast. The RHMSS global version of the DREAM model with  
1121 incorporated ice nucleation parameterization due to dust (Nickovic et al., 2016) predicted the formation of cold clouds over  
1122 the Antarctic. This ice cloud phase was also documented by NASA satellite observations (Fig. 16). The simulation was part of  
1123 a WMO SDS-WAS initiative to include dust impacts on high latitudes in its agenda to better understand the role of mineral  
1124 dust as a climate factor at high latitudes.

1125

NMME–DREAM forecast:  $\log_{10}(\text{IN})$  (IN #/lit) Ullrich  
Valid time: 24JAN2020 21UTC



1126

1127 **Figure 16. Global NMME DREAM model experiments over Australia and the South Pole. Model dust load 22 January 2020; B)**  
1128 **Model  $\log_{10}$  (vertical load of ice nuclei number) (left). NASA MODIS ice cloud phase for 24 January 2020 (right).**

1129

1130 The McMurdo Dry Valleys (MDV) were previously assumed to be a significant regional source of dust (e.g., Bullard, 2016).  
1131 New observations show otherwise. Instead, the McMurdo Ice Shelf's (sometimes called the McMurdo debris bands) debris-  
1132 covered surface is the major dust source. In this study, more details are provided to underline the importance and estimates of  
1133 the size of the areas. The MDV (4 800 km<sup>2</sup>) was estimated to fit Category 3 best. Despite active local aeolian sediment transport  
1134 with many annual occurrences, they are an insignificant source or exporter of dust regionally, thus having only a small but  
1135 poorly known climatic or environmental significance. The MDV are changing quickly with increased ablation, meltwater, and  
1136 permafrost incision, so their importance regarding dust generation may change in the near future. The McMurdo Ice shelf  
1137 "debris bands" fit Category 2 best. Although it is only about 1500 km<sup>2</sup>, the McMurdo Ice shelf is clearly the region's largest  
1138 and most important dust source—active with a continuous supply of new sediment for export and exposed to frequent strong  
1139 winds (with many events during the year), although few have been documented. The aeolian sediment impacts sea ice albedo  
1140 (not directly measured) and marine sedimentation, contributing enough dissolved Fe to potentially support up to 15% of  
1141 primary productivity in the SW Ross Sea (Winton et al., 2014).



1142 Ice core studies from Antarctica ice sheets show that Antarctica receives long-range dust transport from Australia, South  
1143 America, South Africa, and New Zealand (e.g., Bullard, 2016). However, several studies around coastal areas have shown that  
1144 locally, Antarctic sourced dust accumulation rates are at least two orders of magnitude higher than that recorded from the polar  
1145 plateau or global dust models (Chewings et al., 2014; Winton et al., 2014).

#### 1146 **4 Conclusions and outlook**

1147 This study aimed to identify new HLD sources with the focus on their potential climatic and environmental impacts. A  
1148 literature survey on impacts and model calculations on emission, transport and deposition were made to investigate the local,  
1149 regional, and global significance of the HLD sources. We identified 64 new HLD sources. We estimated that in the high  
1150 latitudes, the land area with higher ( $SI \geq 0.5$ ), very high ( $SI \geq 0.7$ ), and the highest potential ( $SI \geq 0.9$ ) for dust emission cover  $>1$   
1151  $670\,000\text{ km}^2$ ,  $>560\,000\text{ km}^2$ , and  $>240\,000\text{ km}^2$ , respectively. These estimations agree with the first HLD sources' estimate of  
1152 an area  $>500\,000\text{ km}^2$  by Bullard et al. (2016), which mainly included the sources with a very high potential for dust emission,  
1153 as classified in this study. Our study shows that active sources cover a significantly larger area, confirmed by over 60 new  
1154 HLD sources with evidence of their dust activity, which is not limited to dry areas. The potential HLD emission areas need  
1155 proof of observed and identified HLD emission sources.

1156 Our modeling results on spatial distribution of the dust sources showed evidence supporting a northern High Latitude Dust  
1157 (HLD) belt, defined as the area north of  $50^\circ\text{N}$ , with a "transitional HLD-source area," extending at latitudes  $50\text{--}58^\circ\text{N}$  in  
1158 Eurasia,  $50\text{--}55^\circ\text{N}$  in Canada, and a "cold HLD-source area," including areas north of  $60^\circ\text{N}$  in Eurasia and north of  $58^\circ\text{N}$  in  
1159 Canada, with currently "no dust source" area between the HLD and LLD dust belt, except for British Columbia. Using the  
1160 global atmospheric transport model SILAM, we estimated that 1.0% of the global dust emission originated from the high-  
1161 latitude regions. About 57% of the dust deposition on snow and the ice-covered Arctic regions came from HLD sources.

1162 Our update provides crucial information on the extent of active HLD sources and their locations. Active HLD sources as  
1163 essential sources of aerosols that directly and indirectly affect climate and the environment in remote regions are often poorly  
1164 understood and predicted. HLD is likely a significant source of atmospheric iron deposition in the Southern Ocean encircling  
1165 Antarctica. More research is needed to quantify the deposition flux of HLD and nutrient (Fe, P, and trace metals such as Co)  
1166 content and solubility, which can then be fed to ocean biogeochemical models to quantify their impact on ocean  
1167 biogeochemistry. HLD is also an active ice-nucleating particle changing cloud properties, which has severe consequences  
1168 when deposited within the cryosphere. However, more studies are needed for HLD from different regions. For example,  
1169 Northern Asia HLD sources are assumed to be numerous but are difficult to access and gain information from. Such points to  
1170 the following main action items for monitoring dust in high latitudes:

1171 · Firstly, the work on HLD sources needs a multidisciplinary combination of field, laboratory, and experimental work;  
1172 remote sensing; and emission, transport and deposition modeling. An increase in observational and modeling studies  
1173 improves HLD monitoring and predicting.

1174 · Secondly, the activity of the currently identified active sources should be followed and reevaluated in the coming  
1175 years and decades.

1176 · Thirdly, research gaps and future research directions essentially include finding, identifying, and characterizing new  
1177 dust sources. As soon as there is evidence of finding a new HLD source, it should be included in the list of dust sources  
1178 and subject to further study.

1179 · Fourthly, the role of different types of road dust in the Arctic could be separately assessed using a standard  
1180 methodology.

1181 Namely, in Arctic communities, road dust as a signature of non-exhaust traffic dust formed via the abrasion and wearing down  
1182 of pavement, traction control materials, vehicle brakes, and tires is a common concern (e.g., Kupiainen et al., 2016; Nordic  
1183 Council of Ministers, 2017). This paper excluded this type of road dust and only included significant anthropogenic road dust  
1184 sources where unpaved roads are a substantial dust source. Unpaved areas of parking lots, storage areas, road shoulders,  
1185 roadside lawn dust, and winter's effects could be considered, too. During winter's cold and wet conditions, dust accumulates  
1186 in snow and ice and the humid road surface texture. As snow and ice melt and street surfaces dry up in spring, high amounts  
1187 of dust become available for suspension. For example, in Finland, north of 60°N, a major anthropogenic dust source comes  
1188 from sand and gravel uptake for building purposes from ridges formed during the Ice Age. These nonrenewable ridges cover  
1189 1.5 million ha. Since 1960, it has been estimated that approximately 40 million tons per year have been utilized (Fig. 211 of  
1190 Wahlström et al., 1996). These open-sand areas are visible in aircraft photos and satellite images. In Finland, long-range  
1191 transported low latitude dust contributes to the dust amounts, too (e.g., Meinander et al., 2021). Another health-significant  
1192 anthropogenic springtime dust source is wintertime pavement traction sanding (Kuhns et al., 2010; Kupiainen, 2007;  
1193 Stojiljkovic et al., 2019). These springtime dust events are annual but local throughout the country. In comparison, the Moscow  
1194 metropolitan area (55°45'N, 37°37'E) is one of the most significant sources of dust at latitudes above 50° N, where dust's  
1195 impact can extend over several hundred kilometers (Adzhiev et al., 2017). Moscow's road dust is mainly generated on paved  
1196 roads, but roadside soils also contribute (Kasimov et al., 2020). Most often, unsealed soils are covered with lawns and are  
1197 widespread in parks and recreational and industrial zones, characterized by heavy pollution, mixed upper horizon, and a high  
1198 degree of soil cover heterogeneity.

1199 This paper aimed to contribute beyond the state-of-the-art of HLD sources by focusing on collecting and providing information  
1200 on the geographical distribution of dust-productive soils and potential dust sources. This is some of the most important

1201 information that is currently lacking but is necessary to perform successful long-range transport and deposition modeling. The  
1202 information on the geographical distribution of dust-productive soils needs evidence and verification on detected dust events  
1203 and is insufficient alone. Therefore, the paper focused on identifying new dust sources, clarifying their climatic and  
1204 environmental importance, and using emission, long-range transport and deposition modeling to study where the potential  
1205 impact areas of the HLD sources are. Our results suggest that future HLD studies should include and update sources within  
1206 the here defined high latitude dust belt, i.e, at 50–58°N in Eurasia and 50–55°N in Canada, and at >60°N in Eurasia and >58°N  
1207 in Canada, as well as sources in the periphery of these regions, especially if sources are highly elevated (Wang et al. 2016).

1208 Icelandic sources have shown that each source, even if nearby, may have different particle size distributions and optical  
1209 properties. A detailed specification of the geographic distribution of potential dust productive soils, verified dust sources, and  
1210 their physical (e.g., particle size distribution, optics, etc.) and mineralogical/chemical (e.g., mineral fractions, chemical  
1211 composition, etc.) properties can contribute to the various topics: predicting dust forecasts (e.g., health protection warnings  
1212 during extreme events); long-range emission, transport and deposition modeling; dust monitoring control; understanding  
1213 extreme and rare events; Arctic protection; aviation control; health; tourist boards; assessing climate, environment, and air  
1214 quality (e.g., Arctic Council Arctic Monitoring and Assessment Program AMAP, and Intergovernmental Panel on Climate  
1215 Change IPCC reports); and implementing HLD in calculations on direct and indirect radiative forcing, including cloud  
1216 formation, cryospheric effects, and modeling the impacts. The new observations in this study improved the representation of  
1217 HLD sources for various approaches and applications related to the observed current, previous, and future environmental  
1218 changes at high latitudes.

1219 In summary, establishing continuous monitoring of HLD sources and their future changes is key to understanding the climatic  
1220 and environmental effects at high latitudes, especially in the Arctic. Climate change causes permafrost thaw, decreases snow  
1221 cover duration, and increases drought, glacial melt, and heatwave intensity and frequency – all leading to increasing the  
1222 frequency of topsoil conditions favorable for dust emission (increasing soil’s exposure to wind erosion) and the probability of  
1223 dust storms. Although dust originates from natural soils, dust sources are also influenced by human activities, e.g., when  
1224 deforestation and land management in cold regions leads to ecosystem collapse and desertification (Prospero et al., 2012;  
1225 Arnalds, 2015). Dust storms from agricultural fields (as reported, e.g., in Poland) can reach distances over 300 km, drastically  
1226 reducing visibility and resulting in hundreds of car accidents and fatalities (Hojan et al., 2019). Whether natural or  
1227 anthropogenic, wildfires can result from new dust sources also (Miller et al., 2012). Hence, human actions can positively and  
1228 negatively influence HLD and its effects. To understand and assess the temporal activity changes in HLD sources and the  
1229 multiple impacts of high-latitude dust on the Earth systems over time, continuous monitoring and regular updates on location,  
1230 particle properties, and activities of current and new HLD sources are needed.

1231

1232

1233

1234 **Competing interests.** The authors declare they have no conflict of interest.

1235 **Special issue statement.** This article is part of the special issue “Arctic climate, air quality, and health impacts from short-  
1236 lived climate forcers (SLCFs): contributions from the AMAP Expert Group (ACP/BG inter-journal SI)”. It is not associated  
1237 with a conference.

## 1238 **Acknowledgements**

1239 This paper was developed as part of the Arctic Monitoring and Assessment Programme (AMAP), AMAP 2021 assessment:  
1240 Arctic climate, air quality, and health impacts from short-lived climate forcers (SLCFs). We are grateful to the anonymous  
1241 referees whose comments have been most valuable and have greatly improved our manuscript. Kaarle Kupiainen, Johanna  
1242 Ikävalko, and Terhikki Manninen are gratefully acknowledged. The staff’s help regarding the stations is highly appreciated.

## 1243 **Financial support**

1244 This research has been supported by the Ministry for Foreign Affairs of Finland (IBA-project No. PC0TQ4BT-25). The study  
1245 of dust composition in Moscow and Tiksi was supported by the Russian Science Foundation (No. 19-77-30004). Firm cores  
1246 collection on southern Spitsbergen, Svalbard, has been co-funded by the Research Council of Norway, Arctic Field Grant 2018  
1247 (No. 282538), funds of the Leading National Research Centre (KNOW) received by the Centre for Polar Studies of the  
1248 University of Silesia, and statutory activities No. 3841/E-41/S/2018 of the Ministry of Science and Higher Education of Poland.  
1249 The Czech Science Foundation projects 20-06168Y, GA20-20240S, and the Ministry of Education, Youth and Sports of the  
1250 Czech Republic projects No. LM2015078 and CZ.02.1.01/0.0/0.0/16\_013/0001708 are acknowledged. The support of the  
1251 EPOS-PL project (No. POIR.04.02.00-14-A003/16), co-financed by the European Union from the funds of the European  
1252 Regional Development Fund (ERDF) to the laboratory facilities at IG PAS used in the study, is also acknowledged. European  
1253 Union COST Action InDust is acknowledged. The preparation of this paper was partially funded by the Icelandic Research  
1254 Fund (Rannis) Grant No. 207057-051. O. Meinander acknowledges funding from the Academy of Finland (ACCC Flagship  
1255 funding grant No. 337552 and BBrCAC No. 341271), H2020 EU-Interact (No. 730938), International Arctic Science  
1256 Committee (IASC Cross-Cutting grant), and the Ministry for Foreign Affairs of Finland (IBA-project No. PC0TQ4BT-20). D.  
1257 Frolov is thankful to Lomonosov Moscow State University (state topic “Danger and risk of natural processes and phenomena”  
1258 No. 121051300175-4). K. Kandler was funded by the Deutsche Forschungsgemeinschaft (DFG, German Research Foundation  
1259 No. 264912134, 416816480, 417012665N). J. King acknowledges NSERC Discovery 2016-05417, CFI 36564, and the CMN  
1260 RES00044975. B. Murray, A. Sanchez-Marroquin, and S. Barr thank the European Research Council (648661 MarineIce) and  
1261 the Natural Environment Research Council (NE/T00648X/1; NE/R006687/1). O. Möhler and N.S. Umo acknowledge the

1262 funding support from Helmholtz Association of German Research Centres through its ‘Changing Earth — Sustaining our  
1263 Future’ Programme. M. Kulmala, N.S. Kasimov, and O. Popovicheva acknowledge funding from the Russian Ministry of  
1264 Education and Science (075-15-2021-574). K. Ranjbar and N.T. O’Neill acknowledge the PAHA project (NSERC-CCAR  
1265 program; RGPCC-433842-2012), the SACIA project (CSA-ESSDA program; 16UASACIA), and the NSERC DG grants of  
1266 O’Neill (RGPIN-05002-2014). I. Semenov, O. Popovicheva, and N. Kasimov acknowledge funding from the M.V.  
1267 Lomonosov Moscow State University (the Interdisciplinary Scientific and Educational School «Future Planet and Global  
1268 Environmental Change» and project No. 121051400083-1). Z. Shi and C. Baldo are funded by the UK Natural Environment  
1269 Research Council (NE/L002493/1; NE/S00579X).

1270

## 1271 **Supplement**

1272 The supplement related to this article is available online at:

1273

## 1274 **Data availability**

1275 Data are mostly included in this article or available on request via personal communication.

1276

## 1277 **Author contribution**

1278 The paper was initiated and lead by O. Meinander. P. Dagsson-Waldhauserová co-coordinated and edited. HLD SI and area  
1279 calculations were by A. Vukovic and B. Cvetkovic. New HLD sources were identified as follows: Alaska, Canada: S. Barr, P.  
1280 Dagsson-Waldhauserová, P., S. Gassó, J. King, B.J. Murray, J.B. McQuaid, N.T. O’Neill, K. Ranjbar. Antarctica: P. Dagsson-  
1281 Waldhauserová, J. Kavan, K. Láska, O. Meinander, E. Shevnina. Denmark and Sweden: O. Meinander. Greenland: A.  
1282 Baklanov, L.G. Benning, P. Dagsson-Waldhauserová, S. Gassó. Iceland: T. Thorsteinsson. Russia: P. Amosov, A. Baklanov,  
1283 P. Enchilik, T. Koroleva, V. Krupskaya, O. Popovicheva, A. Sharapova, I. Semenov, M. Timofeev. Svalbard: B. Barzycka,  
1284 M. Kusiak, M. Laska, M. Lewandowski, B. Luks, A. Nawrot, T. Werner, K. Kandler, N. S. Umo, B.J. Murray, J.B. McQuaid,  
1285 A. Sánchez-Marroquín, O. Möhler. South America, Argentina, and Patagonia: S. Gassó. DREAM model: B. Cvetkovic, S.  
1286 Nickovic. SILAM model: A. Uppstu and M. Sofiev. N. Kasimov, E. Aseyeva, and O. Samonova contributed supplementary  
1287 material on the central part of European Russia (potential dust source). Dust and clouds: B.J. Murray and A. Sánchez-  
1288 Marroquín. Dust and ocean biogeochemistry: Z. Shi and C. Baldo. Dust and atmospheric chemistry: F. Thevenet, M.N.  
1289 Romanias, J.Lasne, D. Urupina. Dust and cryosphere: O. Meinander. All authors contributed significantly to preparing the  
1290 manuscript.

1291

## 1292 **References**

1293 Abbatt, J. P. D., Leaitch, W. R., Aliabadi, A. A., Bertram, A. K., Blanchet, J.-P., Boivin-Rioux, A., Bozem, H., Burkart, J.,  
1294 Chang, R. Y. W., Charette, J., Chaubey, J. P., Christensen, R. J., Cirisan, A., Collins, D. B., Croft, B., Dionne, J., Evans, G. J.,  
1295 Fletcher, C. G., Galí, M., Ghahremaninezhad, R., Girard, E., Gong, W., Gosselin, M., Gourdal, M., Hanna, S. J., Hayashida,  
1296 H., Herber, A. B., Hesarakı, S., Hoor, P., Huang, L., Hussherr, R., Irish, V. E., Keita, S. A., Kodros, J. K., Köllner, F., Kolonjari,  
1297 F., Kunkel, D., Ladino, L. A., Law, K., Levasseur, M., Libois, Q., Liggio, J., Lizotte, M., Macdonald, K. M., Mahmood, R.,  
1298 Martin, R. V., Mason, R. H., Miller, L. A., Moravek, A., Mortenson, E., Mungall, E. L., Murphy, J. G., Namazi, M., Norman,  
1299 A.-L., O'Neill, N. T., Pierce, J. R., Russell, L. M., Schneider, J., Schulz, H., Sharma, S., Si, M., Staebler, R. M., Steiner, N. S.,  
1300 Thomas, J. L., von Salzen, K., Wentzell, J. J. B., Willis, M. D., Wentworth, G. R., Xu, J.-W., and Yakobi-Hancock, J. D.:  
1301 Overview paper: New insights into aerosol and climate in the Arctic, *Atmos. Chem. Phys.*, 19, 2527–2560, doi:10.5194/acp-  
1302 19-2527-2019, 2019.

1303 Achterberg, E. P., Moore, C. M., Henson, S. A., Steigenberger, S., Stohl, A., Eckhardt, S., Avendano, L. C., Cassidy, M.,  
1304 Hembury, D., Klar, J. K., Lucas, M. I., Macey, A. I., Marsay, C. M., and Ryan-Keogh, T. J.: Natural iron fertilization by the  
1305 Eyjafjallajökull volcanic eruption, *Geophysical Research Letters*, 40, 921-926, doi: 10.1002/grl.50221, 2013.

1306 Achterberg, E. P., Steigenberger, S., Marsay, C. M., LeMoigne, F. A. C., Painter, S. C., Baker, A. R., Connelly, D. P., Moore,  
1307 C. M., Tagliabue, A., and Tanhua, T.: Iron Biogeochemistry in the High Latitude North Atlantic Ocean, *Scientific Reports*, 8,  
1308 doi: 10.1038/s41598-018-19472-1, 2018.

1309 Adzhiev, A. H., Bartalyov, S. A., Bekkiev, M. Y., Biryukov, M. V., Biryukova, O. N., Bitjukova, V. R., Bobylev, S. N.,  
1310 Bogdanova, M. D., Bozhilina, E. A., Bronnikova, V. K., et al.: Ecological atlas of Russia, Feoria, Moscow, 510 p., 2017.

1311 AMAP: Black Carbon and Ozone as Arctic Climate Forcers. Arctic Monitoring and Assessment Programme (AMAP), Oslo,  
1312 116, 2015.

1313 Amino, T., Y. Iizuka, S. Matoba, R. Shimada, N. Oshima, T. Suzuki, T. Ando, T. Aoki, and K. Fujita: Increasing dust emission  
1314 from ice free terrain in southeastern Greenland since 2000, *Polar Science*, 100599, doi:10.1016/j.polar.2020.100599, 2020.

1315 Amosov P.V. and Baklanov A.A.: Assessment of dusting intensity on ANOF-2 tailing by using a Westphal D.L. dependency  
1316 // Proceedings of the X International Symposium on Recycling Technologies and Sustainable Development, 4-7 November  
1317 2015, Bor, Serbia. – Bor: University of Belgrade, Technical Faculty, 39-43, 2015.

1318 Anderson, N. J., J. E. Saros, J. E. Bullard, S. M. P. Cahoon, S. McGowan, E. A. Bagshaw, C. D. Barry, R. Bindler, B. T.  
1319 Burpee, J. L. Carrivick, et al.: The Arctic in the twenty-first century: Changing biogeochemical linkages across a paraglacial  
1320 landscape of Greenland. *BioScience*, 67, 118–133, doi:10.1093/biosci/biw158, 2017.

- 1321 Antcibor, I., Eschenbach, A., Zubrzycki, S., Kutzbach, L. et al: Trace metal distribution in pristine permafrost-affected soils  
1322 of the Lena River delta and its hinterland, northern Siberia, Russia. *Biogeosciences* 11:1–15, 2014.
- 1323 Arnalds O.: *The Soils of Iceland*. World Soils Book Series, Springer, Dordrecht, The Netherlands, 2015.
- 1324 Arnalds, O., Thorarinsdottir, E.F., Thorsson, J., Dagsson-Waldhauserová, P., Agustsdottir, A.M.: An extreme wind erosion  
1325 event of the fresh Eyjafjallajökull 2010 volcanic ash. *Nature Scientific Reports* 3, 1257, 2013.
- 1326 Arnalds, O., Olafsson, H., and Dagsson-Waldhauserová, P.: Quantification of iron-rich volcanogenic dust emissions and  
1327 deposition over the ocean from Icelandic dust sources, *Biogeosciences*, 11, 6623–6632, doi: 10.5194/bg-11-6623-2014, 2014.
- 1328 Arnalds, O., Dagsson-Waldhauserová, P., and Olafsson, H.: The Icelandic volcanic aeolian environment: Processes and  
1329 impacts — A review, *Aeolian Res.*, 20, 176–195, doi: 10.1016/j.aeolia.2016.01.004, 2016.
- 1330 Arrigo, K. R., and Van Dijken, G. L.: Interannual variation in air-sea CO<sub>2</sub> flux in the Ross Sea, Antarctica: A model analysis,  
1331 *Journal of Geophysical Research-Oceans*, 112, doi: 10.1029/2006jc003492, 2007.
- 1332 Arrigo, K. R., van Dijken, G., and Long, M.: Coastal Southern Ocean: A strong anthropogenic CO<sub>2</sub> sink, *Geophysical Research*  
1333 *Letters*, 35, doi: 10.1029/2008gl035624, 2008.
- 1334 Atkins, C.B., and Dunbar, G. B. Aeolian sediment flux from sea ice into Southern McMurdo Sound, Antarctica, *Global and*  
1335 *Planetary Change*, 69, 133–141, 2009.
- 1336 Atkinson, J. D., B. J. Murray, M. T. Woodhouse, T. F. Whale, K. J. Baustian, K. S. Carslaw, S. Dobbie, D. O’Sullivan, and T.  
1337 L. Malkin, The importance of feldspar for ice nucleation by mineral dust in mixed-phase clouds, *Nature*, 498, 7454, 355–358,  
1338 doi:10.1038/nature12278, 2013.
- 1339 Aun, M., Lakkala, K., Sanchez,R., Asmi, E., Nollas, F., Meinander, O., Sogacheva, L., De Bock, V., Arola, A., de Leeuw, G.,  
1340 Aaltonen, V., Bolsée, D., Cizkova, K, Mangold, A., Metelka,L., Jakobson, E., Svendby,T., Gillotay, D., and Van Opstal, B.:  
1341 Solar UV radiation measurements in Marambio, Antarctica, during years 2017–2019, *Atmos. Chem. Phys.*, 20, 6037–6054,  
1342 doi:10.5194/acp-20-6037-2020, 2020.
- 1343 Ayling, B. F. and McGowan, H.A.: Niveo-eolian sediment deposits in coastal South Victoria Land, Antarctica: Indicators of  
1344 regional variability in weather and climate, *Arc. Antarct. Alp. Res.*, 38, 3, 313–324, 2006.
- 1345 Bachelder, J., Cadieux, M., Liu-Kang, C., Lambert, P., Filoche, A., Aparecida Galhardi, J., Hadioui, M., Chaput, A., Bastien-  
1346 Thibault, M.-P., Wilkinson, K.J., King, J., and Hayes, P.J.: Chemical and microphysical properties of wind-blown dust near

1347 an actively retreating glacier in Yukon, Canada. *Aerosol Science and Technology* 54:1, 2-20, doi:  
1348 10.1080/02786826.2019.1676394, 2020.

1349 Baddock, M., Mockford, T., Bullard, J.E., and Thorsteinsson, Th.: Pathways of high-latitude dust in the North Atlantic. *Earth*  
1350 *and Planetary Science Letters*, 459: 170 – 182. doi: 10.1016/j.epsl.2016.11.034, 2017.

1351 Baklanov A. and Rigina O. Environmental modeling of dusting from the mining and concentration sites in the Kola Peninsula,  
1352 Northwest Russia. The XI World Clear Air and Environment Congress, 14-18 September 1998, Durban, South Africa,  
1353 IUAPPA-NACA. Durban, v. 1, 4F-3, 1-18, 1998.

1354 Baklanov, A., A. Mahura, L. Nazarenko, N. Tausnev, A Kuchin, and O. Rigina: Modelling of atmospheric Pollution and  
1355 Climate Change in Northern Latitudes. Russian Academy of Sciences, Apatity, Russia, 106 p. Book in Russian,  
1356 <https://search.rsl.ru/ru/record/01006534167>, 2012.

1357 Baldo, C., Formenti, P., Nowak, S., Chevaillier, S., Cazaunau, M., Pangui, E., Di Biagio, C., Doussin, J.-F., Ignatyev, K.,  
1358 Dagsson-Waldhauserová, P., Arnalds, O., MacKenzie, A. R., and Shi, Z.: Distinct chemical and mineralogical composition of  
1359 Icelandic dust compared to northern African and Asian dust, *Atmos. Chem. Phys.*, 20, 13521–13539, doi:10.5194/acp-20-  
1360 13521-2020, 2020.

1361 Baratoux, D., Mangold, N., Arnalds, O., Bardintzeff, J.-M., Platevoët, B., Grégoire, M. and Pinet, P.: Volcanic sands of Iceland  
1362 - Diverse origins of aeolian sand deposits revealed at Dyngjúsandur and Lambahraun. *EARTH SURFACE PROCESSES AND*  
1363 *LANDFORMS Earth Surf. Process. Landforms*, doi: 10.1002/esp.2201, 2011.

1364 Beckett, F., Kylling, A., Sigurðardóttir, G., von Löwis, S., and Witham, C.: Quantifying the mass loading of particles in an ash  
1365 cloud remobilized from tephra deposits on Iceland, *Atmos. Chem. Phys.*, 17, 4401-4418, 2017.

1366 Bertran P, Bosq, M., Quentin Borderie, Coussot, C., Coutard, S., Deschodt, L., Franc, O., Gardère, P., Liard, M., and Wuscher,  
1367 P.: Revised map of European aeolian deposits derived from soil texture data, *Quaternary Science Reviews*, 266, 107085,  
1368 doi:10.1016/j.quascirev.2021.107085, 2021.

1369 Bhattachan, A., L. Wang, M. F. Miller, K. J. Licht, and P. D’Odorico: Antarctica’s Dry Valleys: A potential source of soluble  
1370 iron to the Southern Ocean?, *Geophys. Res. Lett.*, 42, 1912–1918, doi:[10.1002/2015GL063419](https://doi.org/10.1002/2015GL063419), 2015.

1371 Bishop, J. K. B., Davis, R. E., and Sherman, J. T.: Robotic observations of dust storm enhancement of carbon biomass in the  
1372 North Pacific. *Science*, doi:[10.1126/science.1074961](https://doi.org/10.1126/science.1074961), 2002.



- 1373 Bodas-Salcedo, A., K. D. Williams, M. A. Ringer, I. Beau, J. N. S. Cole, J. L. Dufresne, T. Koshiro, B. Stevens, Z. Wang, and  
1374 T. Yokohata: Origins of the Solar Radiation Biases over the Southern Ocean in CFMIP2 Models, *J. Clim.*, 27, 1, 41-56,  
1375 doi:10.1175/jcli-d-13-00169.1, 2014.
- 1376 Bond, T. C., Doherty, S. J., Fahey, D. W., Forster, P. M., Berntsen, T., DeAngelo, B. J., et al.: Bounding the role of black  
1377 carbon in the climate system: a scientific assessment. *J. Geophys. Res. Atmos.* 188, 5380–5552, doi: 10.1002/jgrd.50171,  
1378 2013.
- 1379 Boy, M., Thomson, E. S., Acosta Navarro, J.-C., Arnalds, O., Batchvarova, E., Bäck, J., Berninger, F., Bilde, M., Brasseur,  
1380 Z., Dagsson-Waldhauserová, P., Castarède, D., Dalirian, M., de Leeuw, G., Dragosics, M., Duplissy, E.-M., Duplissy, J.,  
1381 Ekman, A. M. L., Fang, K., Gallet, J.-C., Glasius, M., Gryning, S.-E., Grythe, H., Hansson, H.-C., Hansson, M., Isaksson, E.,  
1382 Iversen, T., Jonsdottir, I., Kasurinen, V., Kirkevåg, A., Korhola, A., Krejci, R., Kristjansson, J. E., Lappalainen, H. K., Lauri,  
1383 A., Leppäranta, M., Lihavainen, H., Makkonen, R., Massling, A., Meinander, O., Nilsson, E. D., Olafsson, H., Pettersson, J.  
1384 B. C., Prisle, N. L., Riipinen, I., Roldin, P., Ruppel, M., Salter, M., Sand, M., Seland, Ø., Seppä, H., Skov, H., Soares, J., Stohl,  
1385 A., Ström, J., Svensson, J., Swietlicki, E., Tabakova, K., Thorsteinsson, T., Virkkula, A., Weyhenmeyer, G. A., Wu, Y., Zieger,  
1386 P., and Kulmala, M.: Interactions between the atmosphere, cryosphere, and ecosystems at northern high latitudes, *Atmos.*  
1387 *Chem. Phys.*, 19, 2015–2061, <https://doi.org/10.5194/acp-19-2015-2019>, 2019.
- 1388 Boyd, P. W., Jickells, T., Law, C. S., Blain, S., Boyle, E. A., Buesseler, K. O., Coale, K. H., Cullen, J. J., de Baar, H. J. W.,  
1389 Follows, M., Harvey, M., Lancelot, C., Levasseur, M., Owens, N. P. J., Pollard, R., Rivkin, R. B., Sarmiento, J., Schoemann,  
1390 V., Smetacek, V., Takeda, S., Tsuda, A., Turner, S., and Watson, A. J.: Mesoscale Iron Enrichment Experiments 1993-2005:  
1391 Synthesis and Future Directions, *Science*, 315, 612-617, doi: 10.1126/science.1131669, 2007.
- 1392 Boyd, P. W., Mackie, D. S., and Hunter, K. A.: Aerosol iron deposition to the surface ocean - Modes of iron supply and  
1393 biological responses, *Mar. Chem.*, 120, 128-143, doi: 10.1016/j.marchem.2009.01.008, 2010.
- 1394 Brabets, T P.: Geomorphology of the lower Copper River, Alaska I by Timothy P. Brabets, U.S. Geological Survey  
1395 professional paper, 1581, <https://pubs.usgs.gov/pp/1581/report.pdf>, 1997.
- 1396 Brédoire, F., Bakker, M.R., Augusto, L., Barsukov, P.A., Derrien, D., Nikitich, P., Rusalimova, O., Zeller, B., Acha, D.L.:  
1397 What is the P value of Siberian soils? *Biogeosci Discuss* 12:19819–19859, 2015.
- 1398 Bullard, J. E.: The distribution and biogeochemical importance of high-latitude dust in the Arctic and Southern Ocean-  
1399 Antarctic regions, *Journal of Geophysical Research-Atmospheres*, 122, 3098-3103, doi: 10.1002/2016jd026363, 2016.

- 1400 Bullard J. and Austin, M.J.: Dust generation on a proglacial floodplain, West Greenland Article in *Aeolian Research* · June  
1401 2011, doi: 10.1016/j.aeolia.2011.01.002, 2011.
- 1402 Bullard, J.E. and Mockford, T.: Seasonal and decadal variability of dust observations in the Kangerlussuaq area, west  
1403 Greenland, Arctic, Antarctic, and Alpine Research, 50:1, S100011, doi: 10.1080/15230430.2017.1415854, 2018.
- 1404 Bullard, J.E., Harrison, S.P., Baddock, M.C., Drake, N., Gill, T.E., McTainsh, G. and Sun, Y.: Preferential dust sources: A  
1405 geomorphological classification designed for use in global dust-cycle models. *Journal of Geophysical Research* 116, doi:  
1406 10.1029/2011JF002061, issn: 0148-0227, 2011.
- 1407 Bullard, J. E., Baddock, M., Bradwell, T., Crusius, J., Darlington, E., Gaiero, D., ... McCulloch, R.: High-latitude dust in the  
1408 Earth system. *Reviews of Geophysics*, 54, 2, 447–485, 2016.
- 1409 Butwin, M.K., Pfeffer, M.A., von Löwis, S., Støren, E., W.N., Bali, E. and Thorsteinsson, T.: Properties of dust source material  
1410 and volcanic ash in Iceland, *Sedimentology*, 67, 6, 3067-3087, doi:10.1111/sed.12734, 2020.
- 1411 Chewings, J., Atkins, C, Dunbar, G., and Golledge, N.: Aeolian sediment transport and deposition in a modern high latitude  
1412 glacial marine environment. *Sedimentology*, v. 61, 6, 1485–1882, doi: 10.1111/sed.12108, 2014.
- 1413 Conca, E., Abollino, O., Giacomino, A., Buoso, S., Traversi, R., Becagli, S., Grotti, M., and Malandrino, M.: Source  
1414 identification and temporal evolution of trace elements in PM10 collected near to Ny-Ålesund (Norwegian Arctic), *Atmos.*  
1415 *Environ.*, 203, 153–165, doi:10.1016/j.atmosenv.2019.02.001, 2019.
- 1416 Coronato, A., Mazzoni, E., Vázquez, M., and Coronato, F.: PATAGONIA Una síntesis de su Geografía Física (Ediciones).  
1417 Río Gallegos, Argentina: Universidad Nacional de la Patagonia Austral. Retrieved from  
1418 [http://www.unpa.edu.ar/sites/default/files/publicaciones\\_adjuntos/PATAGONIA\\_una\\_sintesis\\_de\\_su\\_geografia\\_fisica](http://www.unpa.edu.ar/sites/default/files/publicaciones_adjuntos/PATAGONIA_una_sintesis_de_su_geografia_fisica_web_0.pdf)  
1419 [web\\_0.pdf](http://www.unpa.edu.ar/sites/default/files/publicaciones_adjuntos/PATAGONIA_una_sintesis_de_su_geografia_fisica_web_0.pdf), 2017.
- 1420 Cosentino, N. J., Ruiz-Etcheverry, L. A., Bia, G. L., Simonella, L. E., Coppo, R., Torre, G., et al. Does Satellite Chlorophyll-  
1421 a Respond to Southernmost Patagonian Dust? A Multi-year, Event-Based Approach. *Journal of Geophysical Research:*  
1422 *Biogeosciences*, 125, 12, doi:10.1029/2020JG006073, 2020.
- 1423 Creamean, J.M., Suski, K.J., Rosenfeld, D., Cazorla, A., DeMott, P.J., Sullivan, R.C., White, A.B., Ralph, F.M., Minnis, P.,  
1424 Comstock, J.M., Tomlinson, J.M., Prather, K.A.: Dust and biological aerosols from the Sahara and Asia influence precipitation  
1425 in the Western U.S., *Science*, 339, 6127, 1572-1578, doi:10.1126/science.1227279, 2013.

- 1426 Crespi-Abril, A. C., Soria, G., De Cian, A., and López-Moreno, C.: Roaring forties: An analysis of a decadal series of data of  
1427 dust in Northern Patagonia. *Atmospheric Environment*, doi:10.1016/j.atmosenv.2017.11.019, 2017.
- 1428 Crocchianti,S.; Moroni,B.; Waldhauserová, P.D.; Becagli, S.; Severi, M.; Traversi, R.; Cappelletti, D. Potential Source  
1429 Contribution Function Analysis of High Latitude Dust Sources over the Arctic: Preliminary Results and Prospects. *Atmosphere*  
1430 2021, 12, 347, doi:10.3390/atmos12030347, 2021.
- 1431 Crusius, J.: Dissolved Fe Supply to the Central Gulf of Alaska Is Inferred to Be Derived From Alaskan Glacial Dust That Is  
1432 Not Resolved by Dust Transport Models. *Journal of Geophysical Research: Biogeosciences*, 126, 6, e2021JG006323,  
1433 doi:10.1029/2021JG006323, 2021.
- 1434 Crusius, J., Schroth, A. W., Gassó, S., Moy, C. M., Levy, R. C., and Gatica, M.: Glacial flour dust storms in the Gulf of Alaska:  
1435 Hydrologic and meteorological controls and their importance as a source of bioavailable iron, *Geophysical Research Letters*,  
1436 38, doi: 10.1029/2010gl046573, 2011.
- 1437 Crusius, J., Schroth, A. W., Resing, J. A., Cullen, J., and Campbell, R. W. Seasonal and spatial variabilities in northern Gulf  
1438 of Alaska surface water iron concentrations driven by shelf sediment resuspension, glacial meltwater, a Yakutat eddy, and  
1439 dust. *Global Biogeochemical Cycles*, 31, 6, 942–960, doi:10.1002/2016GB005493, 2017.
- 1440 Csavina, J., Field, J., Taylor, M.P., Gao, S., Landázuri, A., Betterton, E.A., Sáez, A.E.: A review on the importance of metals  
1441 and metalloids in atmospheric dust and aerosol from mining operations, *Science of The Total Environment*, 433, 58-73,  
1442 doi:10.1016/j.scitotenv.2012.06.013, 2012.
- 1443 Cvetkovic, et al., 2021: Fully dynamic numerical prediction model for dispersion of Icelandic mineral dust (submitted), 2021.
- 1444 Dagsson-Waldhauserová P. and Meinander O.: Editorial: Atmosphere - cryosphere interaction in the Arctic, at high latitudes  
1445 and mountains with focus on transport, deposition and effects of dust, black carbon, and other aerosols. *Front. Earth Sci.*, 18  
1446 December 2019, <https://doi.org/10.3389/feart.2019.00337>, 2019.
- 1447 Dagsson-Waldhauserová, P. and Meinander, O. (eds.): Atmosphere – Cryosphere Interaction in the Arctic, at High Latitudes  
1448 and Mountains With Focus on Transport, Deposition and Effects of Dust, Black Carbon, and Other Aerosols. Lausanne:  
1449 Frontiers Media SA. ISSN 1664-8714, ISBN 978-2-88963-504-7, doi: 10.3389/978-2-88963-504-7, e-book, 2020.
- 1450 Dagsson-Waldhauserová, P., O. Arnalds, H. Ólafsson, L. Skrabalova, G. Sigurðardóttir, M. Branis, J. Hladil, R. Skala, T.  
1451 Navratil, L. Chadimova, S. Löwis, T. Thorsteinsson, H. Carlsen, I. Jónsdóttir, Physical properties of suspended dust during  
1452 moist and low wind conditions in Iceland. *Icelandic Agricultural Sciences* 27, 25-39, 2014.

- 1453 Dagsson-Waldhauserová, P., O. Arnalds, H. Olafsson, J. Hladil, R. Skala, T. Navratil, L. Chadimova, O. Meinander: Snow–  
1454 Dust Storm: Unique case study from Iceland, March 6–7, 2013. *Aeolian Res* 16, 69-74, 2015.
- 1455 Dagsson-Waldhauserová P, Magnúsdóttir AÖ, Olafsson H, Arnalds O: The spatial variation of dust particulate matter  
1456 concentrations during two Icelandic dust storms in 2015. *Atmosphere*, 7, 77, 2016.
- 1457 Dagsson-Waldhauserová, P., Renard, J.-B., Olafsson, H., Vignelles, D., Berthet, G., Verdier, N., Duverger, V.: Vertical  
1458 distribution of aerosols in dust storms during the Arctic winter. *Scientific Reports* 6, 1-11, 2019.
- 1459 Dang, C., Warren, S. G., Fu, Q., Doherty, S. J., Sturm, M., and Su, J.: Measurements of light-absorbing particles in snow  
1460 across the Arctic, North America, and China: Effects on surface albedo, *J. Geophys. Res. Atmos.*, 122, 10,149– 10,168,  
1461 doi:10.1002/2017JD027070, 2017.
- 1462 Diaz, M.A., Welch, S.A., Sheets, J.M., Welch, K.A., Khan, A.L., Adams, B.J., McKnight, D.M., Cary, S.C, W.B, Lyons:  
1463 Geochemistry of aeolian material from the McMurdo Dry Valleys, Antarctica: Insights into Southern Hemisphere dust sources.  
1464 *Earth and Planetary Science Letters*, 547, doi:10.1016/j.epsl.2020.116460, 2020.
- 1465 Dijkmans, J. W. A., and Törnqvist, T.E.: Modern periglacial eolian deposits and landforms in the Søndre Strømfjord area,  
1466 West Greenland and their palaeoenvironmental implications. *Meddelelser Om Grønland Geoscience*, 25, 3–39, 1991.
- 1467 Doody, J.P., Ferreira, M., Lombardo, S., Lucius, I., Misdorp, R., Niesing, H., Salman, A., and Smallegange, M. (eds): Living  
1468 with coastal erosion in Europe – sediment and space for sustainability. Results from the EUROSION study, European  
1469 Commission, Office for Official Publications of the European Communities. Available at:  
1470 [http://www.eurosion.org/project/euroasion\\_en.pdf](http://www.eurosion.org/project/euroasion_en.pdf) (last accessed 19 November 2021), 2004.
- 1471 Đorđević Dragana, Tošić Ivana, Sakan Sanja, Petrović Srđan, Đuričić-Milanković Jelena, Finger David C., Dagsson-  
1472 Waldhauserová P.: Can Volcanic Dust Suspended From Surface Soil and Deserts of Iceland Be Transferred to Central Balkan  
1473 Similarly to African Dust (Sahara)? *Frontiers in Earth Science*, 7, doi:10.3389/feart.2019.00142, 2019.
- 1474 Dragosics, M., Meinander, O., Jonsdóttir, T. et al. Insulation effects of Icelandic dust and volcanic ash on snow and ice,  
1475 *Arabian Journal of Geosciences* Volume: 9 Issue: 2, Dust special issue, DOI: 10.1007/s12517-015-2224-6, 2016.
- 1476 Dörnbrack, A., Stachlewska, I. S., Ritter, C., and Neuber, R.: Aerosol distribution around Svalbard during intense easterly  
1477 winds, *Atmos. Chem. Phys.*, 10, 1473–1490, <https://doi.org/10.5194/acp-10-1473-2010>, 2010.
- 1478 Evangelidou, N., Shevchenko, V. P., Yttri, K. E., Eckhardt, S., Sollum, E., Pokrovsky, O. S., Kobelev, V. O., Korobov, V. B.,  
1479 Lobanov, A. A., Starodymova, D. P., Vorobiev, S. N., Thompson, R. L., and Stohl, A.: Origin of elemental carbon in snow

1480 from western Siberia and northwestern European Russia during winter–spring 2014, 2015 and 2016, *Atmos. Chem. Phys.*, 18,  
1481 963–977, <https://doi.org/10.5194/acp-18-963-2018>, 2018.

1482 Finlayson-Pitts, B.J. and Pitts, J.N. Jr., *Chemistry of the upper and lower atmosphere: theory, experiments, and applications*,  
1483 Elsevier, 969 p., 1999.

1484 Flanner, M. G., Zender, C. S., Randerson, J. T., and Rasch, P. T.: Present day climate forcing and response from black carbon  
1485 in snow. *J. Geophys. Res.* 112:D11202. doi: 10.1029/2006JD008003, 2007.

1486 Foroutan, H., et al. Development and evaluation of a physics-based windblown dust emission scheme implemented in the  
1487 CMAQ modeling system, *J Adv Model Earth Syst.*,9, 1, 585–608, 2017.

1488 Forsström, S., Isaksson, E., Skeie, R. B., Ström, J., Pedersen, C. A., Hudson, S. R., Berntsen, T. K., Lihavainen, H.,  
1489 Godtliebsen, F. and Gerland, S.: Elemental carbon measurements in European Arctic snow packs, *J. Geophys. Res. Atmos.*,  
1490 118, 13,614–13,627, 2013.

1491 Fountain, A.G., Levy, J.S., Gooseff, M.N., Van Horn, D: The McMurdo Dry Valleys: A landscape on the threshold of change  
1492 (2014). *Geomorphology* 225, 15, P, 25-35, doi:/10.1016/j.geomorph.2014.03.044, 2014.

1493 Fox, T. A., Barchyn, T. E. and Hugenholtz, C. H.: Successes of soil conservation in the Canadian Prairies highlighted by a  
1494 historical decline in blowing dust, *Environ. Res. Lett.*, 7, 1, doi:10.1088/1748-9326/7/1/014008, 2012.

1495 Frey, W. R., and J. E. Kay: The influence of extratropical cloud phase and amount feedbacks on climate sensitivity, *Climate*  
1496 *Dynamics*, 50, 7, 3097-3116, doi:10.1007/s00382-017-3796-5, 2018.

1497 Gaiero, D. M., Probst, J.-L., Depetris, P. J., Bidart, S. M., and Leleyter, L.: Iron and other transition metals in Patagonian  
1498 riverborne and windborne materials: geochemical control and transport to the southern South Atlantic Ocean. *Geochimica et*  
1499 *Cosmochimica Acta*, 67, 19, 3603–3623, doi:10.1016/S0016-7037(03)00211-4, 2003.

1500 Gaitán, J. J., López, C. R., and Bran, D.: Efectos del pastoreo sobre el suelo y la vegetación en la estepa patagónica. *Ci. Suelo*  
1501 (Argentina), 27, 2, 261–270, 2009.

1502 Gallet, J.-C., Björkman, M. P., Larose, C., Luks, B., Martma, T., and Zdanowicz, C.: Protocols and recommendations for the  
1503 measurement of snow physical properties, and sampling of snow for black carbon, water isotopes, major ions and  
1504 microorganisms, *Norsk Polarinstitutt*, 27 p., 2018.

- 1505 Gardner, A. S. and Sharp, M. J.: A review of snow and ice albedo and the development of a new physically based broadband  
1506 albedo parameterization, *J. Geophys. Res.*, 115, F01009, doi: 10.1029/2009JF001444, 2010.
- 1507 Gassó, S., [twitter.com/SanGassó](https://twitter.com/SanGassó), 2 Gassó, Santiago (@SanGassó). "Sunrise in Alaska and more #highlatitudedust is visible  
1508 in Larsen Bay, just downwind from the Ten Thousand Smokes Valley in @KatmaiNPS, visible in webcams and early GOES17  
1509 image." Nov 2, 2020 , Tweet, <https://twitter.com/SanGassó/status/1323716227793997824?>, 2020a.
- 1510 Gassó, Santiago (@SanGassó)."More #highlatitudedust today in #Alaska , 3 active sources identified in #NOAA20. Surface  
1511 webcams confirm dust presence." Nov 2, 2020 , Twitter. <https://twitter.com/SanGassó/status/1323384615344640000>, 2020b.
- 1512 Gassó, Santiago (@SanGassó). "#highlatitudedust in SE Alaska yesterday several plumes are visible in the spots where there  
1513 is little snow " Jan, 27, 2021. Twitter. <https://twitter.com/SanGassó/status/1354548215186644993021>, 2021a.
- 1514 Gassó, S., [twitter.com/SanGassó](https://twitter.com/SanGassó), 2 Gassó, Santiago (@SanGassó), "A very nice example of #highlatitudedust activity in  
1515 western #Greenland", Oct 19, 2021, <https://twitter.com/SanGassó/status/1450468551379329029>, 2021b.
- 1516 Gassó, S., and Stein, A. F.: Does dust from Patagonia reach the sub-Antarctic Atlantic Ocean? *Geophysical Research Letters*,  
1517 34, 1, L01801. <https://doi.org/10.1029/2006GL027693>, 2007.
- 1518 Gassó, S., and Torres, O.: Temporal Characterization of Dust Activity in the Central Patagonia Desert (Years 1964–2017).  
1519 *Journal of Geophysical Research: Atmospheres*, 124, 6, 3417–3434, [doi:10.1029/2018JD030209](https://doi.org/10.1029/2018JD030209), 2019.
- 1520 Gassó, S., Stein, A., Marino, F., Castellano, E., Udisti, R., and Ceratto, J.: A combined observational and modeling approach  
1521 to study modern dust transport from the Patagonia desert to East Antarctica. *Atmospheric Chemistry and Physics*, 10, 17,  
1522 8287–8303, [doi:10.5194/acp-10-8287-2010](https://doi.org/10.5194/acp-10-8287-2010), 2010.
- 1523 George, C., Ammann, M., D'Anna, B., Donaldson, D. J., Nizkorodov, S A.: Heterogeneous Photochemistry in the Atmosphere.  
1524 *Chem. Rev.* 115, 4218-4258, doi: 10.1021/cr500648z, 2015.
- 1525 Gili, S., Vanderstraeten, A., Chaput, A., King, J., Gaiero, D., Delmonte, B., Vallenga, P., Formenti, P., Di Biagio, C.,  
1526 Cazanau, M. and Pangui, E.: Southern Africa: The Missing Piece To The Dust Provenance Puzzle of East Antarctica?  
1527 *Communications Earth & Environment*, doi: 10.21203/rs.3.rs-923449/v1, 2021.
- 1528 Gillies, J. A., W. G. Nickling, and M. Tilson: Frequency, magnitude and characteristics of aeolian sediment transport:  
1529 McMurdo Dry Valleys, Antarctica, *J. Geophys. Res. Earth Surf.*, 118, 461–479, doi:[10.1002/jgrf.20007](https://doi.org/10.1002/jgrf.20007).2013.

- 1530 Ginoux, P., J. M. Prospero, T. E. Gill, N. C. Hsu, M. Zhao: Global-scale attribution of anthropogenic and natural dust  
1531 sources and their emission rates based on MODIS Deep Blue aerosol products. *Rev. Geophys.* 50, RG3005, 2012.
- 1532 Groot Zwaaftink, C. D., Grythe, H., Skov, H., and Stohl, A.: Substantial contribution of northern high-latitude sources to  
1533 mineral dust in the Arctic, *Journal of Geophysical Research-Atmospheres*, 121, 13678-13697, doi: 10.1002/2016jd025482,  
1534 2016.
- 1535 Groot Zwaaftink, C. D., Arnalds, O., Dagsson-Waldhauserová, P., Eckhardt, S., Prospero, J. M., and Stohl, A.: Temporal and  
1536 spatial variability of Icelandic dust emission and atmospheric transport, *Atmos. Chem. Phys.*, 17, 10865-10878, 2017.
- 1537 Gunnarsson, A., Gardarsson, S. M., Pálsson, F., Jóhannesson, T., and Sveinsson, Ó. G. B.: Annual and interannual variability  
1538 and trends of albedo for Icelandic glaciers. *The Cryosphere* 15, 547–570, 2020.
- 1539 Hadley, D., G. L. Hufford, and J. J. Simpson: Resuspension of relic volcanic ash and dust from Katmai: Still an aviation  
1540 hazard, *Weather Forecast.*, 19, 5, 829–840, doi:10.1175/1520-0434(2004)019<0829:RORVAA>2.0.CO;2, 2004.
- 1541 Hadley, O., and Kirchstetter, T.: Black-Carbon reduction of snow albedo. *Nat. Clim. Change* 2, 437–440. doi:  
1542 10.1038/nclimate1433, 2012.
- 1543 Hardy M. and Cornu S. Location of natural trace elements in silty soils using particle-size fractionation. *Geoderma*, 133, 295-  
1544 308, doi:10.1016/j.geoderma.2005.07.015, 2006.
- 1545 Harrison, A. D., K. Lever, A. Sanchez-Marroquin, M. A. Holden, T. F. Whale, M. D. Tarn, J. B. McQuaid, and B. J. Murray:  
1546 The ice-nucleating ability of quartz immersed in water and its atmospheric importance compared to K-feldspar, *Atmos. Chem.*  
1547 *Phys.*, 19, 17, 11343-11361, doi:10.5194/acp-19-11343-2019, 2019.
- 1548 Hedding DW, Werner Nel, Ryan L. Anderson, Aeolian processes and landforms in the sub-Antarctic: preliminary observations  
1549 from Marion Island, *Polar Research*, 34, 1, 26365, doi:10.3402/polar.v34.26365, 2015.
- 1550 Heindel RC, Lauren E Culler, Ross A Virginia, Rates and processes of aeolian soil erosion in West Greenland, *The Holocene*,  
1551 27,9, 1281-1290, doi:10.1177/0959683616687381, 2017.
- 1552 Hernández, M. A., González, N., and Hernández, L.: Late Cenozoic Geohydrology of Extra-Andean Patagonia, Argentina. In  
1553 J. Rabassa (Ed.), *The Late Cenozoic of Patagonia and Tierra del Fuego*, Vol. 11, 497–509, Elsevier, doi:10.1016/S1571-  
1554 0866(07)10024-5, 2008.

- 1555 Hobbs, W. H.: Wind: The dominant transportation agent within extramarginal zones to continental glaciers. *The Journal of*  
1556 *Geology*, 50, 5, 556–59, doi:10.1086/625072, 1942.
- 1557 Hojan, M., Rurek, M., Więclaw, M., and Krupa, A.: Effects of Extreme Dust Storm in Agricultural Areas (Poland, the Greater  
1558 Lowland). *Geosciences*, 9, 106, doi:10.3390/geosciences9030106, 2019.
- 1559 Hugenholtz, C. H. and Wolfe, S. A.: Rates and environmental controls of aeolian dust accumulation, Athabasca River  
1560 Valley, Canadian Rocky Mountains, *Geomorphology*, 121, 3, 274–282, doi:10.1016/j.geomorph.2010.04.024, 2010.
- 1561 IPCC, 2013: *Climate Change 2013: The Physical Science Basis. Contribution of Working Group I to the Fifth Assessment*  
1562 *Report of the Intergovernmental Panel on Climate Change* [Stocker, T.F., D. Qin, G.-K. Plattner, M. Tignor, S.K. Allen, J.  
1563 Boschung, A. Nauels, Y. Xia, V. Bex and P.M. Midgley (eds.)]. Cambridge University Press, Cambridge, United Kingdom  
1564 and New York, NY, USA, 1535 p., 2013.
- 1565 IPCC, 2019: *IPCC Special Report on the Ocean and Cryosphere in a Changing Climate* [H.-O. Pörtner, D.C. Roberts, V.  
1566 Masson-Delmotte, P. Zhai, M. Tignor, E. Poloczanska, K. Mintenbeck, A. Alegría, M. Nicolai, A. Okem, J. Petzold, B. Rama,  
1567 N.M. Weyer (eds.)]. In press. (last accessed 19 November 2021), 2019.
- 1568 IPCC, 2021: *Climate Change 2021: The Physical Science Basis. Contribution of Working Group I to the Sixth Assessment*  
1569 *Report of the Intergovernmental Panel on Climate Change* [Masson-Delmotte, V., P. Zhai, A. Pirani, S.L. Connors, C. Péan,  
1570 S. Berger, N. Caud, Y. Chen, L. Goldfarb, M.I. Gomis, M. Huang, K. Leitzell, E. Lonnoy, J.B.R. Matthews, T.K. Maycock,  
1571 T. Waterfield, O. Yelekçi, R. Yu, and B. Zhou (eds.)]. Cambridge University Press. In Press, (last accessed 19 November  
1572 2021), 2021.
- 1573 Irish, V. E., et al.: Ice nucleating particles in the marine boundary layer in the Canadian Arctic during summer 2014, *Atmos.*  
1574 *Chem. Phys.*, 19, 2, 1027-1039, doi:10.5194/acp-19-1027-2019, 2019.
- 1575 Ito, A., and Kok, J. F.: Do dust emissions from sparsely vegetated regions dominate atmospheric iron supply to the Southern  
1576 Ocean?, *Journal of Geophysical Research-Atmospheres*, 122, 3987-4002, doi: 10.1002/2016jd025939, 2017.
- 1577 IUSS Working Group WRB: *World Reference Base for Soil Resources 2014, update 2015 International soil classification*  
1578 *system for naming soils and creating legends for soil maps. World Soil Resources Reports No. 106. FAO, Rome, 2015.*
- 1579 Jacobi, H.-W., Obleitner, F., Da Costa, S., Ginot, P., Eleftheriadis, K., Aas, W., and Zanatta, M.: Deposition of ionic species  
1580 and black carbon to the Arctic snowpack: combining snow pit observations with modeling, *Atmos. Chem. Phys.*, 19, 10361–  
1581 10377, <https://doi.org/10.5194/acp-19-10361-2019>, 2019.



- 1582 Janjic Z. I., J. P. Gerrity, Jr. and S. Nickovic: An Alternative Approach to Nonhydrostatic Modeling, *Mon. Wea. Rev.*, 129,  
1583 1164-1178, 2001.
- 1584 Jickells, T., and Moore, C. M.: The importance of Atmospheric Deposition for Ocean Productivity, *Annu. Rev. Ecol. Evol.*  
1585 *Syst.*, 46, 481-501, doi: 10.1146/annurev-ecolsys-112414-054118, 2015.
- 1586 Jickells, T. D., An, Z. S., Andersen, K. K., Baker, A. R., Bergametti, G., Brooks, N., Cao, J. J., Boyd, P. W., Duce, R. A.,  
1587 Hunter, K. A., Kawahata, H., Kubilay, N., laRoche, J., Liss, P. S., Mahowald, N., Prospero, J. M., Ridgwell, A. J., Tegen, I.,  
1588 and Torres, R.: Global iron connections between desert dust, ocean biogeochemistry, and climate, *Science*, 308, 67-71, doi:  
1589 10.1126/science.1105959, 2005.
- 1590 Johnson, M. S., Meskhidze, N., Kiliyanpilakkil, V. P., and Gassó, S.: Understanding the transport of Patagonian dust and its  
1591 influence on marine biological activity in the South Atlantic Ocean. *Atmospheric Chemistry and Physics*, 11, 6, 2487–2502,  
1592 2011.
- 1593 Kanakidou, M., Myriokefalitakis, S., and Tsigaridis, K.: Aerosols in atmospheric chemistry and biogeochemical cycles of  
1594 nutrients, *Environmental Research Letters*, 13, doi: 10.1088/1748-9326/aabccb, 2018.
- 1595 Kandler, K.; Schneiders, K.; Heuser, J.; Waza, A.; Aryasree, S.; Althausen, D.; Hofer, J.; Abdullaev, S.F.; Makhmudov, A.N.  
1596 Differences and Similarities of Central Asian, African, and Arctic Dust Composition from a Single Particle Perspective.  
1597 *Atmosphere* 2020, 11, 269. [doi:10.3390/atmos11030269](https://doi.org/10.3390/atmos11030269), 2020.
- 1598 Kasimov, N. S., Vlasov, D. V., and Kosheleva, N. E.: Enrichment of road dust particles and adjacent environments with metals  
1599 and metalloids in eastern Moscow, *Urban Clim.*, 32, 100638, doi:10.1016/j.uclim.2020.100638, 2020.
- 1600 Kavan, J., Ondruch J, Nývlt D, Hrbáček F, Carrivick JL, Láska K.: Seasonal hydrological and suspended sediment transport  
1601 dynamics in proglacial streams, James Ross Island, Antarctica. *Geografiska Annaler: Series A, Physical Geography* 99, 38-  
1602 55, doi: 10.1080/04353676.2016.1257914, 2017.
- 1603 Kavan, J., Dagsson-Waldhauserová P, Renard JB, Láska K, Ambrožová, K.: Aerosol concentrations in relationship to local  
1604 atmospheric conditions on James Ross Island, Antarctica. *Frontiers in Earth Science* 6: DOI: 10.3389/feart.2018.00207, 2018.
- 1605 Kavan, J., Kamil Láska K, Adam Nawrot A, and Tomasz Wawrzyniak T.: High Latitude Dust Transport Altitude Pattern  
1606 Revealed from Deposition on Snow, Svalbard. *Atmosphere* 2020, 11, 1318; doi:10.3390/atmos11121318., 2020a.

- 1607 Kavan, J, Nývlt D, Láška K, Engel Z, Kňázková M.: High latitude dust deposition in snow on glaciers of James Ross Island,  
1608 Antarctica. *Earth Surface Processes and Landforms*. DOI: 10.1002/esp.4831, 2020b.
- 1609 Khan, A. L., Dierssen, H., Schwarz, J. P., Schmitt, C., Chlus, A., Hermanson, M., Painter, T. H., and McKnight, D. M.: Impacts  
1610 of coal dust from an active mine on the spectral reflectance of Arctic surface snow in Svalbard, Norway, *J. Geophys. Res.*,  
1611 122, 1767–1778, doi:10.1002/2016jd025757, 2017.
- 1612 Kňázková, M., Hrbáček, F., Kavan, J., Nývlt, D. Effect of hyaloclastite breccia boulders on meso-scale periglacial-aeolian  
1613 landsystem in semi-arid Antarctic environment, James Ross Island, Antarctic Peninsula. *Cuadernos de Investigación*  
1614 *Geográfica*. doi: 10.18172/cig.3800, 2020.
- 1615 Koroleva, T. V., Krechetov, P. P., Semenov, I. N., Sharapova, A. V. and Kondrat'ev, A. D.: Transformation of chemical  
1616 composition of snow in the impact areas of the first stage of the expandable launch system Proton in Central Kazakhstan, *Russ.*  
1617 *Meteorol. Hydrol.*, 41(8), 585–591, doi:10.3103/S1068373916080094, 2016.
- 1618 Koroleva, T. V., Sharapova, A. V. and Krechetov, P. P.: A chemical composition of snow on areas exposed to space-rocket  
1619 activities pollution (Altai republic), *Gig. i Sanit.*, doi:10.1882/0016-9900-2017-96-5-432-437, 2017.
- 1620 Kuhlman, H.: Den potentielle jordfygning på danske marker. Teoretiske beregninger vedrørende jordmaterialets  
1621 vindbevægelighed. *Geografisk Tidsskrift - Danish Journal of Geography*, 59. Retrieved from  
1622 <https://tidsskrift.dk/geografisktidsskrift/article/view/46533>, 1960.
- 1623 Kuhns, H., Gillies, J., Etyemezian, V., Nikolich, G., King, J., Zhu, D., Uppapalli, S., Engelbrecht, J., and Kohl, S.: Effect of  
1624 Soil Type and Momentum on Unpaved Road Particulate Matter Emissions from Wheeled and Tracked Vehicles. *Aerosol*  
1625 *Science and Technology - AEROSOL SCI TECH.*, 44, 187-196, doi:10.1080/02786820903516844, 2010.
- 1626 Kupiainen K.: Road dust from pavement wear and traction sanding. *Monographs of the Boreal Environment Research*,  
1627 No. 26, [Mono\\_26.indd \(helsinki.fi\)](#), 2007.
- 1628 Kupiainen, K., Ritola, R., Stojiljkovic, A., Pirjola, L., Malinen, A., and Niemi, J. Contribution of mineral dust sources to street  
1629 side ambient and suspension PM10 samples. *Atmospheric Environment*, 147, 178-189. doi:10.1016/j.atmosenv.2016.09.059,  
1630 2016.
- 1631 Kylling A., Groot Zwaftink, C. D., and Stohl, A.: Mineral dust instantaneous radiative forcing in the Arctic. *Geophysical*  
1632 *Research Letters*, 45, 4290–4298. doi:10.1029/2018GL077346, 2018.

- 1633 Lamy, F., Gersonde, R., Winckler, G., Esper, O., Jaeschke, A., Kuhn, G.; Ullermann, J., Martinez-Garcia, A., Lambert, F.,  
1634 Kilian, R.: Increased dust deposition in the Pacific Southern Ocean during glacial periods. *Science*, 343, 403–407, 2014.
- 1635 Lancaster, N., Nickling, W.G. and Gillies, J.A.: Sand transport by wind on complex surfaces: field studies in the McMurdo  
1636 Dry Valleys, Antarctica. *J. Geophys. Res.*, 115, F03027, 2010.
- 1637 Lappalainen, H. K., Petäjä, T., Vihma, T., Räisänen, J., Baklanov, A., Chalov, S., Esau, I., Ezhova, E., Leppäranta, M.,  
1638 Pozdnyakov, D., Pumpanen, J., Andreae, M. O., Arshinov, M., Asmi, E., Bai, J., Bashmachnikov, I., Belan, B., Bianchi, F.,  
1639 Biskaborn, B., Boy, M., Bäck, J., Cheng, B., Chubarova, N., Duplissy, J., Dyukarev, E., Eleftheriadis, K., Forsius, M.,  
1640 Heimann, M., Juhola, S., Konovalov, V., Konovalov, I., Konstantinov, P., Köster, K., Lapshina, E., Lintunen, A., Mahura, A.,  
1641 Makkonen, R., Malkhazova, S., Mammarella, I., Mammola, S., Buenrostro Mazon, S., Meinander, O., Mikhailov, E., Miles,  
1642 V., Myslenkov, S., Orlov, D., Paris, J.-D., Pirazzini, R., Popovicheva, O., Pulliainen, J., Rautiainen, K., Sachs, T., Shevchenko,  
1643 V., Skorokhod, A., Stohl, A., Suhonen, E., Thomson, E. S., Tsidilina, M., Tynkkynen, V.-P., Uotila, P., Virkkula, A., Voropay,  
1644 N., Wolf, T., Yasunaka, S., Zhang, J., Qiu, Y., Ding, A., Guo, H., Bondur, V., Kasimov, N., Zilitinkevich, S., Kerminen, V.-  
1645 M., and Kulmala, M.: Overview: Recent advances in the understanding of the northern Eurasian environments and of the urban  
1646 air quality in China – a Pan-Eurasian Experiment (PEEX) programme perspective, *Atmos. Chem. Phys.*, 22, 4413–4469,  
1647 doi:10.5194/acp-22-4413-2022, 2022.
- 1648 Lewandowski, M., Kusiak, M.A., Werner, T., Nawrot, A., Barzycka, B., Laska, M., Luks, B.: Seeking the Sources of Dust:  
1649 Geochemical and Magnetic Studies on “Cryodust” in Glacial Cores from Southern Spitsbergen (Svalbard, Norway).  
1650 *Atmosphere* 2020, 11, 1325, doi:[10.3390/atmos11121325](https://doi.org/10.3390/atmos11121325), 2020.
- 1651 Llanos, M. E., Behr, S. J., Gonzalez, J. H., Colombani, E. N., Buono, G. G., and Escobar, J. M.: Informe de las Variaciones  
1652 del Lago Colhue Huapi mediante sensores remotos y su relación con las precipitaciones. Retrieved January 5, 2018, from  
1653 [https://inta.gob.ar/documentos/informe-de-las-variaciones-del-lago-colhue-huapi-mediante-sensores-remotos-y-su-relacion-](https://inta.gob.ar/documentos/informe-de-las-variaciones-del-lago-colhue-huapi-mediante-sensores-remotos-y-su-relacion-con-las-precipitaciones)  
1654 [con-las-precipitaciones](https://inta.gob.ar/documentos/informe-de-las-variaciones-del-lago-colhue-huapi-mediante-sensores-remotos-y-su-relacion-con-las-precipitaciones), 2016.
- 1655 Lutz, S., Anesio, A., Raiswell, R. et al.: The biogeography of red snow microbiomes and their role in melting Arctic glaciers,  
1656 *Nat. Commun.* 7, 11968, 2016.
- 1657 Mahowald, N.: Aerosol Indirect Effect on Biogeochemical Cycles and Climate, *Science*, 334, 794-796, doi:  
1658 10.1126/science.1207374, 2011.
- 1659 Mahowald, N. M., Baker, A. R., Bergametti, G., Brooks, N., Duce, R. A., Jickells, T. D., Kubilay, N., Prospero, J. M., and  
1660 Tegen, I.: Atmospheric global dust cycle and iron inputs to the ocean, *Global Biogeochem. Cy.*, 19, doi:  
1661 10.1029/2004gb002402, 2005.

- 1662 Mahowald, N. M., Kloster, S., Engelstaedter, S., Moore, J. K., Mukhopadhyay, S., McConnell, J. R., Albani, S., Doney, S. C.,  
1663 Bhattacharya, A., Curran, M. A. J., Flanner, M. G., Hoffman, F. M., Lawrence, D. M., Lindsay, K., Mayewski, P. A., Neff, J.,  
1664 Rothenberg, D., Thomas, E., Thornton, P. E., and Zender, C. S.: Observed 20th century desert dust variability: impact on  
1665 climate and biogeochemistry, *Atmos. Chem. Phys.*, 10, 10875-10893, doi: 10.5194/acp-10-10875-2010, 2010.
- 1666 Manninen, T., Anttila, K., Jääskeläinen, E., Riihelä, A., Peltoniemi, J., Räisänen, P., Lahtinen, P., Siljamo, N., Thölix, L.,  
1667 Meinander, O., Kontu, A., Suokanerva, H., Pirazzini, R., Suomalainen, J., Hakala, T., Kaasalainen, S., Kaartinen, H., Kukko,  
1668 A., Hautecoeur, O., and Roujean, J.-L.: Effect of small-scale snow surface roughness on snow albedo and reflectance, *The*  
1669 *Cryosphere*, 15, 793–820, doi:10.5194/tc-15-793-2021, 2021.
- 1670 Markuse, Pierre: High latitude dust storm (silt), Nuussuaq Peninsula, Greenland - October 1st, 2020,  
1671 [https://www.flickr.com/photos/pierre\\_markuse/50447335522/](https://www.flickr.com/photos/pierre_markuse/50447335522/), contains modified Copernicus Sentinel data [2020], processed  
1672 by Pierre Markuse, originally posted to Flickr by Pierre Markuse at [https://flickr.com/photos/24998770@N07/50447335522.](https://flickr.com/photos/24998770@N07/50447335522),  
1673 reviewed on 25 October 2020 by FlickrreviewR 2, licensed under the terms of the cc-by-2.0.2020, 2020.
- 1674 Martin, J. H., and Fitzwater, S. E.: Iron deficiency limits phytoplankton growth in the north-east Pacific sub Arctic, *Nature*,  
1675 331, 341-343, 1988.
- 1676 Martínez-García, A., Sigman, D. M., Ren, H., Anderson, R. F., Straub, M., Hodell, D. A., Jaccard, S. L., Eglinton, T. I., and  
1677 Haug, G. H.: Iron fertilization of the Sub-Antarctic Ocean during the last ice age, *Science*, 343, 1347-1350, 2014.
- 1678 Mazzonia, E., and Vazquez, M.: Desertification in Patagonia. In E. M. Latrubesse (Ed.), *Natural Hazards and Human-*  
1679 *Exacerbated Disasters in Latin America*, Vol. 13, 351–377, Elsevier, doi:10.1016/S0928-2025(08)10017-7, 2009.
- 1680 McCutcheon, J., Lutz, S., Williamson, C. et al.: Mineral phosphorus drives glacier algal blooms on the Greenland Ice Sheet.  
1681 *Nat. Commun.* 12, 570, doi:10.1038/s41467-020-20627-w, 2021.
- 1682 Meinander, O., Kazadzis, S., Arola, A., Riihelä, A., Räisänen, P., Kivi, R., Kontu, A., Kouznetsov, R., Sofiev, M., Svensson,  
1683 J., Suokanerva, H., Aaltonen, V., Manninen, T., Roujean, J.-L., and Hautecoeur, O.: Spectral albedo of seasonal snow during  
1684 intensive melt period at Sodankylä, beyond the Arctic Circle, *Atmos. Chem. Phys.*, 13, 3793–3810, doi:10.5194/acp-13-3793-  
1685 2013, 2013.
- 1686 Meinander, O.; Kontu, A.; Virkkula, A.; et al., Brief communication: Light-absorbing impurities can reduce the density of  
1687 melting snow, *Cryosphere*, Volume: 8 Issue: 3 Pages: 991-995, doi: 10.5194/tc-8-991-2014, 2014.

1688 Meinander, O., Dagsson-Waldhauserová, P., and Arnalds, O.: Icelandic volcanic dust can have a significant influence on the  
1689 cryosphere in Greenland and elsewhere, *Polar Research Volume*: 35, doi: 10.3402/polar.v35.31313, 2016.

1690 Meinander O., Backman, L., Saranko, O., Asmi, E., Rodriguez, E. and Sanchez, R.: Effects of high latitude dust on snow UV  
1691 albedo and solar UV irradiance measured at Marambio during 2013-2017 with comparison to simulated UV irradiances,  
1692 *Geophysical Research Abstracts Vol. 20, EGU2018-2007*, 2018 EGU General Assembly 2018, available at  
1693 <https://meetingorganizer.copernicus.org/EGU2018/EGU2018-2007.pdf>, 2018.

1694 Meinander, O., S. Chalov, H. Lappalainen, J. Ekman, K. Eleftheriadis, D. Frolov, A. Hyvärinen, V. Ivanov, N. Karvosenoja,  
1695 K. Kupiainen, O. Popovicheva, I. Semenov, L. Sogacheva, and The MSU Workshop Participants: About Black Carbon in the  
1696 Arctic and Significance Compared to High-Latitude Dust Sources (Finnish-Russian Workshop at the Lomonosov Moscow  
1697 State University, 17-18 September 2019, in Co-operation with MSU, INAR, PEEEX, MFA/IBA and FMI), In: Tiia Laurila,  
1698 Anna Lintunen, Markku Kulmala (eds.), *Proceedings of The Center of Excellence in Atmospheric Science (CoE ATM) Annual  
1699 Seminar 2019, Report series in aerosol science*, available at: [http://www.faar.fi/wp-](http://www.faar.fi/wp-content/uploads/2019/11/CoE_proceedings_2019-compressed.pdf)  
1700 [content/uploads/2019/11/CoE\\_proceedings\\_2019-compressed.pdf](http://www.faar.fi/wp-content/uploads/2019/11/CoE_proceedings_2019-compressed.pdf), p. 457-465, 2019a.

1701 Meinander O., Dagsson-Waldhauserová P., Björnsson H., Petersen G.N., Moore K., Larsen J.N. and Heininen L.: Report of  
1702 the IASC Workshop on Effects and Extremes of High Latitude Dust, 13-14 FEB 2019, in co-operation with the IceDust Aerosol  
1703 Association, IBA-FIN-BCDUST-project of MFA of Finland and EU COST InDust Action. Available at  
1704 <https://iasc.info/news/iasc-news/472-workshop-report-iasc-workshop-on-effects-and-extremes-of-high-latitude-dust>, last  
1705 accessed 3 June 2021, 2019b.

1706 Meinander, O.; Heikkinen, E.; Aurela, M.; Hyvärinen, A.: Sampling, Filtering, and Analysis Protocols to Detect Black Carbon,  
1707 Organic Carbon, and Total Carbon in Seasonal Surface Snow in an Urban Background and Arctic Finland (>60°N).  
1708 *Atmosphere*, 11, 923, doi:10.3390/atmos11090923, 2020a.

1709 Meinander O., Kontu A., Kouznetsov R., Sofiev M.: Snow Samples Combined With Long-Range Transport Modeling to  
1710 Reveal the Origin and Temporal Variability of Black Carbon in Seasonal Snow in Sodankylä (67°N). *Front. Earth Sci.* 12 June  
1711 2020, doi:10.3389/feart.2020.00153, 2020b.

1712 Meinander, O., Piedehierro, A., Welti, A., Kouznetsov, R., Heinonen, A., Viisanen, Y. and Laaksonen, A.: Saharan dust  
1713 transported and deposited in Finland on February 23rd, 2021. EAC 2021 August 30-September 3 2021, Abstract AAS 19-2  
1714 Paper ID 399, abstract available at:  
1715 [https://www.conftool.com/eac2021/index.php?page=browseSessions&form\\_session=206#paperID399](https://www.conftool.com/eac2021/index.php?page=browseSessions&form_session=206#paperID399); talk available at:  
1716 <https://www.youtube.com/watch?v=ssJ6k8sT0so>. Book of abstracts for the 2021 European Aerosol Conference, A live virtual  
1717 event, hosted by The Aerosol Society, <https://eac2021.co.uk/book-of-abstracts>, 2021, 2021.

1718 Meskhidze, N., Volker, C., Al-Abadleh, H. A., Barbeau, K., Bressac, M., Buck, C., Bundy, R. M., Croot, P., Feng, Y., Ito, A.,  
1719 Johansen, A. M., Landing, W. M., Mao, J. Q., Myriokefalitakis, S., Ohnemus, D., Pasquier, B., and Ye, Y.: Perspective on  
1720 identifying and characterizing the processes controlling iron speciation and residence time at the atmosphere-ocean interface,  
1721 *Mar. Chem.*, 217, 103704, doi: 10.1016/j.marchem.2019.103704, 2019.

1722 Meteosat 2019: Two dust clouds, one from northern Africa and one from Central Europe, travelled north towards Iceland and  
1723 Greenland in late April 2019. Dust over Europe 22 April 2019 12:00 UTC, 23 April 06:00–12:30 UTC, 24 April 06:00 UTC,  
1724 by Jochen Kerkmann and Vesa Nietosvaara (EUMETSAT), Ivan Smiljanicv (SCISYS), Izabela Zablocka (IMGW ), Mike  
1725 Fromm (US Naval Research Laboratory, Published on 22 April 2019, available at: <https://www.eumetsat.int/dust-over-europe>,  
1726 2019.

1727 Miller, M.E., Bowker, M.A., Reynolds, R.L. and Goldstein, H.L.: Post-fire land treatments and wind erosion – lessons from  
1728 the Milford Flat Fire, UT, USA. *Aeolian Research*, 7, 29– 44, 2012.

1729 Mills, M. M., Ridame, C., Davey, M., La Roche, J., and Geider, R. J.: Iron and phosphorus co-limit nitrogen fixation in the  
1730 eastern tropical North Atlantic, *Nature*, 429, 292-294, doi: 10.1038/nature02550, 2004.

1731 Mockford, T., Bullard, J., Thorsteinsson, T.: The dynamic effects of sediment availability on the relationship between wind  
1732 speed and dust concentration. *Earth Surface Processes and Landforms*, 43, 11, 2484–2492, 2018.

1733 Montes, A., Rodríguez, S. S., and Domínguez, C. E.: Geomorphology context and characterization of dunefields developed by  
1734 the southern westerlies at drying Colhué Huapi shallow lake, Patagonia Argentina. *Aeolian Research*, 28, Supplement C, 58–  
1735 70, doi:10.1016/j.aeolia.2017.08.001, 2017.

1736 Moore, C. M., Mills, M. M., Arrigo, K. R., Berman-Frank, I., Bopp, L., Boyd, P. W., Galbraith, E. D., Geider, R. J., Guieu,  
1737 C., Jaccard, S. L., Jickells, T. D., La Roche, J., Lenton, T. M., Mahowald, N. M., Maranon, E., Marinov, I., Moore, J. K.,  
1738 Nakatsuka, T., Oeschler, A., Saito, M. A., Thingstad, T. F., Tsuda, A., and Ulloa, O.: Processes and patterns of oceanic nutrient  
1739 limitation, *Nat. Geosci.*, 6, 701-710, doi: 10.1038/ngeo1765, 2013.

1740 Mori, Tatsuhiro, Goto-Azuma, Kumiko, Kondo, Yutaka, Ogawa-Tsukagawa, Yoshimi, Miura, Kazuhiko, Hirabayashi,  
1741 Motohiro, Oshima, Naga, Koike, M., Kupiainen, Kaarle, Moteki, Nobuhiro, Ohata, Sho, Sinha, P.R., Sugiura, Konosuke, Aoki,  
1742 Teruo, Schneebeli, Martin, Steffen, Konrad, Sato, Atsushi, Tsushima, A., Makarov, V., Nagatsuka, N.: Black Carbon and  
1743 Inorganic Aerosols in Arctic Snowpack, *Journal of Geophysical Research: Atmospheres*. 124, doi:10.1029/2019JD030623,  
1744 2019.

- 1745 Moroni B., Becagli S., Bolzacchini E., Busetto M., Cappelletti D., Crocchianti S., Ferrero L., Frosini D., Lanconelli C., Lupi  
1746 A., Maturilli M., Mazzola M., Perrone G., Sangiorgi G., Traversi R., Udisti R., Viola A. and Vitale V.: Vertical profiles and  
1747 chemical properties of aerosol particles upon Ny-Ålesund (Svalbard Islands). *Advances in Meteorology*,  
1748 doi:10.1155/2015/292081.2015, 2015.
- 1749 Moroni B., Cappelletti D., Ferrero L., Crocchianti S., Busetto M., Mazzola M., Becagli S., Traversi R. and Udisti R.: Local  
1750 vs. long-range sources of aerosol particles upon Ny-Ålesund (Svalbard Islands): mineral chemistry and geochemical records.  
1751 *Rendiconti Lincei. Scienze Fisiche e Naturali*, doi: 10.1007/s12210-016-0533-7, 2016.
- 1752 Moroni B, Arnalds O, Dagsson-Waldhauserová P, Crocchianti S, Vivani R and Cappelletti D. Mineralogical and Chemical  
1753 Records of Icelandic Dust Sources Upon Ny-Ålesund (Svalbard Islands). *Front. Earth Sci.* 6:187, doi:  
1754 10.3389/feart.2018.00187, 2018.
- 1755 Murray, B. J., D. O’Sullivan, J. D. Atkinson, and M. E. Webb: Ice nucleation by particles immersed in supercooled cloud  
1756 droplets, *Chem. Soc. Rev.*, 41, 19, 6519-6554, doi:10.1039/c2cs35200a, 2012.
- 1757 Murray, K.T., Miller, M.F. and Bowser, S.S.: Depositional processes beneath coastal multi-year sea ice. *Sedimentology*, 60,  
1758 391–410, 2013.
- 1759 Murray, B. J., K. S. Carslaw, and P. R. Field: Opinion: Cloud-phase climate feedback and the importance of ice-nucleating  
1760 particles, *Atmos. Chem. Phys.*, 21, 2, 665-679, doi:10.5194/acp-21-665-2021, 2021.
- 1761 Möller, R., Möller, M., Kukla, P. A., and Schneider, C.: Impact of supraglacial deposits of tephra from Grimsvötn volcano,  
1762 Iceland, on glacier ablation. *J. Glaciol.* 62, 933–943, doi: 10.1017/jog.2016.82, 2016.
- 1763 Nagatsuka, Naoko, Goto-Azuma, Kumiko, Tsushima, Akane, Fujita, Koji , Matoba, Sumito, Onuma, Yukihiro, Dallmayr,  
1764 Remi, Kadota, Moe , Hirabayashi, Motohiro, Ogata, Jun, Ogawa-Tsukagawa, Yoshimi, Kitamura, Kyotaro, Minowa,  
1765 Masahiro, Komuro, Yuki , Motoyama, Hideaki , Aoki, Teruo: Variations in mineralogy of dust in an ice core obtained from  
1766 northwestern Greenland over the past 100 years. *Climate of the Past*, 17, 1341-1362, doi: 10.5194/cp-17-1341-2021, 2021.
- 1767 Nemuc, A., Basart, S., Tobias, A., Nickovic, S., Barnaba, F., Kazadzis, S., Mona, L., Amiridis, V., Vukovic, A., Christel, I.,  
1768 Dagsson-Waldhauserová, P., Monteiro, A.: International Network to Encourage the Use of Monitoring and Forecasting Dust  
1769 Products (InDust). *European Review*, 1-13, doi:10.1017/S1062798720000733, 2020.
- 1770
- 1771 Neuman, C. M.: Observations of winter aeolian transport and niveo-aeolian deposition at crater lake, pagnirtung pass,  
1772 N.W.T., Canada, *Permafr. Periglac. Process.*, 1, 3–4, 235–247, doi:10.1002/ppp.3430010304, 1990.

- 1773 Nickling, W.: Eolian sediment transport during dust storms: Slims River valley, Yukon Territory. *Canadian Journal of Earth*  
1774 *Science*, 15, 1069-1084, 1978.
- 1775 Nickling, W. G., and Brazel, A. J.: Surface wind characteristics along the icefield ranges, Yukon Territory, Canada. *Arctic and*  
1776 *Alpine Research*, 17, 125–134. doi:10.2307/1550842, 1985.
- 1777 Nickovic, S., Cvetkovic, B., Madonna, F., Rosoldi, M., Pejanovic, G., Petkovic, S., and Nikolic, J.: Cloud ice caused by  
1778 atmospheric mineral dust – Part 1: Parameterization of ice nuclei concentration in the NMME-DREAM model, *Atmos. Chem.*  
1779 *Phys.*, 16, 11367-11378, doi:10.5194/acp-16-11367-2016, 2016.
- 1780 Nielsdottir, M. C., Moore, C. M., Sanders, R., Hinz, D. J., and Achterberg, E. P.: Iron limitation of the postbloom  
1781 phytoplankton communities in the Iceland Basin, *Global Biogeochemical Cycles*, 23, doi: 10.1029/2008gb003410, 2009.
- 1782 Nordic Council of Ministers. Road dust and PM10 in the Nordic countries. Measures to Reduce Road Dust Emissions from  
1783 Traffic. Publication number 2016:790. Publish date 27.01.17, available at: [https://www.norden.org/en/publication/road-dust-](https://www.norden.org/en/publication/road-dust-and-pm10-nordic-countries)  
1784 [and-pm10-nordic-countries](https://www.norden.org/en/publication/road-dust-and-pm10-nordic-countries) (last accessed 4.11.2021), 2017.
- 1785 Ovadnevaite, J., Ceburnis, D., Plauskaite-Sukiene, K., Modini, R., Dupuy, R., Rimselyte, I., Ramonet, R., Kvietkus, K.,  
1786 Ristovski, Z., Berresheim, H., and O'Dowd, C.D.: Volcanic sulphate and Arctic dust plumes over the North Atlantic Ocean.  
1787 *Atmospheric Environment* 43, 4968-4974, 2009.
- 1788 Pejanovic, G., S. Nickovic, M. Vujadinovic, A. Vukovic, V. Djurdjevic, M. Dacic: Atmospheric deposition of minerals in dust  
1789 over the open ocean and possible consequences on climate. WCRP OSC Climate Research in Service to Society, 24-28 October  
1790 2011, Denver, CO, USA, 2011.
- 1791 Peltoniemi, J. I., Gritsevich, M., Hakala, T., Dagsson-Waldhauserová, P., Arnalds, Ó., Anttila, K., Hannula, H.-R., Kivekäs,  
1792 N., Lihavainen, H., Meinander, O., Svensson, J., Virkkula, A., and de Leeuw, G.: Soot on Snow experiment: bidirectional  
1793 reflectance factor measurements of contaminated snow, *The Cryosphere*, 9, 2323-2337, doi:10.5194/tc-9-2323-2015, 2015.
- 1794 Perron, M. M. G., Strzelec, M., Gault-Ringold, M., Proernse, B. C., Boyd, P. W., and Bowie, A. R.: Assessment of leaching  
1795 protocols to determine the solubility of trace metals in aerosols, *Talanta*, 208, doi: 10.1016/j.talanta.2019.120377, 2020.
- 1796 Popovicheva, O., Diapouli, E., Makshtas, A., Shonija, N., Manousakas, M., Saraga, D., Uttal, T., and Eleftheriadis K.: East  
1797 Siberian Arctic background and black carbon polluted aerosols at HMO Tiksi. *Science of the Total Environment*, 655, 924-  
1798 938, doi.org/10.1016/j.scitotenv.2018.11.165, 2019.



- 1799 Price, H. C., et al.: Atmospheric Ice-Nucleating Particles in the Dusty Tropical Atlantic, *J. Geophys. Res.*, 123, 4, 2175-2193,  
1800 doi:10.1002/2017JD027560, 2018.
- 1801 Prospero, J. M., Ginoux, P., Torres, O., Nicholson, S. E., and Gill, T. E., ENVIRONMENTAL CHARACTERIZATION OF  
1802 GLOBAL SOURCES OF ATMOSPHERIC SOIL DUST IDENTIFIED WITH THE NIMBUS 7 TOTAL OZONE MAPPING  
1803 SPECTROMETER (TOMS) ABSORBING AEROSOL PRODUCT, *Rev. Geophys.*, 40, 1, 1002,  
1804 doi:10.1029/2000RG000095, 2002.
- 1805 Prospero, J.M., Bullard, J.E., Hodgkins, R.: High-latitude dust over the North Atlantic: inputs from Icelandic proglacial dust  
1806 storms. *Science* 335, 1078–1082, 2012.
- 1807 Qin, Y., Abatzoglou, J.T., Siebert, S. et al.: Agricultural risks from changing snowmelt. *Nat. Clim. Chang.* 10, 459–465,  
1808 doi:10.1038/s41558-020-0746-8, 2020.
- 1809 Querol, A. Tobías, N. Pérez, A. Karanasiou, F. Amato, M. Stafoggia, C.P. García-Pando, P. Ginoux, F. Forastiere, S. Gumy,  
1810 P. Mudu: Monitoring the impact of desert dust outbreaks for air quality for health studies. *Environ. Int.*, 130, p. 104867,  
1811 2019.
- 1812 Raiswell, R., Hawkings, J. R., Benning, L. G., Baker, A. R., Death, R., Albani, S., Mahowald, N., Krom, M. D., Poulton, S.  
1813 W., and Wadham, J.: Potentially bioavailable iron delivery by iceberg-hosted sediments and atmospheric dust to the polar  
1814 oceans, *Biogeosciences*, 13, 3887-3900, 2016.
- 1815 Ranjbar, K., O’Neill, N.T., Ivanescu, L., King, J., Hayes, P.L.: Remote sensing of a high- Arctic, local dust event over Lake  
1816 Hazen (Ellesmere Island, Nunavut, Canada), *Atmospheric Environment*, 118102, ISSN 1352-2310,  
1817 doi:10.1016/j.atmosenv.2020.118102, 2021.
- 1818 Richards-Thomas, T., McKenna-Neuman, C., and Power, I.M. Power: Particle-scale characterization of volcanoclastic dust  
1819 sources within Iceland. *Sedimentology*, 68,3, 1137-1158, doi: 10.1111/sed.12821, 2021.
- 1820 Romanias M.N., Y. Ren, B. Grosselin, V. Daele, A. Mellouki, P. Dagsson-Waldhauserová, F. Thevenet: Reactive uptake of  
1821 NO<sub>2</sub> on volcanic particles: A possible source of HONO in the atmosphere, *Journal of Environmental Sciences*, Vol 95, pp  
1822 155-164, September 2020. doi: 10.1016/j.jes.2020.03.042, 2020.
- 1823 Ryan-Keogh, T. J., Macey, A. I., Nielsdottir, M. C., Lucas, M. I., Steigenberger, S. S., Stinchcombe, M. C., Achterberg, E. P.,  
1824 Bibby, T. S., and Moore, C. M.: Spatial and temporal development of phytoplankton iron stress in relation to bloom dynamics  
1825 in the high-latitude North Atlantic Ocean, *Limnology and Oceanography*, 58, 533-545, doi: 10.4319/lo.2013.58.2.0533, 2013.

- 1826 Rymer, K.: Aeolian activity in central Spitsbergen (Ebba Valley) in the years 2012–2017. In Proceedings of the XXXVII Polar  
1827 Symposium “Polar Change—Global Change”, Poznan, Poland, 7–10 June 2018; p. 61, 2018.
- 1828 Rymer, K.G., Rachlewicz, G., Buchwal, A., Temme, A.J.A.M., Reimann, T., van der Meij, W.M.: Contemporary and past  
1829 aeolian deposition rates in periglacial conditions (Ebba Valley, central Spitsbergen). *Catena* 211, 105974, 2022.
- 1830 Samonova O.A. and Aseyeva E.N.: Particle size partitioning of metals in humus horizons of two small erosional landforms in  
1831 the middle Protva basin – a comparative study. *GEOGRAPHY, ENVIRONMENT, SUSTAINABILITY*, 13, 1, 260-271,  
1832 doi:10.24057/2071-9388-2019-116, 2020.
- 1833 Sanchez-Marroquin, A. O. Arnalds, K. J. Baustian-Dorsi, J. Browse, P. Dagsson-Waldhauserová, A. D. Harrison, E. C. Maters,  
1834 K. J. Pringle, J. Vergara-Temprado, I. T. Burke, J. B. McQuaid, K. S. Carslaw, B. J. Murray: Iceland is an episodic source of  
1835 atmospheric ice-nucleating particles relevant for mixed-phase clouds. *Science Advances* 6, 26, eaba8137,  
1836 doi:10.1126/sciadv.aba8137, 2020.
- 1837 Šantl-Temkiv, T., R. Lange, D. Beddows, U. Rauter, S. Pilgaard, M. Dall’Osto, N. Gunde-Cimerman, A. Massling, and H.  
1838 Wex: Biogenic Sources of Ice Nucleating Particles at the High Arctic Site Villum Research Station, *Environ. Sci. Technol.*,  
1839 53, 18, 10580-10590, doi:10.1021/acs.est.9b00991, 2019.
- 1840 Schroth, A. W., Crusius, J., Sholkovitz, E. R. and Bostick, B. C.: Iron solubility driven by speciation in dust sources to the  
1841 ocean, *Nat. Geosci.*, 2, 5, 337–340, doi:10.1038/ngeo501, 2009.
- 1842 Schroth, A. W., Crusius, J., Gassó, S., Moy, C. M., Buck, N. J., Resing, J. A., and Campbell, R. W.: Atmospheric deposition  
1843 of glacial iron in the Gulf of Alaska impacted by the position of the Aleutian Low, *Geophysical Research Letters*, 44, 5053-  
1844 5061, doi: 10.1002/2017gl073565, 2017.
- 1845 Schuler, T. V., Kohler, J., Elagina, N., Hagen, J. O. M., Hodson, A. J., Jania, J. A., Kääb, A. M., Luks, B., Małecki, J., Moholdt,  
1846 G., Pohjola, V. A., Sobota, I., and Van Pelt, W. J. J.: Reconciling Svalbard Glacier Mass Balance, *Front Earth Sci.*, 8, 156,  
1847 doi:10.3389/feart.2020.00156, 2020.
- 1848 Semenkov, I. N. and Koroleva, T. V.: The spatial distribution of fractions and the total content of 24 chemical elements in soil  
1849 catenas within a small gully’s catchment area in the Trans Urals, Russia, *Appl. Geochemistry*, 106, 1–6, doi:  
1850 10.1016/j.apgeochem.2019.04.010, 2019.
- 1851 Semenkov, I. and Yakushev, A.: Dataset on heavy metal content in background soils of the three gully catchments at Western  
1852 Siberia, *Data Br.*, doi:10.1016/j.dib.2019.104496, 2019.

- 1853 Semenov, I. N., Usacheva, A. A. and Miroshnikov, A. Y.: Distribution of global fallouts cesium-137 in taiga and tundra  
1854 catenae at the Ob River basin, *Geol. Ore Depos.*, 57, 2, 138–155, doi:10.1134/S1075701515010055, 2015a.
- 1855 Semenov, I. N., Miroshnikov, A. Y., Asadulin, E. E., Usacheva, A. A., Velichkin, V. I. and Laverov, N. P.: The Ob river  
1856 basin as a source of Kara Sea contamination with global fallout of Cesium-137, *Dokl. Earth Sci.*, 463, 1, 704–706,  
1857 doi:10.1134/S1028334X1507003X, 2015b.
- 1858 Semenov, I. N., Krupskaya, V. and Klink, G.: Data on the concentration of fractions and the total content of chemical elements  
1859 in catenae within a small catchment area in the Trans Urals, Russia, *Data in Brief*, 29, doi: 10.1016/j.dib.2019.104224, 2019.
- 1860 Semenov, I. N., Sharapova, A. V., Koroleva, T. V., Klink, G. V., Krechetov, P. P. and Lednev, S. A.: Nitrogen-containing  
1861 substances in the snow of the fall areas of the Proton launch vehicle stages in 2009 – 2019, *Led i sneg*, 61, 301-310, doi:  
1862 10.31857/S2076673421020090, 2021.
- 1863 Sharapova, A. V., Semenov, I. N., Koroleva, T. V., Krechetov, P. P., Lednev, S. A. and Smolenkov, A. D.: Snow pollution  
1864 by nitrogen-containing substances as a consequence of rocket launches from the Baikonur Cosmodrome, *Sci. Total Environ.*,  
1865 709, 136072, doi: 10.1016/j.scitotenv.2019.136072, 2020.
- 1866 Shepherd, G., Terradellas E., Baklanov A., Kang A., Sprigg W., Nickovic S., Darvishi Bolorani A., Al-Dousari A., Basart  
1867 S., Benedetti A. et al.: Global assessment of sand and dust storms, UNEP, WMO, UNCCD; United Nations Environment  
1868 Programme, 123 p., [URL:http://apps.unep.org/publications/pmtdocuments/Global\\_assessment\\_of\\_sand\\_and\\_dust\\_storms-](http://apps.unep.org/publications/pmtdocuments/Global_assessment_of_sand_and_dust_storms-2016.pdf)  
1869 [2016.pdf](http://apps.unep.org/publications/pmtdocuments/Global_assessment_of_sand_and_dust_storms-2016.pdf), 2016.
- 1870 Shi, Z., Krom, M. D., Jickells, T. D., Bonneville, S., Carslaw, K. S., Mihalopoulos, N., Baker, A. R., and Benning, L. G.:  
1871 Impacts on iron solubility in the mineral dust by processes in the source region and the atmosphere: A review, *Aeolian*  
1872 *Research*, 5, 21-42, doi: 10.1016/j.aeolia.2012.03.001, 2012.
- 1873 Shugar, D. H., Clague, J. J., Best, J. L., Schoof, C., Willis, M. J., Copland, L., Roe, G. H.: River piracy and drainage basin  
1874 reorganization led by climate-driven glacier retreat. *Nature Geoscience* 10, 370, 2017.
- 1875 Sofiev, M., Vira, J., Kouznetsov, R., Prank, M., Soares, J., Genikhovich, E.: Construction of the SILAM Eulerian atmospheric  
1876 dispersion model based on the advection algorithm of Michael Galperin, *Geosci. Model Developm.* 8, 3497-3522, 2015.
- 1877 Speirs, J.C., McGowan, H.A. and Neil, D.T. Meteorological controls on sand transport and dune morphology in a polar-desert:  
1878 Victoria Valley, Antarctica. *Earth Surf. Proc. Land.*, 33, 1875–1891, 2008.

- 1879 Spolaor A, Moroni B, Luks B, Nawrot A, Roman M, Larose C, Stachnik Ł, Bruschi F, Koziol K, Pawlak F, Turetta C, Barbaro  
1880 E, Gallet J-C and Cappelletti D. Investigation on the Sources and Impact of Trace Elements in the Annual Snowpack and the  
1881 Firn in the Hansbreen (Southwest Spitsbergen). *Front. Earth Sci.* 8:536036, doi: 10.3389/feart.2020.536036, 2021.
- 1882 Stockdale, A., Krom, M. D., Mortimer, R. J., Benning, L. G., Carslaw, K. S., Herbert, R. J., Shi, Z., Myriokefalitakis, S.,  
1883 Kanakidou, M., and Nenes, A.: Understanding the nature of atmospheric acid processing of mineral dusts in supplying  
1884 bioavailable phosphorus to the oceans, *Proc Natl Acad Sci U S A*, 113, 14639-14644, doi: 10.1073/pnas.1608136113, 2016.
- 1885 Stojiljkovic, A., Kauhaniemi, M., Kukkonen, J., Kupiainen, K., Karppinen, A., Denby, B. R., Kousa, A., Niemi, J. V., and  
1886 Ketzel, M.: The impact of measures to reduce ambient air PM10 concentrations originating from road dust, evaluated for a  
1887 street canyon in Helsinki, *Atmos. Chem. Phys.*, 19, 11199–11212, doi: 10.5194/acp-19-11199-2019, 2019.58-9, 2019.
- 1888 Storelvmo, T., I. Tan, and A. V. Korolev: Cloud Phase Changes Induced by CO2 Warming—a Powerful yet Poorly Constrained  
1889 Cloud-Climate Feedback, *Current Climate Change Reports*, 1, 4, 288-296, doi:10.1007/s40641-015-0026-2, 2015.
- 1890 Sweeney M., Mason J. A., Mechanisms of dust emission from Pleistocene loess deposits, Nebraska, USA, *Journal of*  
1891 *Geophysical Research* 118, 3, 1460-1471, doi:10.1002/jgrf.20101, 2013.
- 1892 Tagliabue, A., and Arrigo, K. R.: Iron in the Ross Sea: 1. Impact on CO2 fluxes via variation in phytoplankton functional  
1893 group and non-Redfield stoichiometry, *Journal of Geophysical Research: Oceans*, 110, 2005.
- 1894 Tan, I., and T. Storelvmo: Evidence of Strong Contributions From Mixed-Phase Clouds to Arctic Climate Change, *Geophys.*  
1895 *Res. Lett.*, 46, 5, 2894-2902, doi:10.1029/2018GL081871, 2019.
- 1896 Tang, M, Cziczo, D.J., Grassian, V. H.: Interactions of sater with mineral dust aerosol: Water adsorption, hygroscopicity, cloud  
1897 condensation, and ice nucleation. *Chem. Rev.* 116, 4205-4259, 2016.
- 1898 Tarr, R. S., and L. Martin. Glacier deposits of the continental type in Alaska, *Geology*, 21, 289–300, doi:10.1086/622063,  
1899 1913.
- 1900 Television Midtvest 2021, video link: [Se videoen: Kraftig blæst får biler til at forsvinde i støvsky | TV MIDTVEST](#), 2021.
- 1901 Terradellas, E., Nickovic, S., and Zhang, X. Y.: Airborne dust: a hazard to human health, environment and society. *WMO*  
1902 *Bull*, 64, 2, 42-46, 2015.
- 1903 Terradellas, E., Zhang, X. Y, Farrel, D., Nickovic, S., and Baklanov, A.: Airborne dust: Overview of atmospheric dust content  
1904 in 2016. *WMO Airborne Dust Bull* 1, 1-3, 2017.

- 1905 Tobo, Y. K. Adachi, P. J. DeMott, T. C. J. Hill, D. S. Hamilton, N. M. Mahowald, N. Nagatsuka, S. Ohata, J. Uetake, Y.  
1906 Kondo, M. Koike: Glacially sourced dust as a potentially significant source of ice nucleating particles. *Nat Geosci*, 12, 4, 253-  
1907 258, doi:10.1038/s41561-019-0314-x, 2019.
- 1908 Urupina D., Lasne, J., Romanias, M., Thiery, V., Dagsson-Waldhauserová, P., Thevenet, F.: Uptake and surface chemistry of  
1909 SO<sub>2</sub> on natural volcanic dusts, *Atmospheric Environment*, Vol 217, pp 116942, DOI: 10.1016/j.atmosenv.2019.116942, 2019.
- 1910 UNCCD / Vukovic, A.: Sand and Dust Storms Source Base-map. Visualization Tool. <https://maps.unccd.int/sds/> and  
1911 <https://www.youtube.com/watch?v=4tsbspJvuAs>, 2021.
- 1912 USGCRP: Impacts, Risks, and Adaptation in the United States: The Fourth National Climate Assessment, Volume II. In: D.  
1913 R. Reidmiller, C. W. Avery, D. R. Easterling, K. E. Kunkel, K. L. M. Lewis, T. K. Maycock, and B. C. Stewart (Eds.).  
1914 Washington, DC, doi:10.7930/NCA4.2018, 2018.
- 1915 Usher, C.R., Michel, A.E., and Grassian, V.H.: *Chemical Reviews*, 103, 12, 4883-4940, doi: 10.1021/cr020657y, 2003.
- 1916 Valle, H. F. Del, Elissalde, N. O., Gagliardini, D. A., and Milovich, J.: Status of desertification in the Patagonian region:  
1917 Assessment and mapping from satellite imagery. *Arid Soil Research and Rehabilitation*, 12, 2, 95–121,  
1918 doi:10.1080/15324989809381502, 1998.
- 1919 Varga, G., Dagsson-Waldhauserová, P., Gresina, F. and Helgadóttir A.: Saharan dust and giant quartz particle transport  
1920 towards Iceland. *Scientific Reports* 11, 11891, 2021.
- 1921 Vergara-Temprado, J., A. K. Miltenberger, K. Furtado, D. P. Grosvenor, B. J. Shipway, A. A. Hill, J. M. Wilkinson, P. R.  
1922 Field, B. J. Murray, and K. S. Carslaw: Strong control of Southern Ocean cloud reflectivity by ice-nucleating particles, *P. Natl.*  
1923 *Acad. Sci. USA*, doi:10.1073/pnas.1721627115, 2018.
- 1924 von Friesen, L.W. and Riemann, L.: Nitrogen Fixation in a Changing Arctic Ocean: An Overlooked Source of Nitrogen?  
1925 *Frontiers in Microbiology*, 11, 1664-302X, doi: 10.3389/fmicb.2020.596426, 2020.
- 1926 Vukovic, A.: Report on consultancy to develop Global Sand and Dust Source Base Map, no. CCD/18/ERPA/21, UNCCD,  
1927 2019.
- 1928 Vukovic Vimic, A.: Global high-resolution dust source map, InDust webinar, 21 April 2021, [https://cost-](https://cost-indust.eu/events/indust-events)  
1929 [indust.eu/events/indust-events](https://cost-indust.eu/events/indust-events), 2021.

- 1930 Wang, Q., Fan, X. & Wang, M.: Evidence of high-elevation amplification versus Arctic amplification. *Sci Rep*, 6, 19219.  
1931 <https://doi.org/10.1038/srep19219>, 2016.
- 1932 Wahlström E., Reinikainen, T. and Hallanaro E.-L.: *Ympäristön tila Suomessa*, ISBN 951-662-523-1, 364 p., 1996.
- 1933 Wheaton, E. E.: Prairie dust storms — A neglected hazard, *Nat. Hazards*, 5, 1, 53–63, doi:10.1007/BF00127139, 1992.  
1934
- 1935 Wheaton, E. E. and Chakravarti, A. K.: Dust storms in the Canadian Prairies, *Int. J. Climatol.*, 10, 8, 829–837,  
1936 doi:10.1002/joc.3370100805, 1990.
- 1937 Wientjes, I. G., R. S. Van De Wal, G. J. Reichert, A. Sluijs, and J. Oerlemans: Dust from the dark region in the western ablation  
1938 zone of the Greenland ice sheet, *The Cryosphere*, 5, 589–601, doi:10.5194/tc-5-589-2011, 2011.
- 1939 Winton, V. H. L., Dunbar, G. B., Bertler, N. A. N., Millet, M. A., Delmonte, B., Atkins, C. B., Chewings, J. M., and Andersson,  
1940 P.: The contribution of aeolian sand and dust to iron fertilization of phytoplankton blooms in southwestern Ross Sea,  
1941 Antarctica, *Global Biogeochemical Cycles*, 28, 423-436, doi: 10.1002/2013gb004574, 2014.
- 1942 Winton, V.H.L., Dunbar, G.B., Atkins, C.B., Bertler, N.A.N., Delmonte, B., Andersson, P., Bowie, A., Edwards, R.: The origin  
1943 of lithogenic sediment in the south-western Ross Sea and implications for iron fertilization. *Antarctic Science*,  
1944 doi:10.1017/S095410201600002X, 2016a.
- 1945 Winton, V. H. L., Edwards, R., Delmonte, B., Ellis, A., Andersson, P. S., Bowie, A., Bertler, N. A. N., Neff, P., and Tuohy,  
1946 A.: Multiple sources of soluble atmospheric iron to Antarctic waters, *Global Biogeochemical Cycles*, 30, 421-437, doi:  
1947 10.1002/2015gb005265, 2016b.
- 1948 Wolfe S.A.: *Cold-Climate Aeolian Environments*, Reference Module in Earth Systems and Environmental Sciences,  
1949 10.1016/B978-0-12-818234-5.00036-5, 2020.
- 1950 Zhu, L., Ives, A., Zhang, C., Guo, Y., and Radeloff, V.: Climate change causes functionally colder winters for snow cover-  
1951 dependent organisms. *Nature Climate Change*, 9, 1-8, doi:10.1038/s41558-019-0588-4, 2019.
- 1952 Zhu, Y., Toon, O.B., Jensen, E.J. et al.: Persisting volcanic ash particles impact stratospheric SO<sub>2</sub> lifetime and aerosol optical  
1953 properties. *Nat Commun* 11, 4526, doi:10.1038/s41467-020-18352-5, 2020.
- 1954 Zwoliński, Z., Kostrzewski, A., and Pulina, M. (Eds.): *Dawne i współczesne geokosystemy Spitsbergenu* [Ancient and  
1955 modern geocosystems of Spitsbergen], Bogucki Wydawnictwo Naukowe, Poznań, 456 p., 2013.